ISSN 0169-6548

# Communications on Hydraulic and Geotechnical Engineering

Simulation of a Surf Zone with a Barred Beach;
Report 1: Wave Heights and Wave Breaking

1996

M. Boers

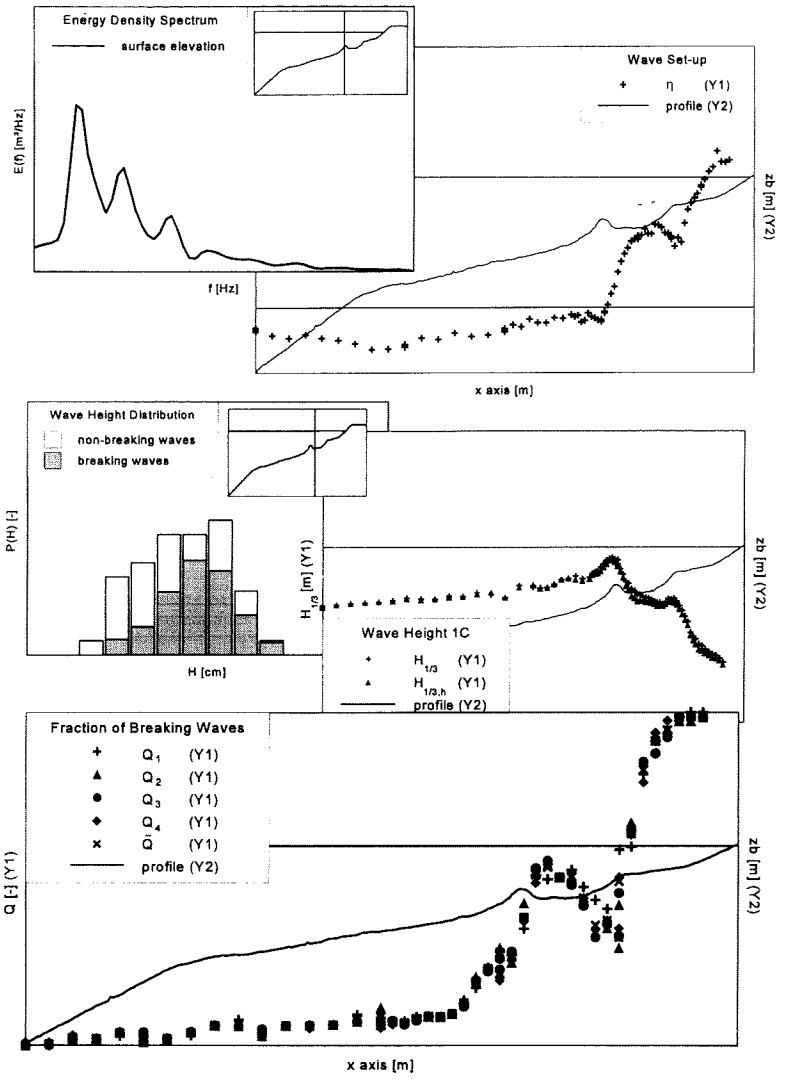


TU Delft
Delft University of Technology

**Faculty of Civil Engineering**

# Simulation of a Surf Zone with a Barred Beach; Part 1: Wave Heights and Wave Breaking

by

M. Boers

1996

Communications on Hydraulic
and Geotechnical Engineering

Report No. 96-5

Delft University of Technology
Department of Civil Engineering
Division of Hydraulic and Geotechnical Engineering

## ACKNOWLEDGEMENTS

The author thanks Dr. Richard Simons for the use of the shear stress plate of the University College of London. Futher, the author thanks all people mentioned in Chapter 1 for their contributions to the measurements. Special thanks are paid to Mark Voorendt, who gave much of his precious time to make the measurements a success.

## CONTENTS

# 1 INTRODUCTION

The present report describes some of the results obtained during experiments in the Large Wave Flume of the Fluid Mechanics Laboratory of the Delft University of Technology.

The experiments are part of the PhD-work of M. Boers. They follow on the LIP 11D-experiments, carried out in the Delta Flume of Delft Hydraulics in spring 1993. During the LIP 11D-experiments much information was obtained about physical parameters in the surf zone such as wave heights, wave set-up and velocities.

The experiments have the following objectives:

- To add measuring data to the LIP 11D-data
- To obtain data which can reconstruct the mass, momentum and energy balances
- To obtain detailed information about regions with steep gradients of wave heights and wave set-up (onshore slope of breaker bar and toe of foreshore)
- To obtain information about the breaking behaviour of waves
- To measure bed shear stresses
- To measure turbulence motions

The objective of this report is to distribute the results of the measurements among researchers working in the field of coastal engineering. Futher, it gives information about the accuracy of the measuring data.

The following people are involved in the experiments:

Project team:
M. Boers (manager) and M.Z. Voorendt (assistant)

Advisors:
Dr. J. van de Graaff, G. Klopman and Dr. J.A. Roelvink

Assistance from the laboratory:
Dr. H.L. Fontijn, R. Booij, J.F. van de Brugge, K. de Bruin, J.A. van Duin, J. Groeneveld, F. Kalkman, Mrs. H. Klaasman, H.J. Monteny, J. Tas, A. den Toom, J. Tukker

Assistance with the Shear Stress Plate:
Dr. R. Simons, B. Fairman, R. MacIver (University College of London)

Assistance with the laser-Doppler velocimetry:
H. Godefroy (Delft Hydraulics)

The results of the experiments are described in two reports. Report 1 (the present report) describes the experimental set-up [Chapter 2], wave height measurements and the video recordings of the wave breaking [Chapter 3]. The results of velocities and shear stress measurements are described in Report 2 [Boers, 1996]. Some of the results are already published by Boers and Van de Graaff [1995].


The results of the analysis of the measurements is presented in many figures. Data are also available in files [Enclosure A]. When a file is described, a file icon is put in the margin. The files can be requested from:

Marien Boers
Delft University of Technology
Department of Civil Engineering
Division of Hydraulic and Geotechnical Engineering
Stevinweg 1
2628 CN, Delft
The Netherlands
e-mail: M.Boers@ct.tudelft.nl

# 2 EXPERIMENTAL SET-UP

## 2.1 General

The present chapter discusses the set-up of the experiments performed in the Large Wave Flume of the Fluid Mechanics Laboratory of the Delft University of Technology from March until October 1995.

The experiments are aimed to be a Froude scaled reproduction of the LIP 11D-experiments, which were carried out in the Delta Flume of Delft Hydraulics in spring 1993 [Roelvink and Reniers, 1995]. The geometric scaling factor is $n_l$ = 5.6. Because of some technical limitations, a perfect scaled reproduction is not reached.

## 2.2 Set-up of Wave Flume

The geometry of the Large Wave Flume of the Delft University of Technology is presented in Table 2.1.

| Geometry Wave Flume | Size [m] |
|---|---|
| Length | 40 |
| Width | 0.80 |
| Height | 1.05 |

*Table 2.1* Geometry of Wave Flume

The flume has a piston-type wave board allowing for a translatory motion. A reflection compensation system prevents the re-reflection of incoming waves against the wave board. These incoming waves are determined from the wave board velocity and the wave gauges installed at the wave board front. The wave board moves over a span of about 0.50 m.

Beach profile

A beach profile is built in the wave flume according to a profile present during the LIP 11D-experiment 1B. This profile has a breaker bar and a surf zone trough. The mega-ripples which were present during the LIP 11D-experiments are not reproduced. Because it is not possible within the present experiments to adapt the profile for the Wave Conditions 1A and 1C, a perfect reproduction of the corresponding LIP 11D-experiments is not reached.

Figure 2.1 shows the beach profile with the coordination system used during the experiments. The origin of the 'x axis' is at the toe of the profile. The origin of the 'z axis' is at the bottom of the flume for profile measurements and at the bed of the profile for the velocity measurements.

A fixed bottom profile is used, because the wave conditions have to be similar for all experiments. The profile is built up with a fill of sand and a concrete top layer. This concrete layer is smoothed to reduce the bed roughness.

Six boxes covered with a concrete top layer are installed inside the profile for measurements with a shear stress plate. During experiments with this plate the concrete top layer is removed to install the shear stress plate [Figures 2.2, 2.3].

Matrices of PVC are placed in the concrete bottom layer. When the laser-Doppler velocimetry has to measure the velocities in the bottom boundary layer, a special matrix is applied which has two grooves with the shape of the LDV [Figure 2.4]. This matrix is coarsened to get a similar bed roughness as the concrete top layer.

The concrete top layer, the PVC matrices and the shear stress plate have different bed roughnesses. This will give differences between the velocities in the bottom boundary layer and between the bed shear stresses.

File After the construction of the beach profile, the profile was sounded with a gauging-rod. The results are given in File **PROFILE.TAB**.

The still water level during the experiments is z = 0.75 m above the bottom of the wave flume. The water level is controlled and re-supplied daily. The loss of water is about 1 - 2 mm per day. The water in the wave flume is refreshed regularly to remove algae and other debris. The water temperature is between 20 - 23°C.

## 2.3 Wave Generation

Three different types of wave conditions are generated during the experiments. The required wave conditions at the wave board are given in Table 2.2. Because the span of the wave board is too short to generate waves which should be present according to the LIP 11D-experiment 1B, the wave height of Wave Condition 1B is reduced with about 8%. This means that the reproduction of Wave Condition 1B of the LIP 11D-experiments is not perfect either.

Because it is one of the objectives to measure turbulence motions, a relative short signal of irregular waves is produced (a cycle), which is repeated several times. This enables the technique of ensemble averaging over the various cycles, which is applied to determine the turbulence motions [Klopman, 1994].

The program STIR of Delft Hydraulics produces the signal for the generation of the waves. Second order harmonics for both subharmonic and superharmonic frequencies are generated [Delft Hydraulics, 1992(A); Klopman and Van Leeuwen, 1990].

| Wave Condition | $H_{sig,0}$ [m] | $T_p$ [s] | No. of Cycles | Cycle Period [s] |
|---|---|---|---|---|
| 1A | 0.16 | 2.1 | 11 | 157.079 |
| 1B | 0.22 | 2.1 | 11 | 157.079 |
| 1C | 0.10 | 3.4 | 7 / 11 | 245.441 |

*Table 2.2* Input Values of Wave Parameters in the Program STIR

Table 2.2 gives the input values for the program STIR. The produced signal is sent to the wave board with a frequency of 110 Hz.

Because the span of the wave board is restricted, it was necessary to apply a high-pass filter on this signal with a cut-off frequency of $0.2*f_p$ for Wave Condition 1B and $0.1*f_p$ for the Wave Conditions 1A and 1C.

| **Wave Condition** | **$H_{sig,0}$ [m]** | **$T_p$ [s]** |
|---|---|---|
| 1A | 0.157 | 2.05 |
| 1B | 0.206 | 2.03 |
| 1C | 0.103 | 3.33 |

*Table 2.3* Measured Wave Parameters in the Wave Flume at location x = 0 m

The measured wave parameters at location x = 0 m are presented in Table 2.3. These parameters show good correspondence with the required parameters in Table 2.2. Note that the distance between the wave board and the measuring location is about 4.5 m.

The measured energy density spectra for the wave conditions at location x = 0 m are presented in the Figures 2.5, 2.6 and 2.7. These figures show the minimum, the mean and the maximum values of E(f) of at least 17 (1B: 18) experiments. It appears that the deviation of E(f) over the experiments is very small (hardly visible), which indicates an accurate reproduction of the wave conditions during the various experiments.

Besides, these figures show Jonswap spectra with the same content of energy. It appears that the spectra of the measured signal have a lot of energy in the superharmonic frequencies. Consequently the energy in the first harmonics of the measured signal is much lower than according to the Jonswap spectrum. The

energy in the subharmonic frequencies of the measured signals are satisfactory low. Further information about the energy density spectra from the measured signals is given in Section 3.2.

Two different procedures of wave generation are used during the measurements:
Procedure 1
Every experiment starts with the still water condition in the wave flume (the wave board does not work). First, the still water situation is measured for the determination of the still water level and the shear stress of the plate when the water is at rest. This is a necessary step for the determination of the wave set-up and the mean bed shear stresses during the experiment. When the experiment comes to an end, the waves diminish and the still water condition reappears. The measurements of the first wave cycle are not used in the data analysis. Velocity measurements during experiments following this procedure should be taken at locations where the turbulence becomes stable very fast, like the bottom boundary layer or regions with intense breaking.
Procedure 2
Wave generation starts long before an experiment to get a stable level of turbulence throughout the flume. This procedure is required when accurate velocity measurements are carried out in regions outside the bottom boundary layer and outside the breaking region. Measurements of the wave set-up or the mean bed shear stress are impossible.

## 2.4 Instrumentation

The present section gives information about the instrumentation, which is used during the experiments. The tasks of the instruments used are discussed together with their strong and weak points and the way they are applied.

Table 2.4 gives an overview of all instruments used during the experiments. Further, information is given about the sample frequency $f_s$ and the provider of the instruments (UCL: University College of London; DH: Delft Hydraulics; DUT:

Delft University of Technology).

| Instrument | Number | $f_s$ [Hz] | Provider |
|---|---|---|---|
| wave gauge (WG) | 6 | 20 | DUT |
| laser-Doppler velocimetry (LDV) | 2 | 100 | DUT/DH |
| electro-magnetic flow meter (EMF) | 1 | 20 | DUT |
| shear stress plate (SSP) | 1 | 20 | UCL |
| video | 1 | - | DUT |

*Table 2.4* Instrumentation used during experiments

Measurements are carried out at two different sample frequencies (20 Hz and 100 Hz). Therefore, two data acquisition systems are needed. Because there is a time lag between the beginning of the measurements, a synchronisation of both systems is required. For this reason, one of the LDV channels is also sampled with a sample frequency of 20 Hz.

wave gauge [Figure 2.8]

The wave gauges have the following tasks:

- Wave characteristics are measured with the wave gauges. Outside the surf zone the waves are measured every 1 m. Within the surf zone, the distance between two measurements decreases to 0.20 m. The results of the measurements are discussed in Chapter 3.
- Wave gauges are used to check the wave conditions in the wave flume. On fixed locations, surface elevations are measured during several experiments. The measured signals are used to quantify the accuracy of the reproduction of the wave conditions in the flume. At location x = 0 m, a wave gauge is employed during all tests.

A wave gauge consists of two silvered copper wires, which measure the electric

resistance of the water in between. When the surface elevation is low, the resistance is high and vice versa.

When the wave gauges are used to measure the wave characteristics, they are calibrated every day. Further, at every position the still water level is measured before the generation of waves starts. When the wave gauges are used for the control of the wave conditions only, there is a calibration of at least one time a week.

The use of wave gauges has a number of strong points:

- Wave gauges are easy installed and removed on various locations.
- Wave gauges measure the free surface elevation directly. Measurements with pressure transducers have to be transformed using some wave theory to derive the free surface elevation. The relation between the pressure and the free surface elevation is non-linear, depending also on the velocity.
- Wave gauges measure very high wave frequencies, which show a strong decline of the pressure oscillations in downward direction and are probably not detected by pressure transducers.

Wave gauges have also a weak point:

- When a wave breaks, air bubbles are generated. The influence of the air bubbles on the electric resistance of the water is unknown.

Laser-Doppler velocimetry [Figures 2.9, 2.10]

The task of the LDV is the measuring of flow velocities at a very accurate level, to enable the study of the turbulence motions and velocities in the bottom boundary layer [Boers, 1996].

The LDV's used during the experiments are immersed in the water and measure according to the forward scatter technique. Horizontal and vertical velocities are determined from the Doppler frequency shift, caused by the motion of small particles in the water. Calibration coefficients can be computed from the geometry

of the laser beams.

Only one of the LDV's is able to measure flow velocities when the probe is immersed temporary. The other one is only operational when the probe is immersed during the whole experiment.

The immersible LDV has several strong points:

- It is possible to measure velocities over the whole profile, i.e., from bottom boundary layer to wave crest.
- Horizontal and vertical velocities are measured at one position at the same time.
- The accuracy of the measurements is very high because of the small measuring volume where the Doppler shift is measured (0.1 $mm^3$).
- The system is easy to operate at various locations.
- The disturbance of the signal by air bubbles is relatively small, because the laser beams are relatively short.
- There is no calibration needed.

Of course, there are also some weak points:

- Because the system is immersible, the measuring device interferes with the flow velocities. The distance between transmitter and receiver is about 4 cm.
- The LDV has a large weight and consists of very sensitive units. The system is therefore highly vulnerable for damage.
- The equipment is quite expensive.

Electro-magnetic Flow Meter [Figure 2.11]

The EMF has two tasks:

- The instrument is used to check the wave conditions just like the wave gauges.
- Velocities are measured above the shear stress plate. These velocities are necessary to determine the pressure gradients which influence the

measurements of the shear stress plate.

The EMF measures the flow velocities from the perturbations of the electromagnetic field caused by the water motion. Although this instrument is very easy to use, it is not used to measure the characteristics of the flow velocities, because the large measuring volume filters most of the turbulence motions near the bed.

Shear Stress Plate [Figure 2.11]
The tasks of the shear stress plate is the measuring of the bed shear stresses at six locations along the profile [Table 2.5].

| **Location** | **Coordinate [m]** |
|---|---|
| 1 | 8.10 |
| 2 | 14.37 |
| 3 | 17.00 |
| 4 | 19.67 |
| 5 | 22.35 |
| 6 | 23.95 |

*Table 2.5* Locations where bed shear stresses are measured

This instrument measures a combination of the desired shear stress acting on the plate and a spurious force due to the pressure gradient acting on the edges of the plate. To determine the shear stress, it is necessary to measure:

- the total force on the plate during the experiments
- the force on the plate before and after the experiments during still water conditions
- the velocity above the plate to estimate the pressure gradient

The instrument has to be re-calibrated after every major installation.

Although the shear stress plate is very sensitive to debris, which hinder the free moving of the plate, the measurements give good insight in the bed shear stresses in the wave flume [Boers, 1996].

Video

The task of the video is the recording of the breaking of waves [Section 3.7]. The recording takes place at a position above the wave flume. The whole wave flume is split up into intervals of 5 m, which are recorded separately.

# 3 WAVE HEIGHTS AND WAVE BREAKING

## 3.1 General

The results of the measurements related to the waves in the wave flume are presented in this chapter. Information is given about the following topics:

- spectral analysis
- statistical analysis
- wave celerity and wave group celerity
- reflection of waves
- wave energy flux
- analysis of wave breaking

Most information comes from the measurements of the surface elevation. Velocity measurements are used to analyse the reflection of the waves and video recordings are used to study the breaking of the waves.

All results presented are also available in files. All files are in 'ASCII'-format except the files with extension '**XLS**'. These files are in 'Microsoft Excel'-format. The wildcard characters used in the filenames have the following meaning:

| | |
|---|---|
| *#### | location of the measurement *100 (e.g., 1960 means: location x = 19.60 m) |
| *## | wave condition (1A, 1B or 1C) |

A list of files is given in Enclosure A.

## 3.2 Spectral Analysis

In this section a spectral analysis is made of the measured surface elevations. The program SPECTRUM computes the energy density spectrum and some relevant spectral parameters [Delft Hydraulics, 1992 (B)]. Before the spectral analysis, the mean value of the measured surface elevations is subtracted from the signal.

The energy density spectrum is computed directly using a Fast Fourier Transform algorithm. The accuracy of the computation is increased by a 50% overlap of the data sequences and Hanning filtering in the frequency domain. Spectral leakage is reduced by using a cosine time window.

| Condition | N | M | β [Hz] | ν | $\epsilon_r$ | Δf [Hz] |
|---|---|---|---|---|---|---|
| 1A | 512 | 122 | 0.1024 | 317.2 | 0.0794 | 0.0395 |
| 1B | 512 | 122 | 0.1024 | 317.2 | 0.0794 | 0.0395 |
| 1C | 512 | 115 | 0.1024 | 299 | 0.0818 | 0.0395 |

*Table 3.1* Accuracy of the spectral analysis

Table 3.1 gives information about the accuracy of the computations. The symbols used have the following meaning:

N: number of measuring data in one sequence

M: number of sequences

β: $\frac{2.6 f_s}{N+1}$ frequency resolution

ν: $2.6M$ degrees of freedom

$\epsilon_r$: $\sqrt{\frac{2}{\nu}}$ relative error estimate

Δf: frequency bandwidth


Figures 3.1, 3.2 and 3.3 give a lot of graphs with the energy density spectrum at the various locations in the wave flume. The location of the measurements is presented at the right upper corner of the graphs. Also the number of measuring series put in the graph is given. (Because these series are very similar, they cannot be distinguished discretely.) The energy density spectra are also available in the Files SP_X####.##.

File

The Files **SPEC_TAB.**** give more information about the spectra, namely:

| | | |
|---|---|---|
| $m_0$ | $\int_0^\infty E(f)\,df$ | zeroth order spectral moment |
| $m_2$ | $\int_0^\infty f^2 E(f)\,df$ | second order spectral moment |
| $m_4$ | $\int_0^\infty f^4 E(f)\,df$ | fourth order spectral moment |
| $E(f)_{max}$ | | maximum spectral value |
| $f_p$ | | frequency with maximum spectral value |
| $T_p$ | $\frac{1}{f_p}$ | period with maximum spectral value |
| $f_{p,D}$ | $\frac{\int_{f_l}^{f_h} fE(f)\,df}{\int_{f_l}^{f_h} E(f)} \quad [f_l < f_p < f_h \wedge E(f_l) = E(f_h) = 0.8\,E(f_p)]$ | dominant peak frequency |
| $T_{p,D}$ | $\frac{1}{f_{p,D}}$ | dominant period |
| $T_{0,2}$ | $\sqrt{\frac{m_0}{m_2}}$ | mean zero-crossing period |
| $T_{2,4}$ | $\sqrt{\frac{m_2}{m_4}}$ | mean period local maxima |
| $\epsilon_2$ | $\sqrt{\frac{m_0 m_2}{m_1^2} - 1}$ | narrowness parameter |
| $\epsilon_4$ | $\sqrt{1 - \frac{m_2^2}{m_0 m_4}}$ | broadness parameter |
| $\kappa$ | $\frac{\sqrt{(\int_0^\infty E(f)\cos(T_{0,2} f)\,df)^2 + (\int_0^\infty E(f)\sin(T_{0,2} f)\,df)^2}}{m_0}$ | spectral width/narrowness parameter |
| $H_{m0}$ | $4\sqrt{m_0}$ | significant wave height from spectrum |

File The Files **HM0_TAB.###** give information about the energy content of the subharmonic frequencies (low frequencies) and the first order and superharmonic frequencies (high frequencies). The subharmonic frequencies are eliminated with a high-pass filter. The frequency range is from 0.2 Hz (1A, 1B) and 0.15 Hz (1C) upwards. The following parameters are given:

| | | |
|---|---|---|
| $m_0$ | $\int_0^\infty E(f)\,df$ | zeroth order spectral moment of unfiltered signals |
| $m_{0,h}$ | $\int_{f_l}^\infty E(f)\,df$ | zeroth order spectral moment of the high frequencies |
| $m_{0,l}$ | $m_0 - m_{0,h}$ | zeroth order spectral moment of the low frequencies |
| $H_{m0}$ | $4\sqrt{m_0}$ | significant wave height from spectrum (unfiltered signals) |
| $H_{m0,h}$ | $4\sqrt{m_{0,h}}$ | significant wave height of high frequencies |
| $H_{m0,l}$ | $4\sqrt{m_{0,l}}$ | significant wave height of low frequencies |

The significant wave heights are presented in the Figures 3.4, 3.5 and 3.6.

Discussion of the results

Energy density spectra are measured at many locations in the wave flume. The distance between these locations is less than or equal to one metre. The Figures 3.1, 3.2 and 3.3 show that the differences of the spectrum between all adjacent measurements are very small. This indicates that the measurements are quite accurate and that the measurements cover all important developments of the waves.

In a number of locations measurements have been carried out more than once. (This can be read from the legend.) In the Figures 3.1, 3.2 and 3.3, these series often cannot be distinguish discretely. This indicates that the reproduction of the waves in the flume during the measurements is satisfactory good.

The measured spectra give good insight in the development and dissipation of the superharmonic frequencies. For Wave Condition 1C even three superharmonic peaks are found.

Energy in the subharmonic frequency range is in particular present in the breaker zone. At the foreshore the energy density of the subharmonic frequencies even exceeds the energy density of the dominant peak frequency of the high frequencies.

At the toe of the profile (x = 0 m), energy in the subharmonic frequencies is almost negligible compared with the energy density of the first order frequencies. This is an indication that the compensation of the reflected energy by the wave board is working well.

The energy content of the high frequencies is decreasing throughout the flume for the Wave Conditions 1A and 1B. This is apparently due to wave breaking. Wave Condition 1C shows an increase of the wave height offshore of the breaker bar (shoaling). A strong decrease of the energy content is present onshore of the breaker bar and at the foreshore for all wave conditions.

The energy content of the low frequencies shows a moderate but steady increase throughout the whole wave flume. The influence of the breaker bar is only of importance for Wave Condition 1A.

### 3.3 Statistical Analysis

The measured surface elevations are analysed with the programs STATIST and WAVES [Delft Hydraulics, 1992(B)]. The program STATIST computes a number of relevant statistical parameters from the surface elevation. The program WAVES analyses the extreme values and the zero-crossings of the signals.

File The results of STATIST are given in the Files **STAT_TAB.****:

| | | |
|---|---|---|
| $\overline{\eta_0}$ | $E[\eta_0]$ | still water level |
| $\overline{\eta}$ | $E[\eta]$ | mean water level |
| $\sigma_\eta$ | $\sqrt{E[(\eta-\overline{\eta})^2]}$ | standard deviation of surface elevation |
| $\eta_{rms}$ | $\sqrt{E[\eta^2]}$ | root mean square value of surface elevation |
| $\eta_{min}$ | $\min[\eta]$ | minimum value of surface elevation |
| $\eta_{max}$ | $\max[\eta]$ | maximum value of surface elevation |
| $\gamma_{1,\eta}$ | $\frac{E[(\eta-\overline{\eta})^3]}{E[(\eta-\overline{\eta})^2]^{\frac{3}{2}}}$ | skewness of surface elevation |
| $\gamma_{2,\eta}$ | $\frac{E[(\eta-\overline{\eta})^4]}{E[(\eta-\overline{\eta})^2]^2} - 3$ | kurtosis of surface elevation |
| GF | | groupiness factor |

The Figures 3.7, 3.8 and 3.8 show the wave set-up for all wave conditions. The wave set-up is computed as the difference between the mean water level and the still water level. The measuring of the still water level is discussed in Section 2.3.

The program WAVES uses measured surface elevations with the mean value subtracted. Again a high-pass filter is applied on the signal. Both the unfiltered and the filtered signals are analysed. The frequency range is from 0.2 Hz (1A, 1B) and 0.15 Hz (1C) upwards.

File The following results are given in the Files **WAVE_TAB.****:

| | |
|---|---|
| N | number of waves |
| $T_m$ | mean wave period |
| $H_{1/3}$ | mean wave height of highest 1/3 waves |
| $a_{c,1/3}$ | mean crest amplitude of highest 1/3 waves |
| $a_{t,1/3}$ | mean trough amplitude of highest 1/3 waves |
| $H_{1/10}$ | mean wave height of highest 1/10 waves |
| $a_{c,1/10}$ | mean crest amplitude of highest 1/10 waves |

| | |
|---|---|
| $a_{t,1/10}$ | mean trough amplitude of highest 1/10 waves |
| $H_{1/100}$ | 1/100 exceeded wave height |
| $a_{c,1/100}$ | 1/100 exceeded crest amplitude |
| $a_{t,1/100}$ | 1/100 exceeded trough amplitude |
| $H_{max}$ | maximum wave height |
| $a_{c,max}$ | maximum crest amplitude |
| $a_{t,max}$ | maximum trough amplitude |
| $\gamma$ | correlation function gamma (from H) |
| $\kappa$ | correlation function kappa (from H) |
| $\gamma_\kappa$ | gamma computed from kappa |

The Figures 3.10, 3.11 and 3.12 show the significant wave height $H_{1/3}$ for the filtered and the unfiltered signal.

Discussion of the results

The wave set-up in the wave flume shows little scatter according to the Figures 3.8, 3.9 and 3.10. Only Wave Condition 1A has two measurements which don't fit in the trend of the other measurements.

In all wave conditions, there are two regions with a discontinuity of the gradient of the wave set-up. The first region is located just onshore of the breaker bar, the other region is located at the beginning of the foreshore. Offshore of both regions, the gradient of the wave set-up is negative. (Here it is more proper to speak about a wave set down.) Onshore of the regions, the wave set-up increases with a steep gradient.

The significant wave heights derived from the individual wave heights of the records [Figures 3.10, 3.11 and 3.12] look quite similar to the significant wave height derived from the energy density spectrum. There are some minor dissimilarities; most remarkable is larger difference between the unfiltered and filtered results of the wave heights derived from the spectra.

## 3.4 Wave Celerity and Wave Group Celerity

Wave celerity and wave group celerity are computed from two wave measurements at different but close locations. With a cross-correlation analysis the time lag between both measurements is computed. The distance between the two measurements divided by the time lag gives the required celerity. The distance between the measurements is 2 m.

In many cases the two measurements are taken during different experiments. To reduce the error caused by different starting times of these measurements, corrections are made by cross-correlating the measurements taken at $x = 0$ m.

The celerity of the waves is computed with the following steps:

- A high-pass filter is applied to remove the free low frequency waves. (Free low frequency waves have a different celerity.) Cut-off values are identical to the values used in the spectral analysis.
- The wave celerity is computed from the cross-correlation for every cycle of irregular waves to enable a statistical analysis [Section 2.3]. When the result is not realistic, which happens occasionally, it is not included in the analysis.

A high-pass filter is also applied to get the wave group celerity. After the filtering, some additional steps are made:

- The signal is squared to get the energy.
- A low-pass filter is applied to remove high frequencies, which are not part of the wave group. The cut-off values of the frequency range are 0.48 Hz (1A, 1B) and 0.35 Hz (1C).
- The same statistical analysis as the wave celerity is made.


The following parameters are found in the Files **CELC_TAB.****:

c mean wave celerity

| | |
|---|---|
| $\sigma_c$ | standard deviation wave celerity |
| $n_c$ | number of cycles with realistic wave celerity |
| $c_g$ | mean wave group celerity |
| $\sigma_{cg}$ | standard deviation wave group celerity |
| $n_{cg}$ | number of cycles with realistic wave group celerity |

The mean wave celerity and wave group celerity are presented in the Figures 3.13, 3.14 and 3.15.

Discussion of the results

The results of the wave celerity look more regular than the results of the wave group celerity. Outside the breaker region, there is some spreading of the wave group velocity. Within the breaker region, there are some discontinuities, although the spreading is less.

The wave celerity generally follows the depth. The gradients of the wave celerity are not so sharp as the gradients of the profile. This is because the wave celerity is computed over a distance of 2 m, which causes dissipation of the results. The distance of 2 m is an optimum. To get the same accuracy for a shorter distance, the sample frequency of the measurements has to be decreased and therefore the number of data in the cross-correlation has to be increased.

There are some minor differences in the wave celerity and wave group celerity of the between the Wave Conditions 1A and 1B. These differences are possibly caused by differences of the wave set-up.

The wave celerity and wave group celerity are computed for a number of cycles with irregular waves. The standard deviation of the result is generally very small and in many cases even zero. (This conclusion cannot be read from the figures.)

At many locations the wave group celerity exceeds the wave celerity, especially in the breaker region. This happens for all wave conditions. According to linear

wave theory the wave group celerity should be less or equal to the wave celerity. A good explanation for this phenomenon cannot be given, although it is remarked that this also occurs for capillary waves.

### 3.5 Reflection of Waves

The reflection of wave energy is derived from the horizontal and vertical velocity measurements using linear wave theory. The method is described by Hughes [1993].

This method is quite applicable in the region of breaking waves, because velocity measurements are carried out at the same location. Dissipation of wave energy between two measurements has therefore no influence on the outcome of the computations.

To improve the accuracy, computations are carried out at three depths at every location. Tables with the positions of the measurements used (horizontal and vertical) can be read in Enclosure B.

Figures 3.16, 3.17 and 3.18 show the spectra of incoming and reflected wave energy. When the coherence $\gamma$ of the horizontal and vertical velocity is less than 0.85, no results are presented. An exception is made for location x = 27.03 of Wave Condition 1C, where results with a coherence of more than 0.80 are presented. The spectra are represented against a logarithmic scale, to make the reflected spectra more visible.

Further, energy density spectra from adjacent wave gauges are put in the figures. The positions of these wave gauges can also be read from the tables in Enclosure B.

The reflection coefficient and the coherence outside the breaker region are presented as a function of the frequency in the Figures 3.19, 3.20 and 3.21. When

the coherence declines, the reflection coefficient becomes unreasonable high. The overall reflection coefficient is given in Table 3.2. Only results with a coherence more than 0.85 are used.

| Wave Condition | Location [m] | Reflection Coefficient $c_r$ |
|---|---|---|
| 1A | 14.37 | 0.14 |
| 1B | 8.10 | 0.19 |
| 1C | 8.10 | 0.12 |

*Table 3.2* Reflection Coefficient outside Breaker Region

File The following information about the wave reflection as function of the frequency is given in the Files **RF_X####.****:

$E_{uu}(f)$ energy of horizontal velocity

$E_{ww}(f)$ energy of vertical velocity

$E_{\eta\eta,in}(f)$ incoming wave energy

$E_{\eta\eta,ref}(f)$ reflected wave energy

$\gamma(f)$ $\sqrt{\frac{E_{uw}(f)^2}{E_{uu}(f)E_{ww}(f)}}$ coherence between horizontal and vertical velocity

$c_r(f)$ $\sqrt{\frac{E_{\eta\eta,ref}(f)}{E_{\eta\eta,in}(f)}}$ reflection coefficient

Discussion of the results

The incoming spectra have a similar shape as the spectra of the wave gauges. In most cases, the incoming spectra is a bit smaller than the spectra of the wave gauges. The spreading of the incoming spectra is generally small. Differences between the incoming spectra and the spectra of the wave gauges are probably caused by the shortcomings of the linear wave theory and inaccuracies in the estimated water depth, which is applied in the computations of the incoming spectra.

The spreading of the reflected spectra is different for the various locations. Because the energy density of reflected spectra is about 50-100 times less than the incoming spectra, the computation of the reflected spectra is quite sensible to inaccuracies. Although some of the results should not be trusted (1A, 22.05 m; 1C, 21.35 m) there are many results, which give a good impression of the reflection of wave energy.

It is a disadvantage of the applied method that the derivation of the reflection of low frequency waves is quite inaccurate. In this frequency domain, the coherence between the horizontal and vertical velocity is generally quite low. Even when results are shown because the coherence exceeds 0.85, the results should be treated with caution (1B, 20.90 m; 1C, 22.37 m). This is a pity, because especially the low frequency waves reflect at the beach.

The reflection coefficients, presented in Table 3.2, are rather high compared with the normally assumed reflection coefficient of about 0.05.

The Figures 3.19, 3.20 and 3.21 show that the reflection coefficient is quite sensible to the coherence between the horizontal and vertical velocity measurements.

### 3.6 Wave Energy Flux

Figures 3.22, 3.23 and 3.24 show the wave energy flux for the three wave conditions. The wave energy flux is calculated by multiplying the wave group celerity with the energy of the waves ($m_{0,h}$; low frequency energy is not included). It should be considered that the energy of waves consists partly of reflected waves. This is not taken into account in the computations.

The wave energy flux of the reflected waves is shown in the Figures 3.25, 3.26 and 3.27. The wave group celerity of the reflected waves is assumed equal to the negative value of the wave group celerity of the incoming waves. The wave energy

is taken from the frequency interval between 0.4 Hz and 1 Hz.


The data representing the wave energy flux of the measured waves are available in the Files **FWE_TAB.##**. The Files **FRE_TAB.##** contain the data of the reflected wave energy flux.

Discussion of the results

The wave energy flux, presented in the Figures 3.22, 3.23 and 3.24 shows some spreading in the region outside the breaker zone, which is apparently caused by the spreading of the wave group celerity. Within the breaker zone the results are well in line with each other.

The gradient of the wave energy flux is generally zero or negative, which corresponds with the idea of dissipation of wave energy. (Positive gradients caused by spreading are not taken into account.) Exceptions are the beginning of the foreshore for the Wave Conditions 1A and 1B. The positive gradient of the wave energy flux, which is present over a very short distance is probably caused by the positive gradient of the wave group celerity at this location.

The reflected wave energy flux shows a lot of spreading of the results, especially onshore of the breaker bar. Therefore, conclusions should be drawn with caution. Following the reflected wave energy flux in offshore direction, there is a sharp increase in the surf zone trough. This indicates that much reflection happens in this region. Just onshore of the breaker bar the flux reaches a peak, which decreases at the breaker bar. Here there is apparently dissipation of the reflected wave energy. Outside the breaker bar, the reflected wave energy flux becomes uniform.

## 3.7 Analysis of Wave Breaking

The breaking of waves in the flume is analysed with the measurements of the surface elevation and the video measurements. These measurements are coupled,

which enables the study of the wave breaking in combination with the evolution of the individual waves.

First the program WAVES calculates a number of parameters from the measured surface elevations. For the Wave Conditions 1A and 1C, this signal is a band-pass filtered. The measurements are taken at an interval of 1 m for the section 0 - 15 m and ca. 0.5 m for the section 15 - 28.5 m. The following parameters are calculated:

| | |
|---|---|
| $t_c$ | passing time of crest |
| $a_c$ | crest amplitude |
| $t_t$ | passing time of trough (which is the trough before the crest) |
| $a_t$ | trough amplitude |
| $t_z$ | passing time of upward zero-crossing (which is the zero-crossing before the crest) |
| $H_u$ | upward zero-crossing wave height |
| $T_u$ | upward zero-crossing wave period |

All parameters are put into a spreadsheet file (Microsoft Excel). Every individual wave has its parameters distributed over separated worksheets but similar addresses of the cells. Every column contains the results of one location (Figure 3.28).

The passing time of the crests are sorted so the patterns of the individual waves can be read in the rows of the worksheet (Figure 3.28). This enables the study at the development of the various parameters of each individual wave.

For many waves, it is not possible to follow the wave through the whole flume. Often, two or more waves are united to one wave, which starts with more than one maximum. This behaviour sometimes complicates the analysis of wave breaking.

Now the patterns of the individual waves are determined, it is possible to follow them on the video recordings. For every wave condition, there are six video

recordings, each covering 5 m of the wave flume. Every recording has five wave cycles, from which the last four cycles are used in the analysis.

The video recordings are related to the passing time of a crest at a certain location. From the spreadsheet file this passing time is extracted and then the corresponding wave is searched at the video recording. Then, the wave is examined for breaking or non-breaking. When a wave breaks, the length of the roller is estimated too [Figure 3.28]. All information is put into the spreadsheet file.

The estimate of the length of the roller is based on the 'white' turbulence which can be noticed when a wave breaks. Because such an estimate is not very accurate, the length of the roller is given in decimetres. All the work has been done by one single observer, so there are no inaccuracies caused by any different interpretation of the video recordings.


The spreadsheet Files are available with the names **WAV_BR##.XLS**. In this Files the following worksheets are available:

| | |
|---|---|
| T-CREST($t_c$) | passing time of crest |
| CREST ($a_c$) | crest amplitude |
| T-TROUGH ($t_t$) | passing time of trough |
| TROUGH ($a_t$) | trough amplitude |
| T-WAVES ($t_z$) | passing time of upward zero-crossing |
| WAVES ($H_u$) | upward zero-crossing wave height |
| PERIOD ($T_u$) | upward zero-crossing wave period |
| BREAKING ($N_Q$) | number of cycles that wave breaks (max = 4) |
| ROLLER ($r_m$) | mean length of roller |
| Q*i* (Q) | breaking (1) or non-breaking (0) for cycle *i* |
| R*i* (r) | length of roller for cycle *i* |

Because the video recordings cover sections of 5 m and the beginning of each section joins with the previous section, the positions 5 m, 10 m, 15 m, 20 m and

25 m are examined twice.

The wave celerity, which is analysed in Section 3.4, can also be computed by taking the first derivative of the wave patterns. Figures 3.29, 3.30 and 3.31 show the celerity of the crest, the trough and the zero-crossing for all wave conditions. The results can also be found in the Files **CELW_TAB.****. These files contain the following parameters:

| | |
|---|---|
| $c_c$ | celerity of wave crest |
| $c_t$ | celerity of wave trough |
| $c_z$ | celerity of zero-crossing (upward) |

Another interesting parameter is the vertical asymmetry of the waves. This asymmetry $\zeta$ is defined as:

$$\zeta = \frac{t_c - t_t}{T}$$

The vertical asymmetry is presented in the Figures 3.32, 3.33 and 3.34. The Files **ASYM_TAB.**** contain this parameter as:

| | |
|---|---|
| zeta ($\zeta$) | vertical asymmetry of waves |

The breaking behaviour of the waves is available in the Files **BRW_TAB.****. This behaviour is also illustrated in the Figures 3.35, 3.36 and 3.37. These files have the following parameters:

| | |
|---|---|
| Q | fraction of breaking waves |
| r | average length of roller (all waves) |
| $r_Q$ | average length of roller (breaking waves only) |

The Files **PH_X####.**** contain the distribution of the wave heights at the various locations. Distinction is made between the non-breaking waves and the breaking waves. This information is also presented in the Figures 3.38, 3.39 and 3.40.


The statistical information of these wave height distributions in the wave flume is given in the Files **PH_TAB.###** (mean and standard deviation). This information is also given in the Figures 3.41, 3.42 and 3.43.

Discussion of the results

Minor differences exist between the wave celerity computed with cross-correlation and the wave celerity derived from the pattern. The biggest differences occur outside the breaker region.

At certain locations the celerity of the crest differs from the celerity of the trough, which results in a change of the asymmetry of the waves:

$$\frac{d\zeta}{dx} = \frac{1}{c_c T} - \frac{1}{c_t T}$$

Outside the breaker region the waves are almost vertically symmetric; at the breaker bar the crest moves faster than the trough and the waves become asymmetric. At the end of the surf zone trough the symmetry restores, but at the foreshore the waves become more asymmetric again.

The waves of Wave Condition 1B show more asymmetry than the waves of the Wave Conditions 1A and 1C. A possible effect reason is that the superharmonic frequencies of Wave Condition 1A and 1C are filtered before the analysis.

The breaker characteristics shown in the Figures 3.35, 3.36 and 3.37 look quite reliable. Results for adjacent locations are good in line with each other and although the overlap between two sections with different video recordings is visible, the disturbances are small. Since the observations are made over four cycles of irregular waves it is possible to analyse the results statistically. From the Figures 3.35, 3.36 and 3.37 it appears that the spreading of the results is low, especially for r and Q; when Q is low there is some spreading in the results of $r_Q$.

The figures give an accurate overview of the wave breaking in the flume. The distance between the measurements is small enough to follow all changes of the breaking behaviour.

Waves break at every location in the flume for Wave Condition 1B. For Wave Condition 1A wave breaking starts shortly onshore of the toe of the profile; for Wave Condition 1C waves break only just offshore of the breaker bar.

The breaker characteristics of the Wave Conditions 1A and 1B are quite comparable. Wave breaking reaches a peak just onshore of the breaker bar and decreases further in the surf zone trough. At the foreshore the breaking increases again. Wave breaking onshore of the breaker bar is more intense for Wave Condition 1B, but Wave Condition 1A is most intense at the foreshore.

Remarkable is the strong increase and decrease of $r_Q$ offshore of the breaker bar during Wave Condition 1A. This phenomenon is less visible for Wave Condition 1B. Further it appears that $r_Q$ has comparable sizes for all wave conditions.

It is interesting to relate the observed breaking characteristics with other phenomena like:

- wave energy flux
- wave set-up
- wave asymmetry

There is an apparent relation between the breaking of waves and the wave energy flux. Breaking of waves is one of the most important causes of the dissipation of wave energy. It is fascinating to see the close relation between the gradient of the wave energy flux and a breaking characteristic like r.

When there is almost no wave breaking (Wave Condition 1A and 1C), the gradient of the wave energy flux is about zero. For Wave Condition 1B, where wave breaking occurs through the whole flume, the gradient of the wave energy flux is

always negative.

Just onshore of the breaker bar there is a large decrease of the wave energy flux which corresponds to the heavy breaking observed from the video recordings. Further in the surf zone trough the gradient of the wave energy flux becomes less steep, which corresponds with the decrease of breaking. For Wave Condition 1C there is an almost uniform breaking of the waves through the whole surf zone trough. This corresponds with an almost uniform gradient of the wave energy flux.

At the foreshore the wave breaking intensifies again for all wave conditions. Again this corresponds with a larger decrease of the wave energy flux.

Since the wave set-up is related to the radiation stress and thus the wave energy, there is also a relation between wave breaking and wave set-up. Indeed the discontinuities of the gradient of the wave set-up corresponds with sharp increases of the breaking of waves.

It is interesting to see a relation between wave breaking and wave asymmetry. Wave asymmetry has an impact on the steepness of the wave front, which is an important parameter for wave breaking.

The wave height distribution of breaking and non-breaking waves is one of the results of the coupling of the wave height measurements with the video recordings [Figures 3.38, 3.39 and 3.40]. The results look trustworthily, because it appears that the probability of wave breaking is highest for the biggest waves.

Also the statistical analysis of the distribution of the wave heights gives useful information. It is possible to divide the wave flume in four sections:

- In the region offshore from the breaker bar where most of the waves do not break, there is a lot of spreading of the statistical results. The mean of the breaking waves is quite uniform. Apparently the waves are breaking because of exceedence of the critical wave steepness.

- At a certain position, the water depth gets an influence on the height of breaking waves. This position differs for each wave condition (Wave Condition 1A: 15 m; Wave Condition 1B: 13 m; Wave Condition 1C: 17 m). Onshore from this position the mean height of the breaking waves decreases linearly until the top of the breaker bar.
- Just onshore of the breaker bar the mean height of the breaking waves decreases with a big jump. Further onshore the decrease of the mean continues moderately, probably because of the dissipation of the wave by the roller. The mean value of the non-breaking waves increases in this region.
- At the beginning of the foreshore the mean height of the breaking waves again decreases with a jump. At the foreshore there is a strong decrease of the mean wave height.

The standard deviation of the breaking wave height is less than the standard deviation of the non-breaking wave height for most of the locations. In the first region there is a lot of spacial spreading in the standard deviation of the breaking waves. In the other regions the standard deviation at one location is more in line with the adjacent locations.

## REFERENCES


Boers, M. and J. van de Graaff. 1995. Mass and Momentum Balance in the Surf Zone. *Coastal Dynamics '95*, Gdansk, pp. 257-268

Boers, M. 1996. Simulation of a Surf Zone with a Barred Beach; Report 2: Velocities and Shear Stresses. *Communications on Hydraulic and Geotechnical Engineering*, No. 96-6, Delft University of Technology.

Delft Hydraulics. 1992(A). AUKE/pc; Control Signals for Wave Makers; Part 2 Program STIR.

Delft Hydraulics. 1992(B). AUKE/pc; Process Document; Processing of Series.

Hughes, S.A. 1993. Laboratory Wave Reflection Analysis using co-located Gages. *Coastal Engineering*, Vol. 20, pp. 223-247.

Klopman, G and P.J. van Leeuwen. 1990. An Efficient Method for the Reproduction of Non-linear Random Waves. *Proc. 22nd Int. Conf. Coastal Engng*, Delft, The Netherlands, pp. 478-488.

Klopman, G. 1994. Vertical Structure of the Flow due to Waves and Currents; Laser-Doppler Flow Measurements for Waves following or opposing a Current. *Delft Hydraulics*, Progress Report H 840.30 Part II.

Roelvink, J.A. and A.J.H.M. Reniers. 1995. LIP 11D Delta Flume Experiments. A dataset for profile model validation. *Delft Hydraulics*, Report H 2130.

## ENCLOSURE A DATAFILES

Enclosure A gives a list of the available files with results from the analysis of the measurements described in the present report. The contents of these files is described in the Chapters 2 and 3.

The **profile** is given in the file:
PROFILE.TAB

The **energy density spectra** of the measurements of the surface elevation are given in files:

| | | | | | |
|---|---|---|---|---|---|
| SP_X0000.1A | SP_X0000.1B | SP_X0000.1C | SP_X0100.1A | SP_X0100.1B | SP_X0100.1C |
| SP_X0200.1A | SP_X0200.1B | SP_X0200.1C | SP_X0300.1A | SP_X0300.1B | SP_X0300.1C |
| SP_X0400.1A | SP_X0400.1B | SP_X0400.1C | SP_X0500.1A | SP_X0500.1B | SP_X0500.1C |
| SP_X0600.1A | SP_X0600.1B | SP_X0600.1C | SP_X0700.1A | SP_X0700.1B | SP_X0700.1C |
| SP_X0800.1A | SP_X0800.1B | SP_X0800.1C | SP_X0900.1A | SP_X0900.1B | SP_X0900.1C |
| SP_X1000.1A | SP_X1000.1B | SP_X1000.1C | SP_X1100.1A | SP_X1100.1B | SP_X1100.1C |
| SP_X1200.1A | SP_X1200.1B | SP_X1200.1C | SP_X1300.1A | SP_X1300.1B | SP_X1300.1C |
| SP_X1400.1A | SP_X1400.1B | SP_X1400.1C | SP_X1500.1A | SP_X1500.1B | SP_X1500.1C |
| SP_X1550.1A | SP_X1550.1B | SP_X1550.1C | SP_X1600.1A | SP_X1600.1B | SP_X1600.1C |
| SP_X1650.1A | SP_X1650.1B | SP_X1650.1C | SP_X1700.1A | SP_X1700.1B | SP_X1700.1C |
| SP_X1750.1A | SP_X1750.1B | SP_X1750.1C | SP_X1800.1A | SP_X1800.1B | SP_X1800.1C |
| SP_X1850.1A | SP_X1850.1B | SP_X1850.1C | SP_X1900.1A | SP_X1900.1B | SP_X1900.1C |
| SP_X1920.1A | SP_X1920.1B | SP_X1920.1C | SP_X1940.1A | SP_X1940.1B | SP_X1940.1C |
| SP_X1960.1A | SP_X1960.1B | SP_X1960.1C | SP_X1980.1A | SP_X1980.1B | SP_X1980.1C |
| SP_X2000.1A | SP_X2000.1B | SP_X2000.1C | SP_X2020.1A | SP_X2020.1B | SP_X2020.1C |
| SP_X2040.1A | SP_X2040.1B | SP_X2040.1C | SP_X2060.1A | SP_X2060.1B | SP_X2060.1C |
| SP_X2080.1A | SP_X2080.1B | SP_X2080.1C | SP_X2100.1A | SP_X2100.1B | SP_X2100.1C |
| SP_X2120.1A | SP_X2120.1B | SP_X2120.1C | SP_X2140.1A | SP_X2140.1B | SP_X2140.1C |
| SP_X2160.1A | SP_X2160.1B | SP_X2160.1C | SP_X2180.1A | SP_X2180.1B | SP_X2180.1C |
| SP_X2200.1A | SP_X2200.1B | SP_X2200.1C | SP_X2220.1A | SP_X2220.1B | SP_X2220.1C |
| SP_X2240.1A | SP_X2240.1B | SP_X2240.1C | SP_X2260.1A | SP_X2260.1B | SP_X2260.1C |
| SP_X2280.1A | SP_X2280.1B | SP_X2280.1C | SP_X2300.1A | SP_X2300.1B | SP_X2300.1C |
| SP_X2320.1A | SP_X2320.1B | SP_X2320.1C | SP_X2340.1A | SP_X2340.1B | SP_X2340.1C |
| SP_X2360.1A | SP_X2360.1B | SP_X2360.1C | SP_X2380.1A | SP_X2380.1B | SP_X2380.1C |
| SP_X2400.1A | SP_X2400.1B | SP_X2400.1C | SP_X2420.1A | SP_X2420.1B | SP_X2420.1C |
| SP_X2440.1A | SP_X2440.1B | SP_X2440.1C | SP_X2460.1A | SP_X2460.1B | SP_X2460.1C |
| SP_X2480.1A | SP_X2480.1B | SP_X2480.1C | SP_X2500.1A | SP_X2500.1B | SP_X2500.1C |
| SP_X2520.1A | SP_X2520.1B | SP_X2520.1C | SP_X2540.1A | SP_X2540.1B | SP_X2540.1C |
| SP_X2560.1A | SP_X2560.1B | SP_X2560.1C | SP_X2580.1A | SP_X2580.1B | SP_X2580.1C |

| | | | | | |
|---|---|---|---|---|---|
| SP_X2600.1A | SP_X2600.1B | SP_X2600.1C | SP_X2620.1A | SP_X2620.1B | SP_X2620.1C |
| SP_X2640.1A | SP_X2640.1B | SP_X2640.1C | SP_X2656.1A | SP_X2656.1B | SP_X2656.1C |
| SP_X2680.1A | SP_X2680.1B | SP_X2680.1C | SP_X2700.1A | SP_X2700.1B | SP_X2700.1C |
| SP_X2725.1A | SP_X2725.1B | SP_X2725.1C | SP_X2750.1A | SP_X2750.1B | SP_X2750.1C |
| SP_X2775.1A | SP_X2775.1B | SP_X2775.1C | SP_X2800.1A | SP_X2800.1B | SP_X2800.1C |
| SP_X2825.1A | SP_X2825.1B | SP_X2825.1C | SP_X2850.1A | SP_X2850.1B | SP_X2850.1C |

These files give information about the location of the measurements, the testrun(s) and the measuring device(s). Further, the lowest frequency ($f_0$), the highest frequency ($f_N$) and the frequency interval (df) are given. The energy density spectum is given as $E(f_i)$ $i \in \{0, N\}$, where $f_i = i * df$. The files sp_x1300.## have a frequency interval different from all other files!

**Spectral parameters** are given in the files:
SPEC_TAB.1A SPEC_TAB.1B SPEC_TAB.1C

The **energy content** of the low frequency and high frequency waves and the corresponding **significant wave heights** are given in the files:
HM0_TAB.1A HM0_TAB.1B HM0_TAB.1C

**Statistical information** about the surface elavation is given in the files:
STAT_TAB.1A STAT_TAB.1B STAT_TAB.1C

Information derived from the **zero-crossings and extreme values** is given in the files:
WAVE_TAB.1A WAVE_TAB.1B WAVE_TAB.1C

**Wave celerity and wave group celerity** are given in the files:
CELC_TAB.1A CELC_TAB.1B CELC_TAB.1C

Information about the **incoming and reflected spectra** is given in the files:

| | | | | | |
|---|---|---|---|---|---|
| RF_X1437.1A | RF_X0810.1B | RF_X0810.1C | RF_X1700.1A | RF_X1437.1B | RF_X1437.1C |
| RF_X1880.1A | RF_X1700.1B | RF_X1700.1C | RF_X1967.1A | RF_X1880.1B | RF_X1880.1C |
| RF_X2037.1A | RF_X1967.1B | RF_X1967.1C | RF_X2071.1A | RF_X2037.1B | RF_X2037.1C |
| RF_X2090.1A | RF_X2090.1B | RF_X2090.1C | RF_X2108.1A | RF_X2135.1B | RF_X2135.1C |
| RF_X2205.1A | RF_X2239.1B | RF_X2237.1C | RF_X2235.1A | RF_X2395.1B | RF_X2395.1C |

RF_X2395.1A RF_X2475.1B RF_X2475.1C RF_X2475.1A RF_X2556.1B RF_X2703.1C

The **wave energy flux** is given in the files:
FWE_TAB.1A FWE_TAB.1B FWE_TAB.1C

The **flux of the reflected wave energy** is given in the files:
FRE_TAB.1A FRE_TAB.1B FRE_TAB.1C

The **patterns of the waves** with information about **wave breaking and other wave parameters** are given in the EXCEL-files:
WAV_BR1A.XLS WAV_BR1B.XLS WAV_BR1C.XLS

The **celerity of crest, trough and zero-crossing** is given in the files:
CELW_TAB.1A CELW_TAB.1B CELW_TAB.1C

The **vertical asymmetry** of waves is given in the files:
ASYM_TAB.1A ASYM_TAB.1B ASYM_TAB.1C

**Breaking parameters** are given in the files:
BRW_TAB.1A BRW_TAB.1B BRW_TAB.1C

The **probability distribution of breaking and non-breaking waves** is given in the files:
PH_XTAB.1A PH_XTAB.1B PH_XTAB.1C

**Statistical information** about the probability distribution of breaking and non-breaking waves is given in the files:
PH_TAB.1A PH_TAB.1B PH_TAB.1C

## ENCLOSURE B COORDINATES OF WAVE REFLECTION

Enclosure B gives the coordinates of the velocity measurements used to calculate the reflection of wave energy. The location of the nearest wave gauge is given too.

| $x_{ldv}$ | $z_{1,ldv}$ | $z_{2,ldv}$ | $z_{3,ldv}$ | $x_{wg}$ |
|---|---|---|---|---|
| 14.37 | 0.22 | 0.23 | 0.24 | 14.00 |
| 17.00 | 0.15 | 0.18 | 0.21 | 17.00 |
| 18.80 | 0.12 | 0.15 | 0.18 | 19.00 |
| 19.67 | 0.09 | 0.12 | 0.14 | 19.60 |
| 20.37 | 0.08 | 0.10 | 0.12 | 20.40 |
| 20.71 | 0.05 | 0.07 | 0.09 | 20.80 |
| 20.90 | 0.07 | * | * | 21.00 |
| 21.08 | 0.04 | 0.05 | 0.06 | 21.00 |
| 22.05 | 0.03 | 0.05 | * | 22.00 |
| 22.35 | 0.11 | * | * | 22.40 |
| 23.95 | 0.09 | 0.105 | 0.12 | 24.00 |
| 24.75 | 0.05 | 0.06 | 0.07 | 24.80 |

*Table B.1* Coordinates of velocity measurements and wave gauges (Condition 1A)

| $x_{ldv}$ | $z_{1,ldv}$ | $z_{2,ldv}$ | $z_{3,ldv}$ | $x_{wg}$ |
|---|---|---|---|---|
| 8.10 | 0.31 | 0.34 | 0.37 | 8.00 |
| 14.37 | 0.16 | 0.19 | 0.22 | 14.00 |
| 17.00 | 0.14 | 0.17 | 0.20 | 17.00 |
| 18.80 | 0.14 | 0.17 | 0.19 | 19.00 |
| 19.67 | 0.11 | 0.13 | 0.15 | 19.60 |
| 20.37 | 0.10 | 0.12 | * | 20.40 |
| 20.90 | 0.08 | 0.09 | 0.10 | 20.80 |
| 21.35 | 0.105 | 0.12 | 0.13 | 21.40 |
| 22.39 | 0.12 | 0.13 | 0.14 | 22.40 |
| 23.95 | 0.09 | 0.105 | 0.115 | 24.00 |
| 24.75 | 0.05 | 0.06 | 0.07 | 24.80 |
| 25.56 | 0.05 | 0.06 | 0.07 | 25.60 |

*Table B.2* Coordinates of velocity measurements and wave gauges (Condition 1B)

| $x_{ldv}$ | $z_{1,ldv}$ | $z_{2,ldv}$ | $z_{3,ldv}$ | $x_{wg}$ |
|---|---|---|---|---|
| 8.10 | 0.28 | 0.31 | 0.34 | 8.00 |
| 14.37 | 0.17 | 0.20 | 0.23 | 14.00 |
| 17.00 | 0.07 | 0.12 | 0.18 | 17.00 |
| 18.80 | 0.165 | 0.18 | 0.195 | 19.00 |
| 19.67 | 0.12 | 0.135 | 0.15 | 19.60 |
| 20.37 | 0.09 | 0.105 | 0.12 | 20.40 |
| 20.90 | 0.075 | 0.09 | * | 20.80 |
| 21.35 | 0.075 | 0.09 | 0.105 | 21.40 |
| 22.37 | 0.09 | 0.105 | 0.12 | 22.40 |
| 23.95 | 0.09 | 0.105 | 0.12 | 24.00 |
| 24.75 | 0.045 | 0.06 | 0.08 | 24.80 |
| 27.03 | 0.035 | 0.04 | * | 27.00 |

*Table B.3* Coordinates of velocity measurements and wave gauges (Condition 1C)

## FIGURES

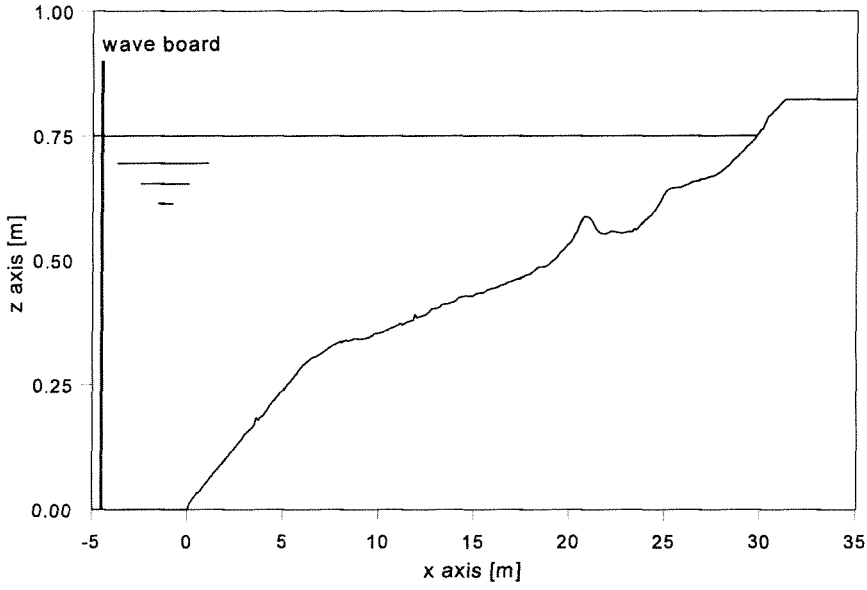


*Figure 2.1* Beach Profile in Wave Flume with the Coordinate System

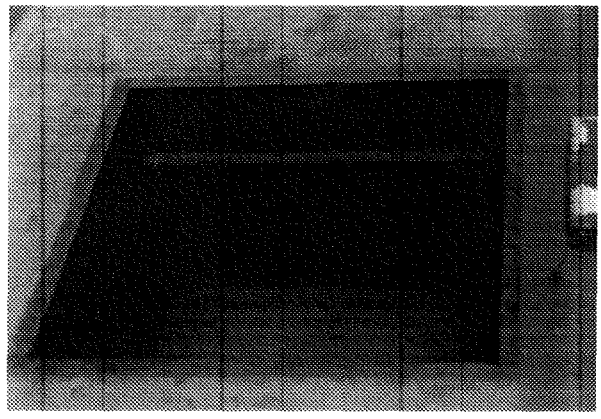

*Figure 2.2* Box in Profile for Shear Stress Plate

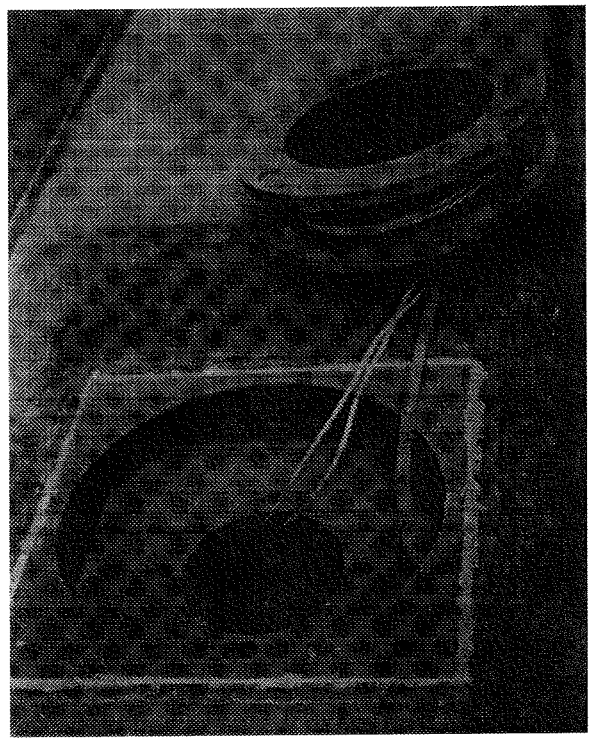

*Figure 2.3* Installation of Shear Stress Plate

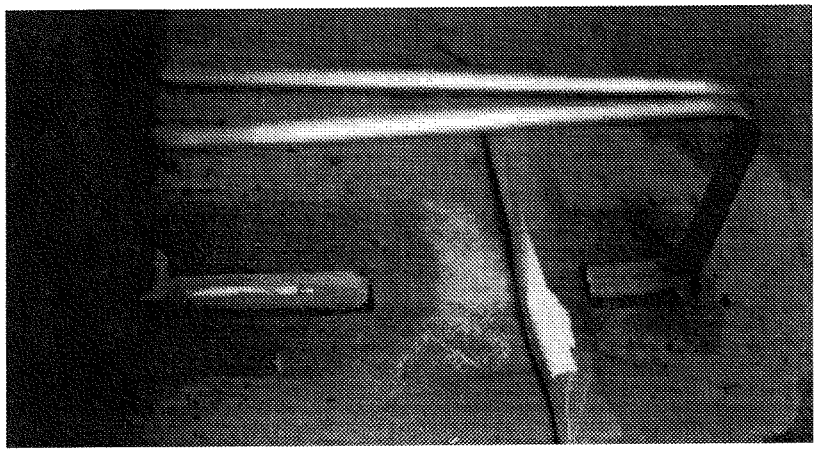

*Figure 2.4* PVC Matrix for LDV

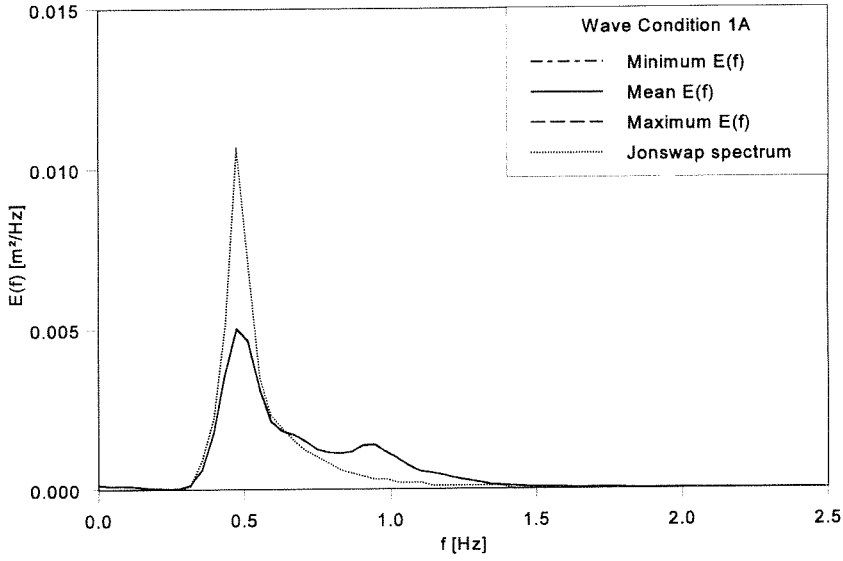


*Figure 2.5* Energy Spectrum at x = 0 m; Wave Condition 1A

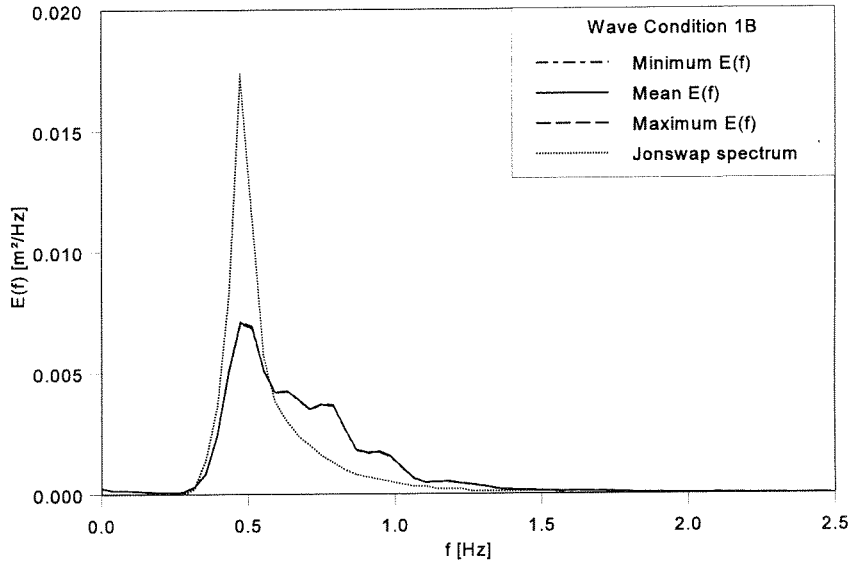


*Figure 2.6* Energy Spectrum at x = 0 m; Wave Condition 1B

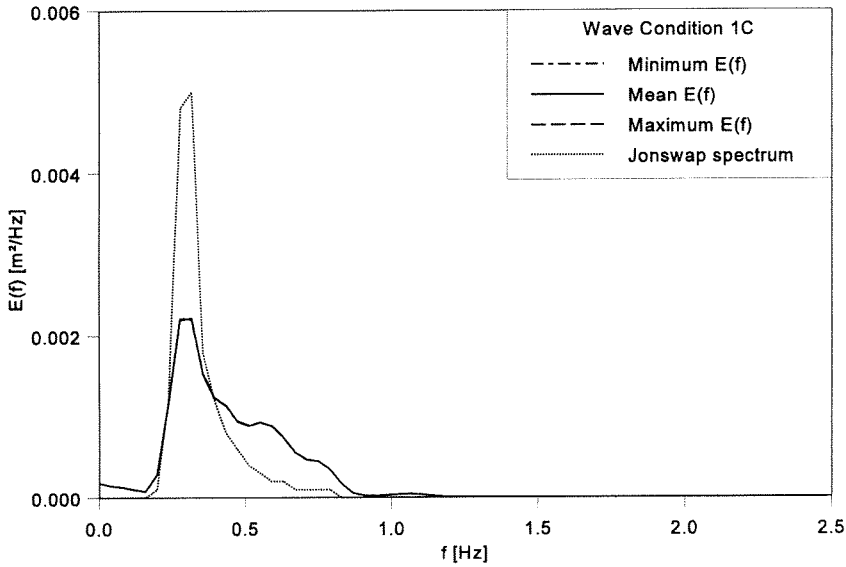


*Figure 2.7* Energy Spectrum at x = 0 m; Wave Condition 1C

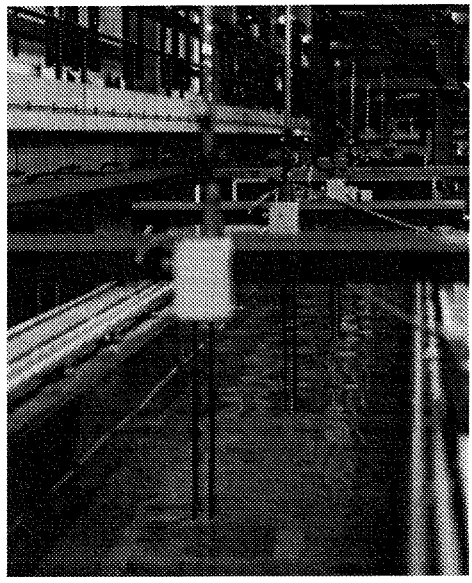

*Figure 2.8* Wave Gauges

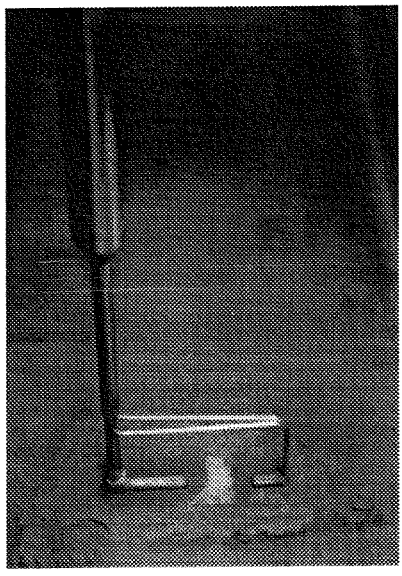

*Figure 2.9* LDV Instrument (Detail)

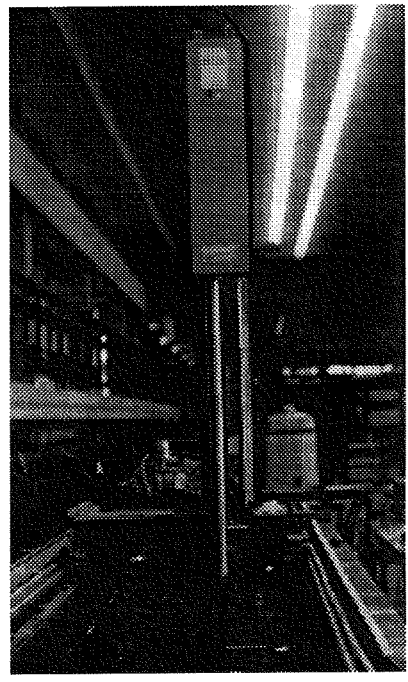

*Figure 2.10* LDV Instrument

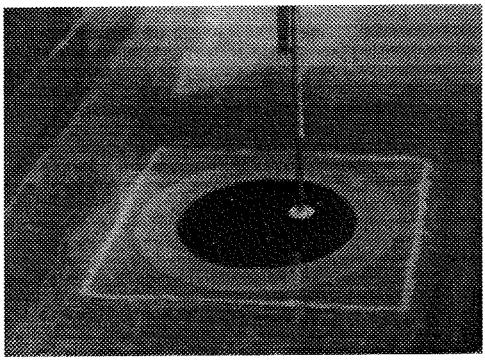

*Figure 2.11* EMF with Shear Stress Plate

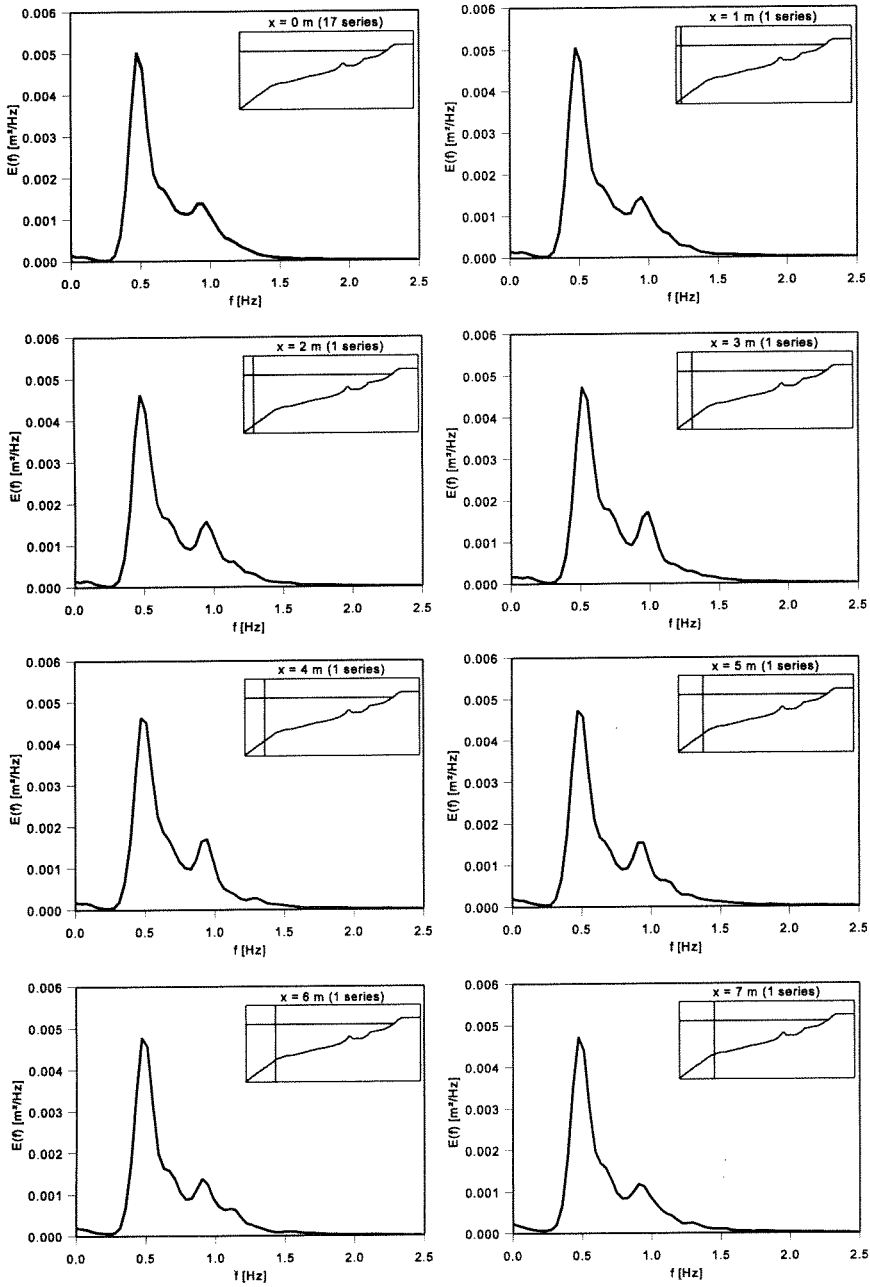


*Figure 3.1a* Energy Density Spectrum of Surface Elevation (1A; x = 0 - 7 m)

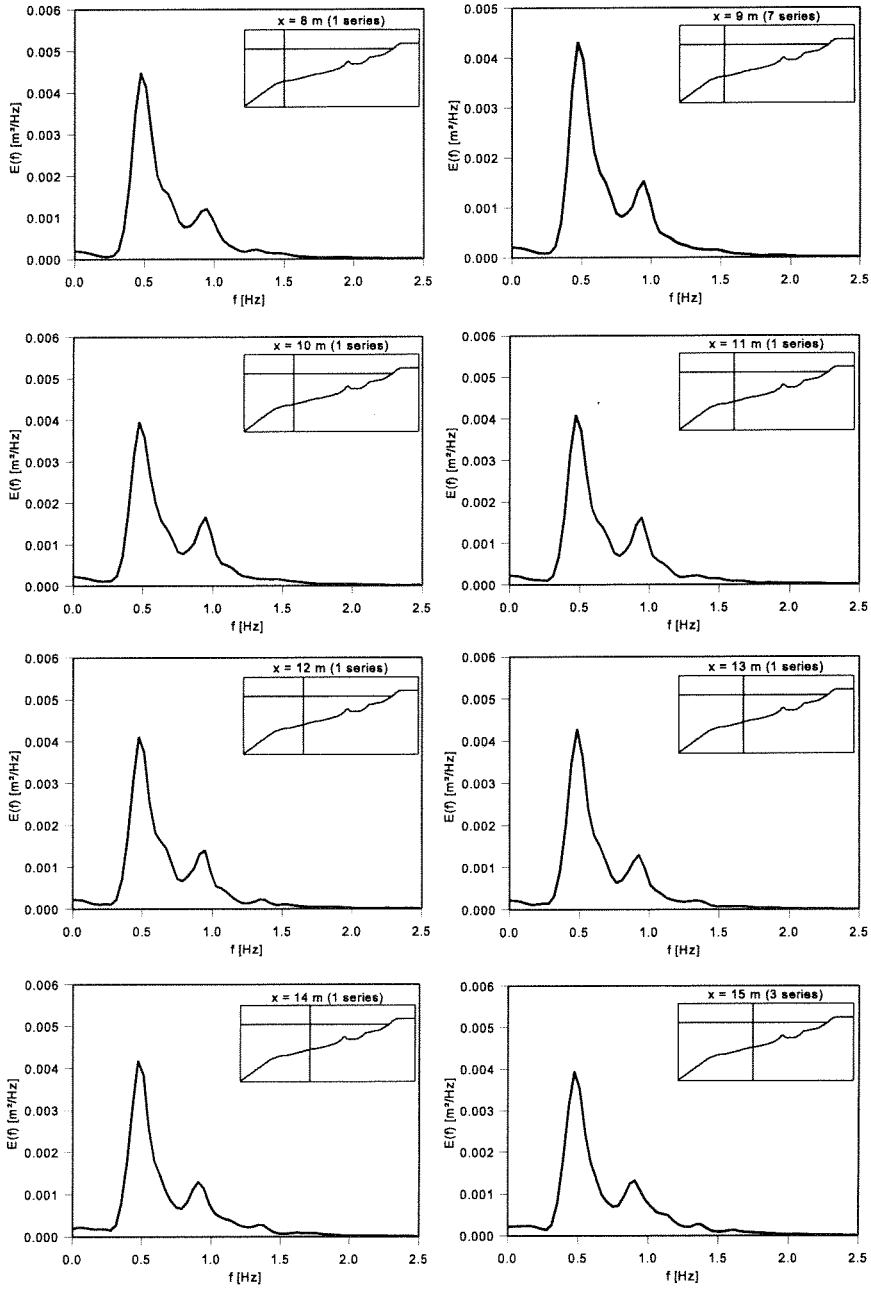


*Figure 3.1b* Energy Density Spectrum of Surface Elevation (1A; x = 8 - 15 m)

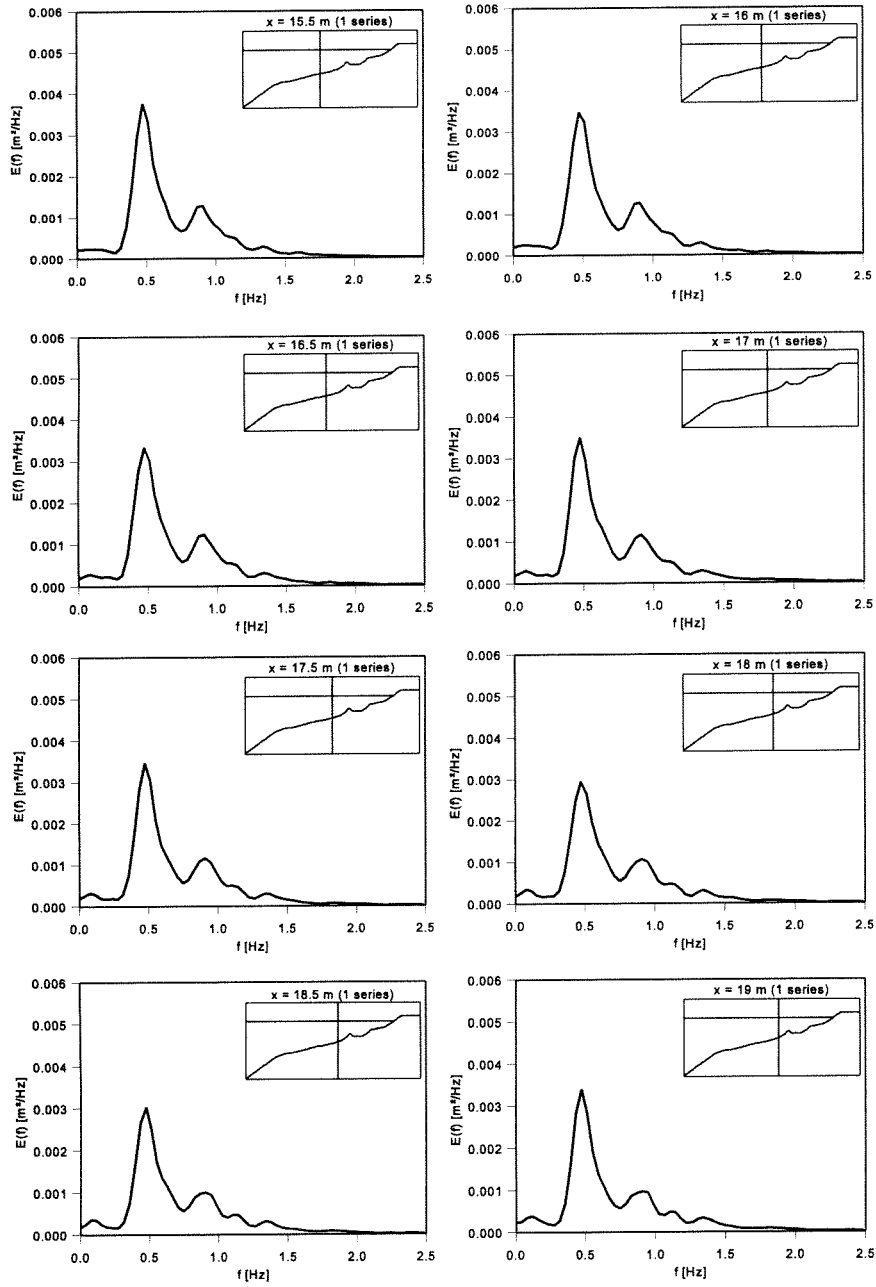


*Figure 3.1c* Energy Density Spectrum of Surface Elevation (1A; x = 15.5 - 19 m)

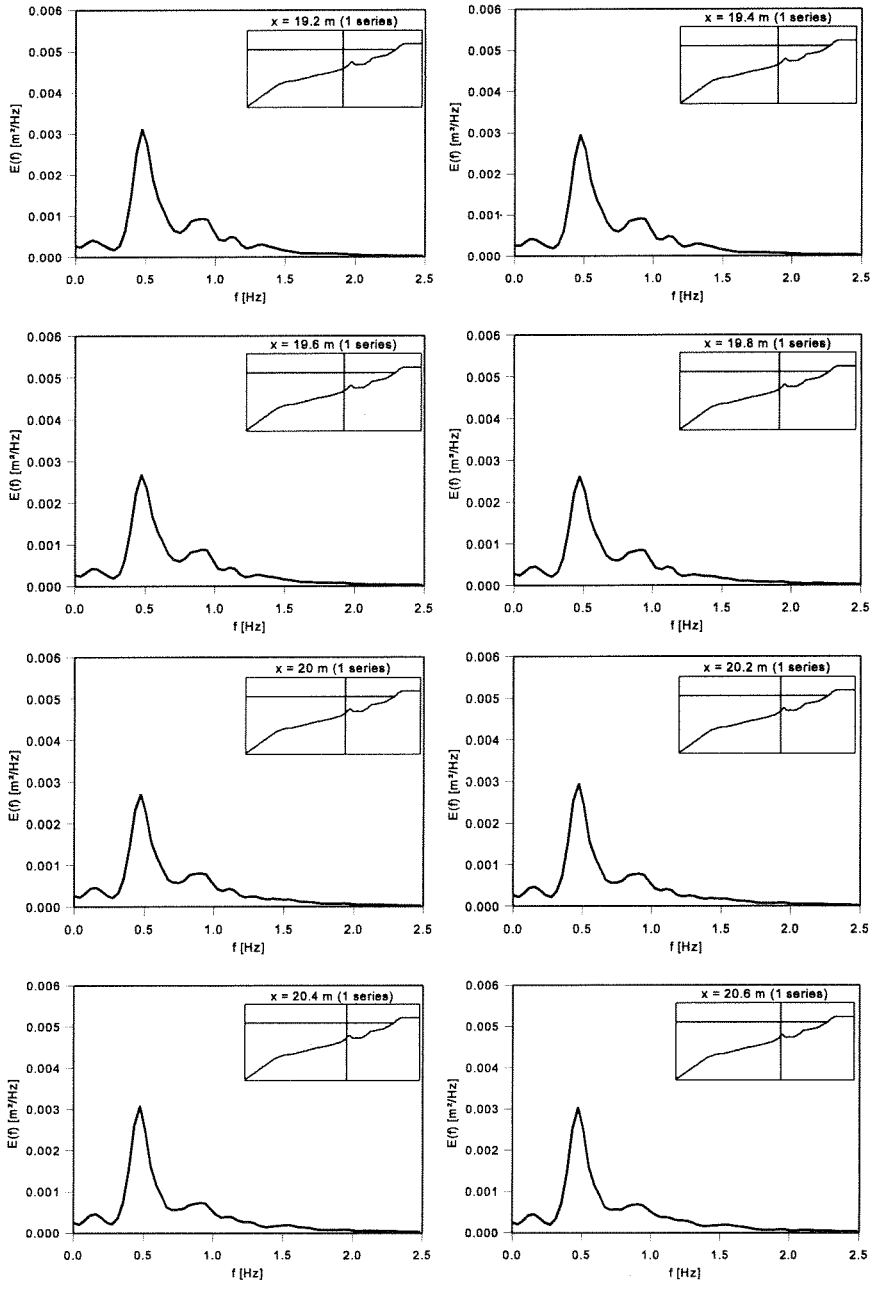


*Figure 3.1d* Energy Density Spectrum of Surface Elevation (1A; x = 19.2 - 20.6 m)

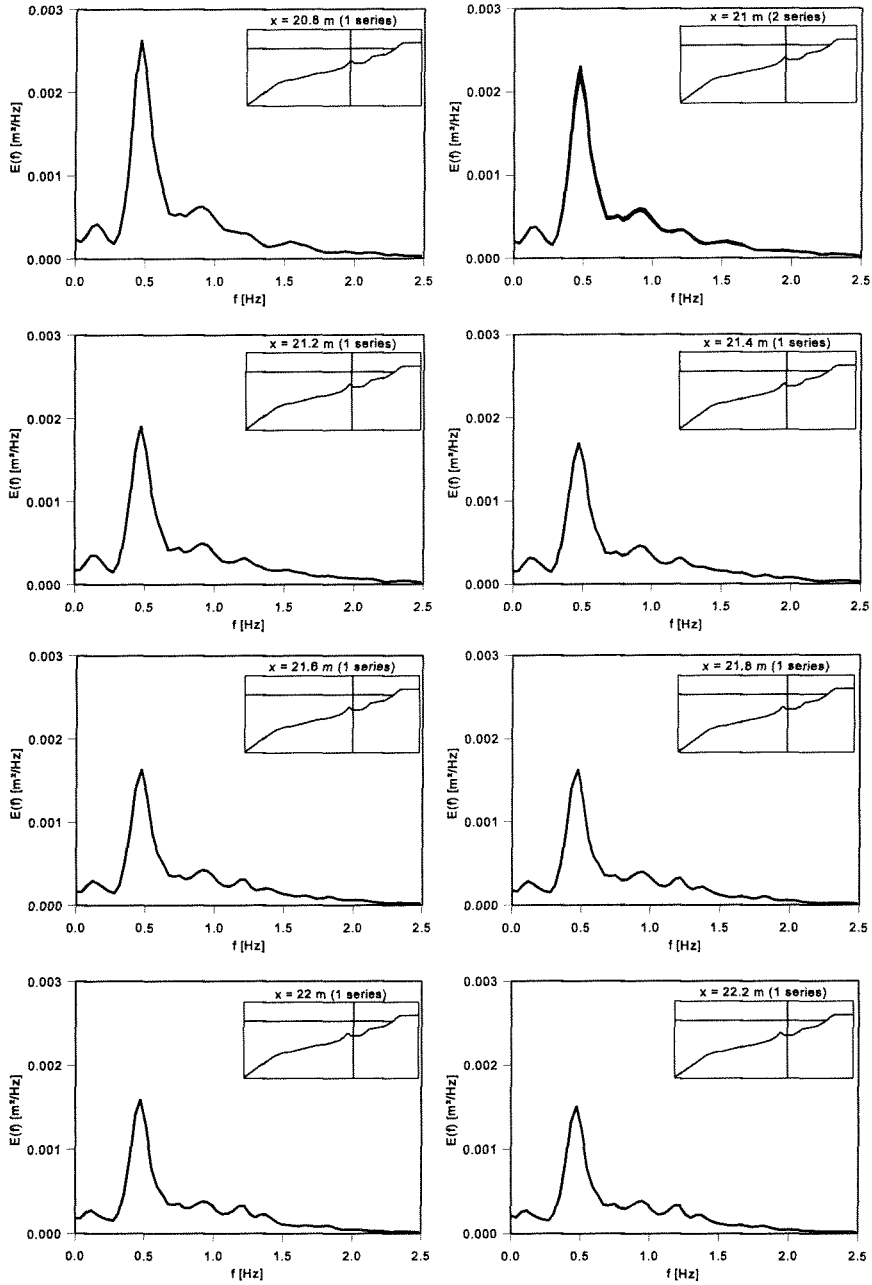


*Figure 3.1e* Energy Density Spectrum of Surface Elevation (1A; x = 20.8 - 22.2 m)

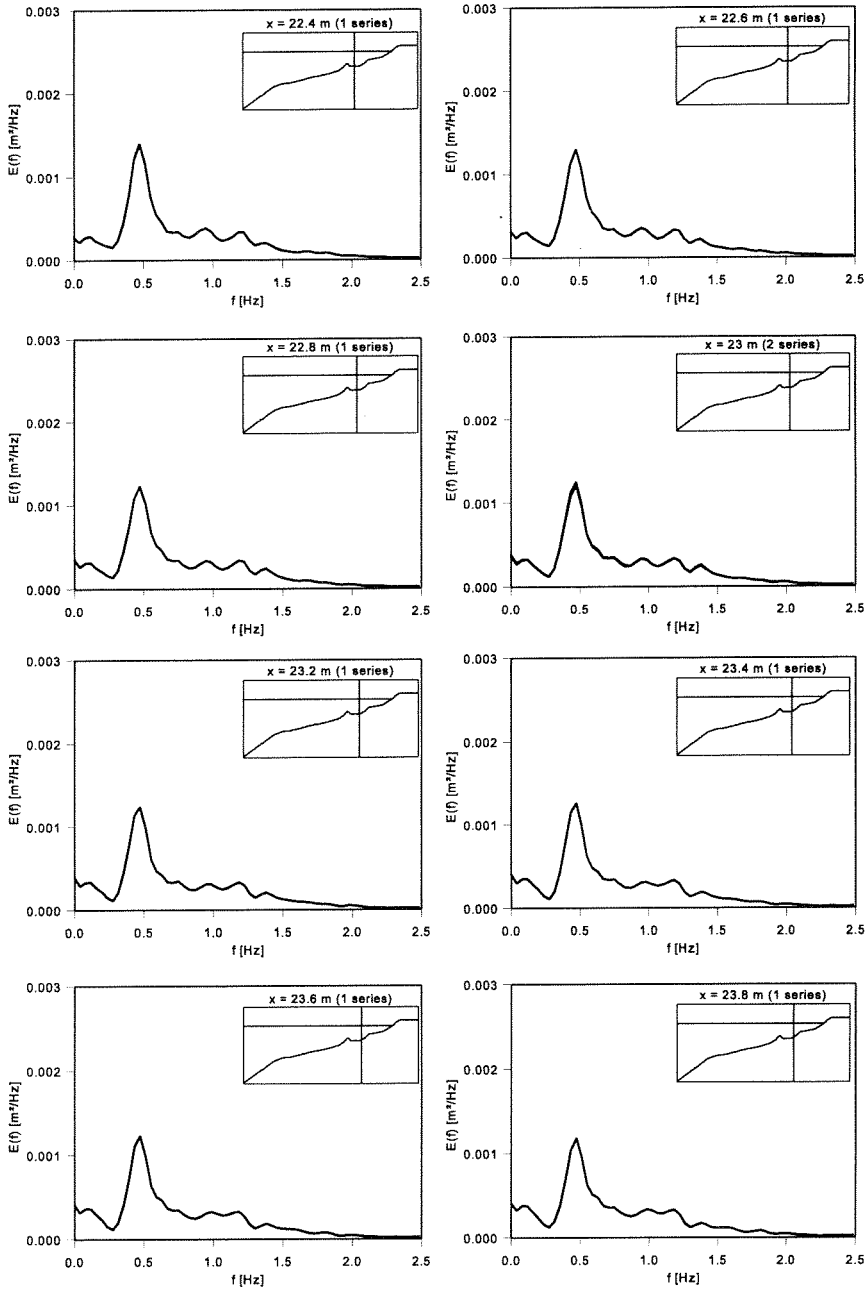


*Figure 3.1f* Energy Density Spectrum of Surface Elevation (1A; x = 22.4 - 23.8 m)

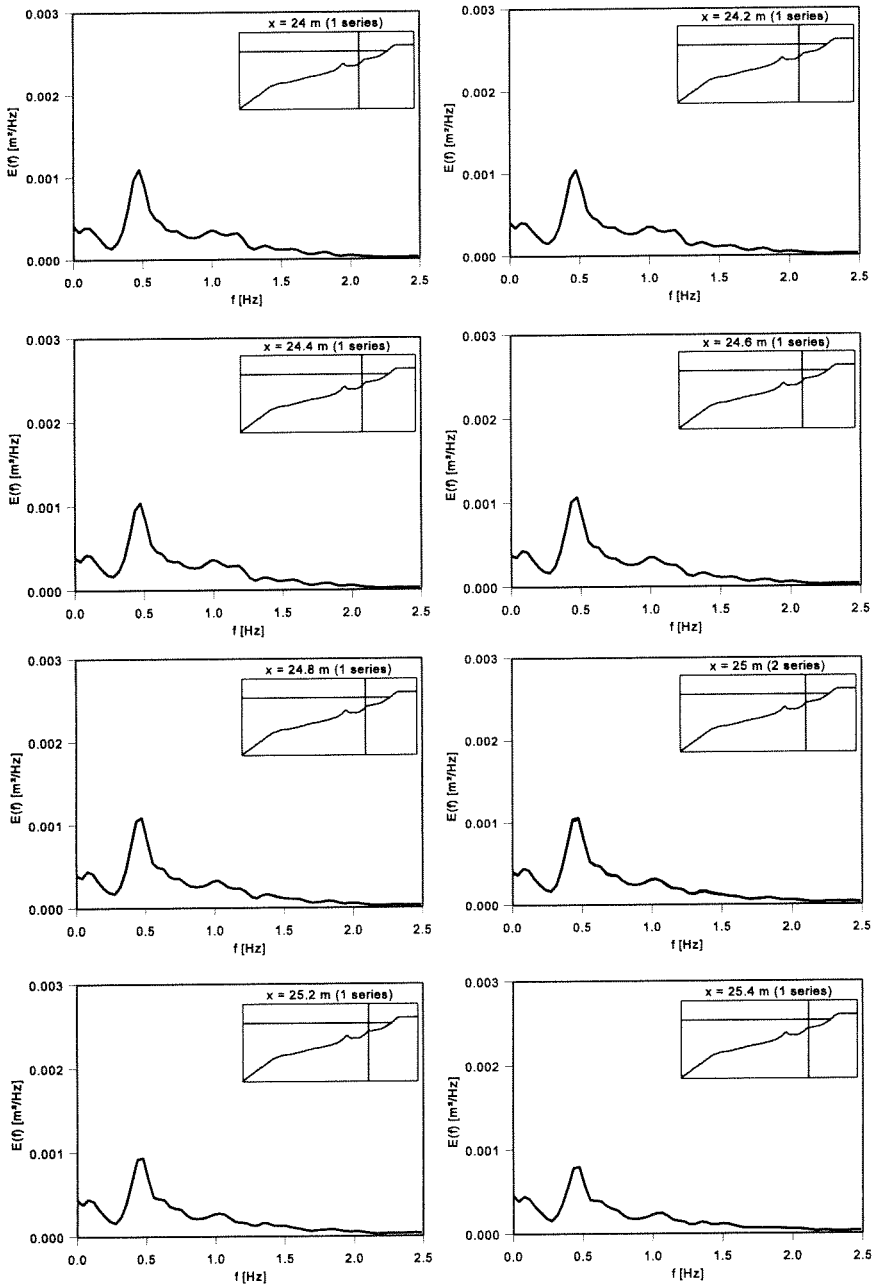


*Figure 3.1g* Energy Density Spectrum of Surface Elevation (1A; x = 24 - 25.4 m)

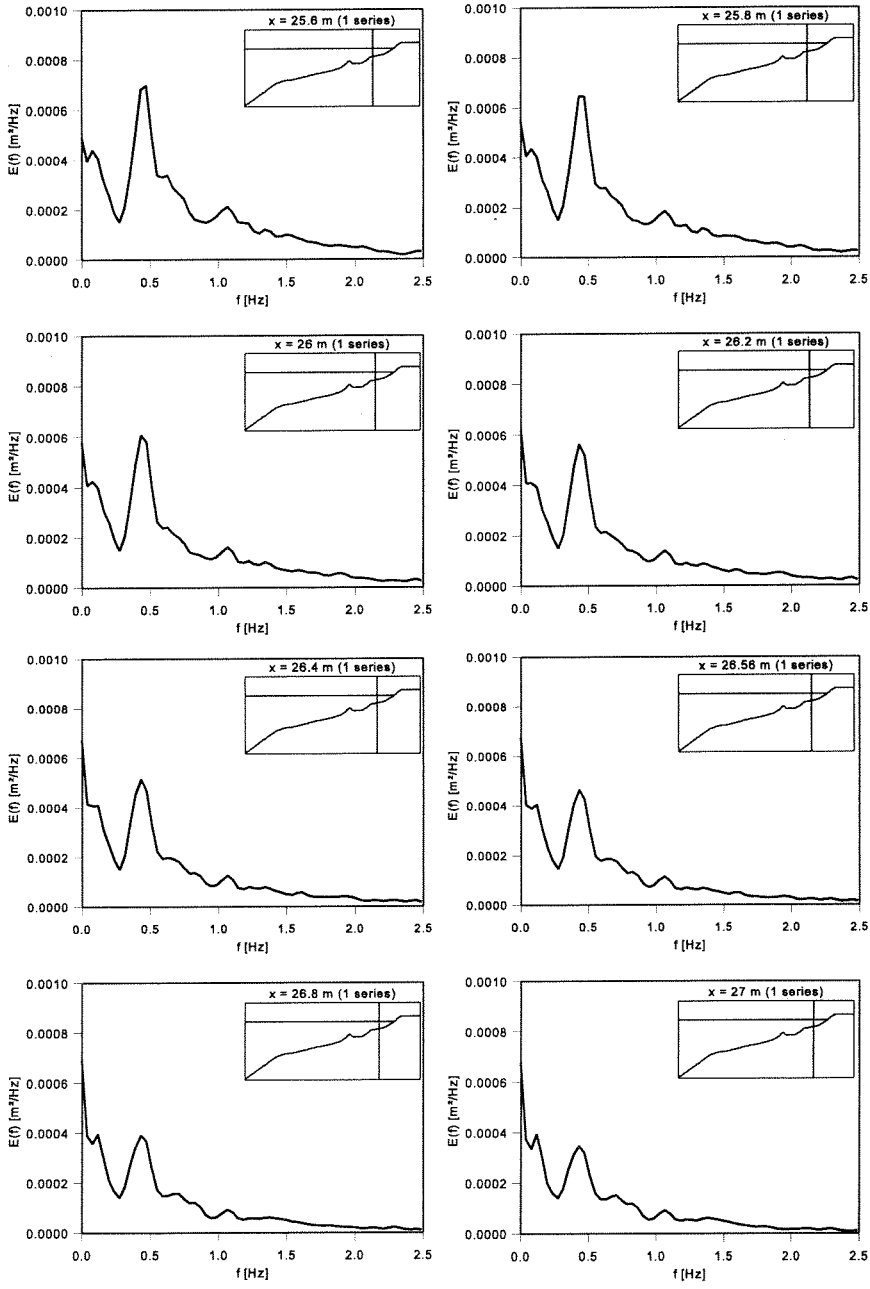


*Figure 3.1h* Energy Density Spectrum of Surface Elevation (1A; x = 25.6 - 27 m)

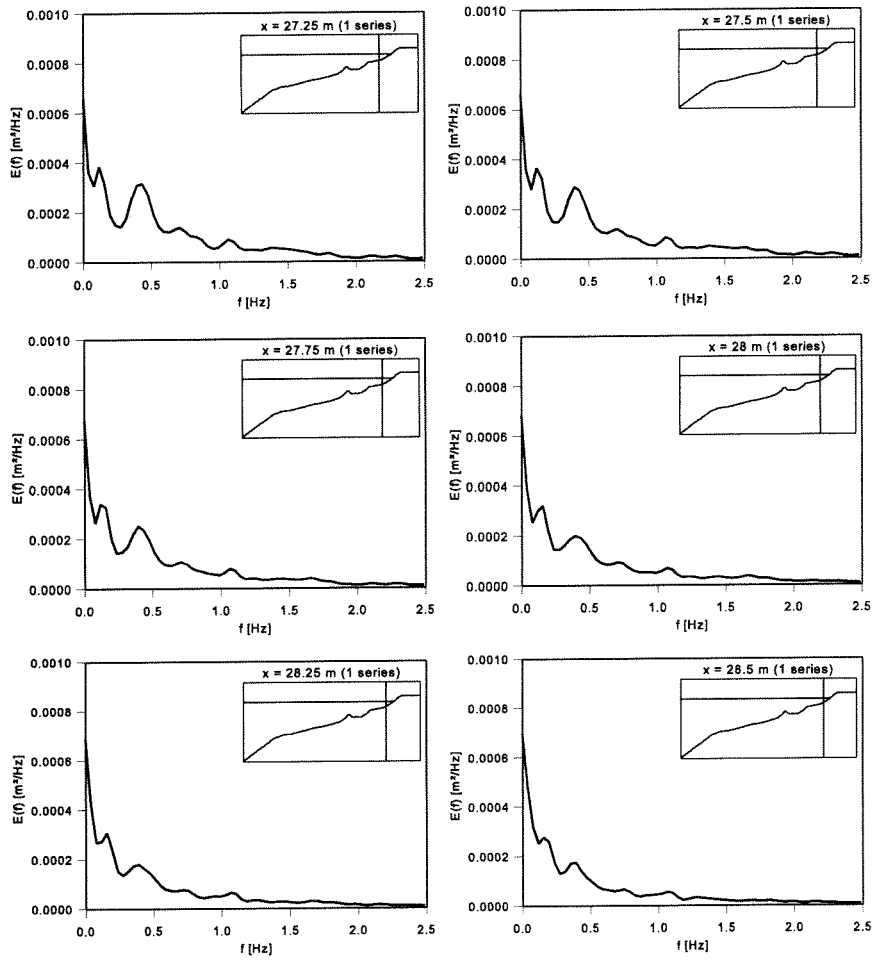


*Figure 3.1i* Energy Density Spectrum of Surface Elevation (1A; x = 27.25 - 28.5 m)

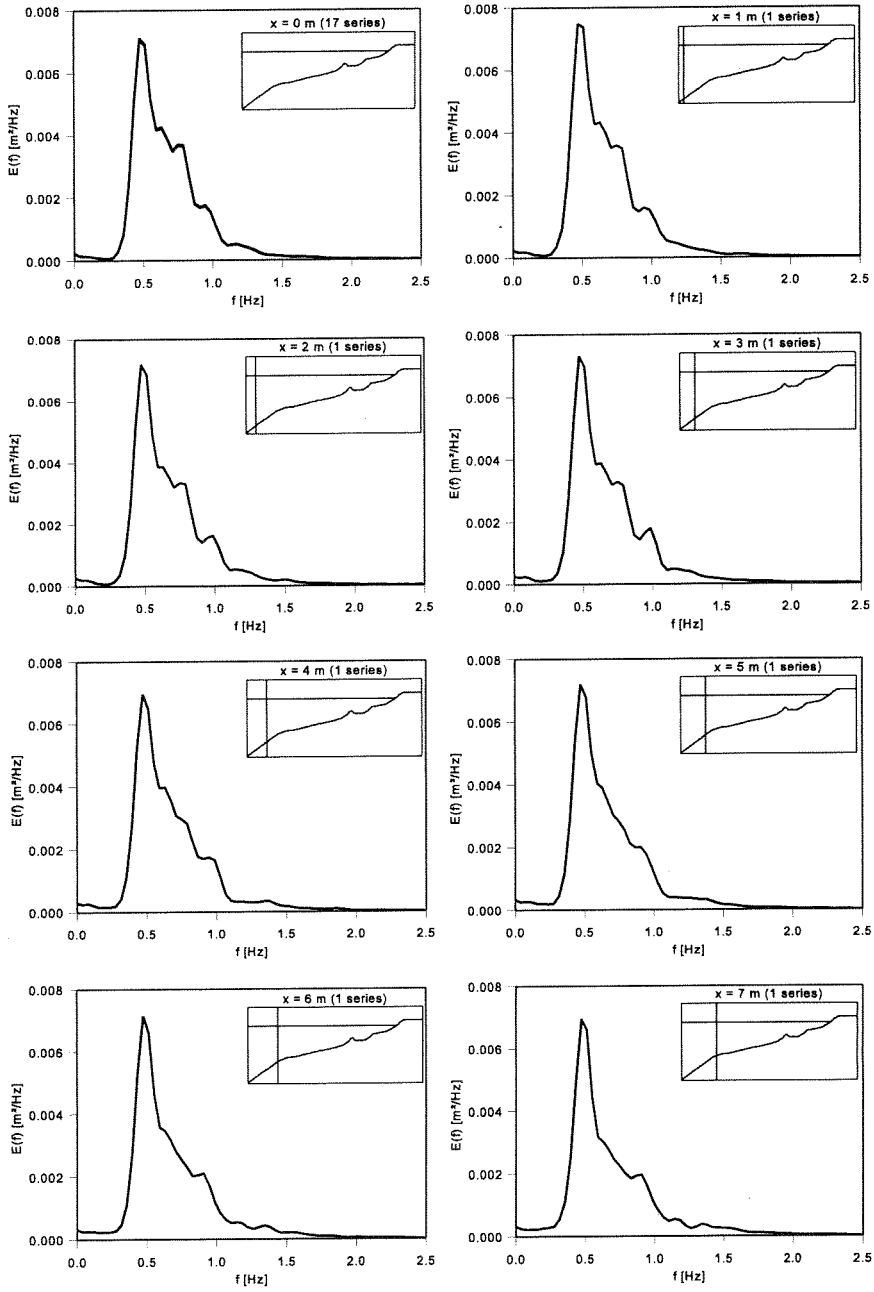


*Figure 3.2a* Energy Density Spectrum of Surface Elevation (1B; x = 0 - 7 m)

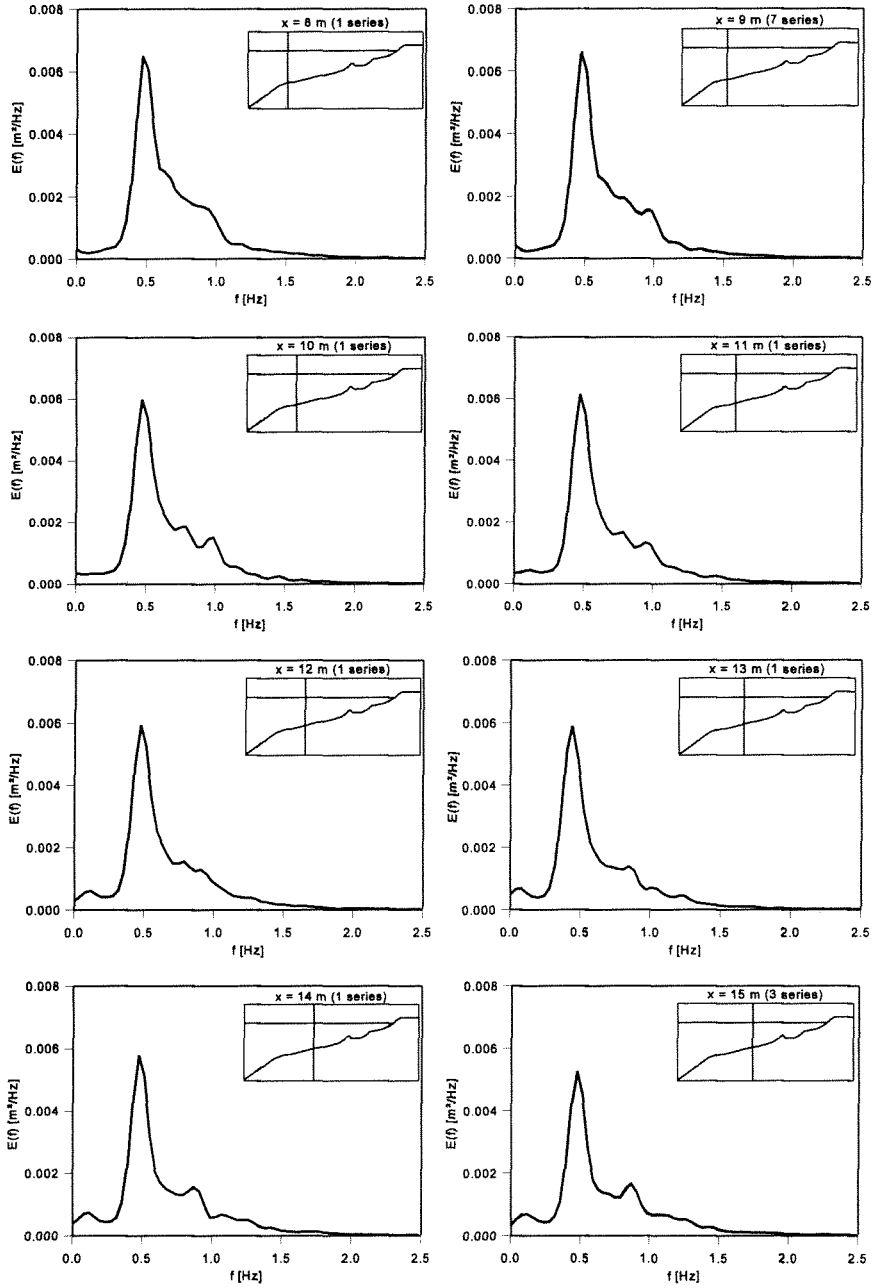


*Figure 3.2b* Energy Density Spectrum of Surface Elevation (1B; x = 8 - 15 m)

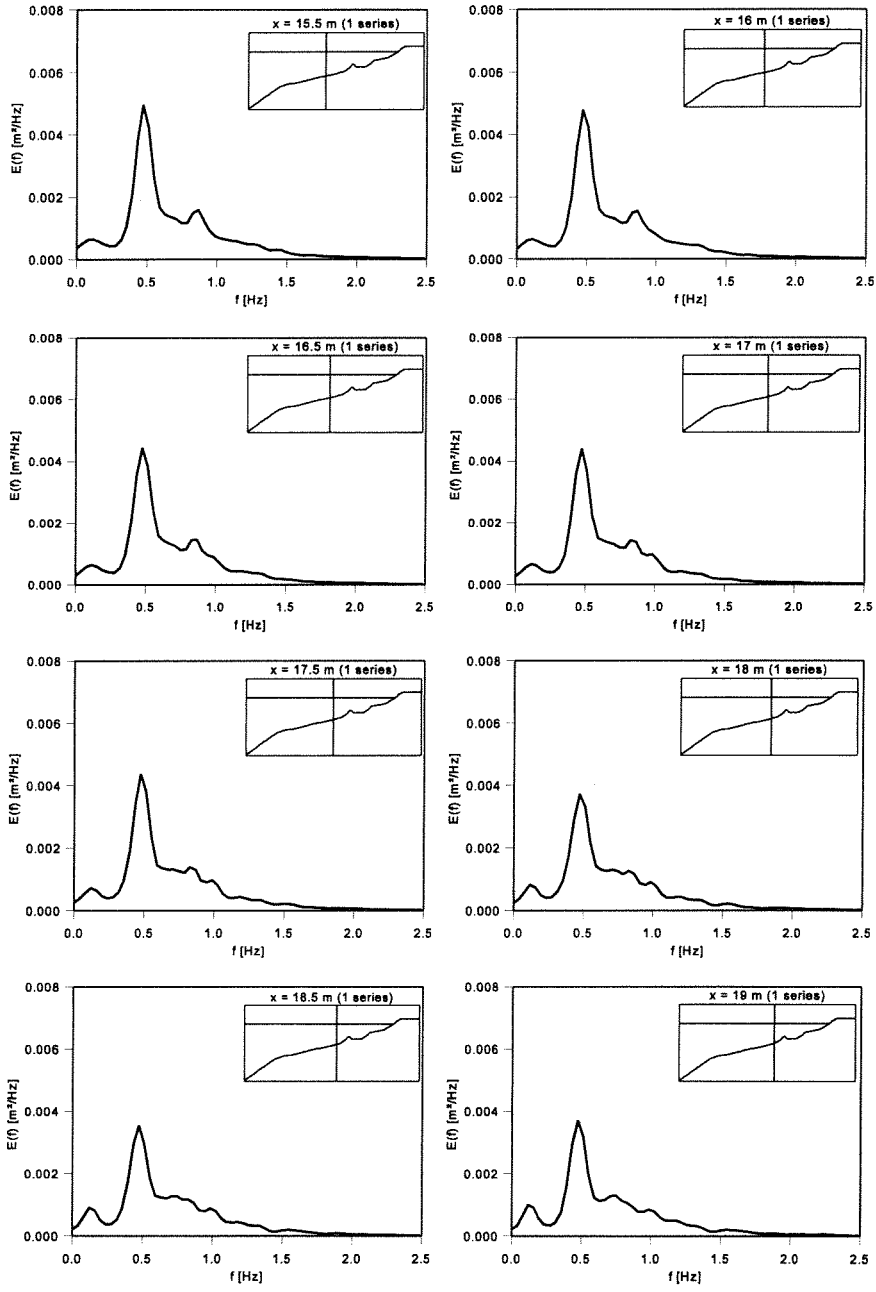


*Figure 3.2c* Energy Density Spectrum of Surface Elevation (1B; x = 15.5 - 19 m)

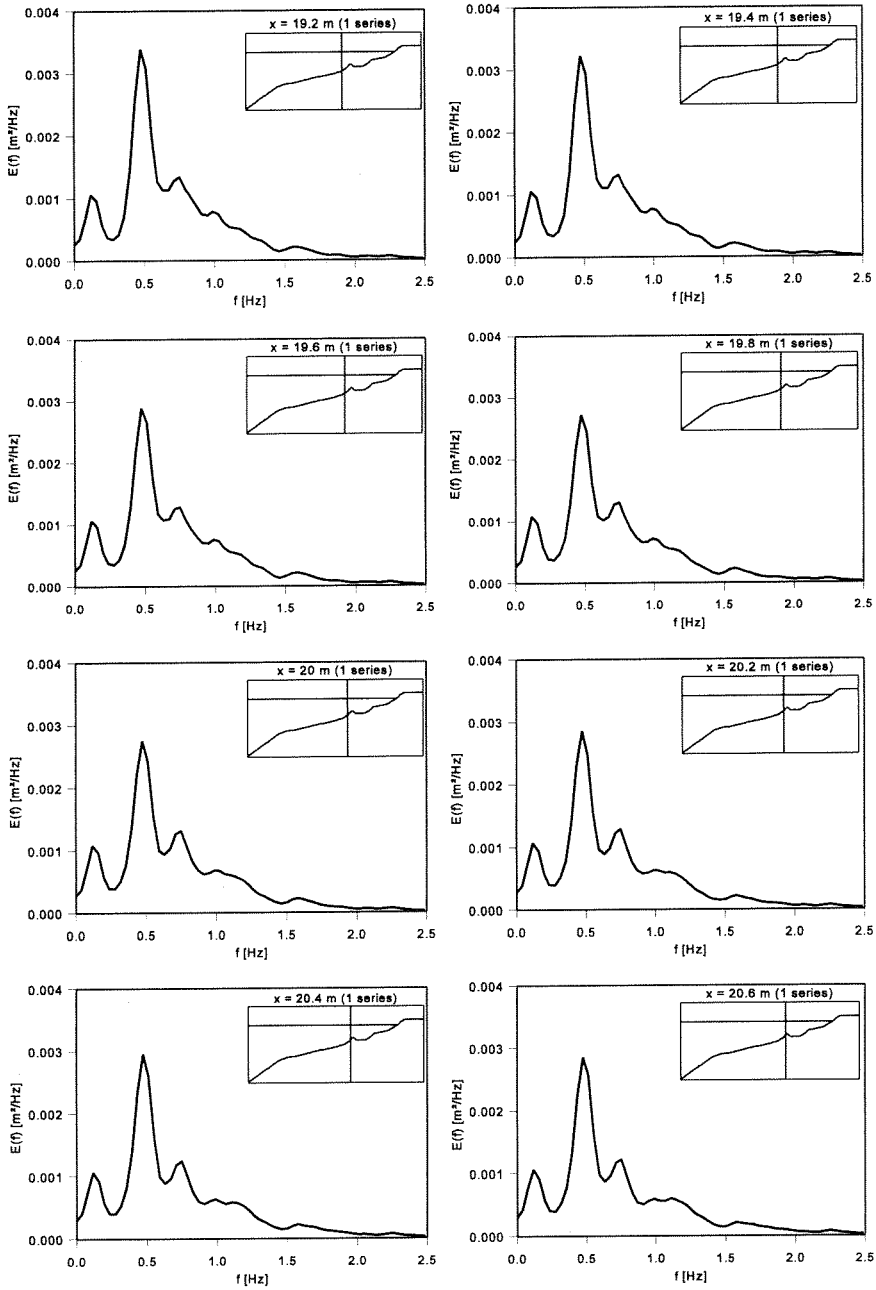


*Figure 3.2d* Energy Density Spectrum of Surface Elevation (1B; x = 19.2 - 20.6 m)

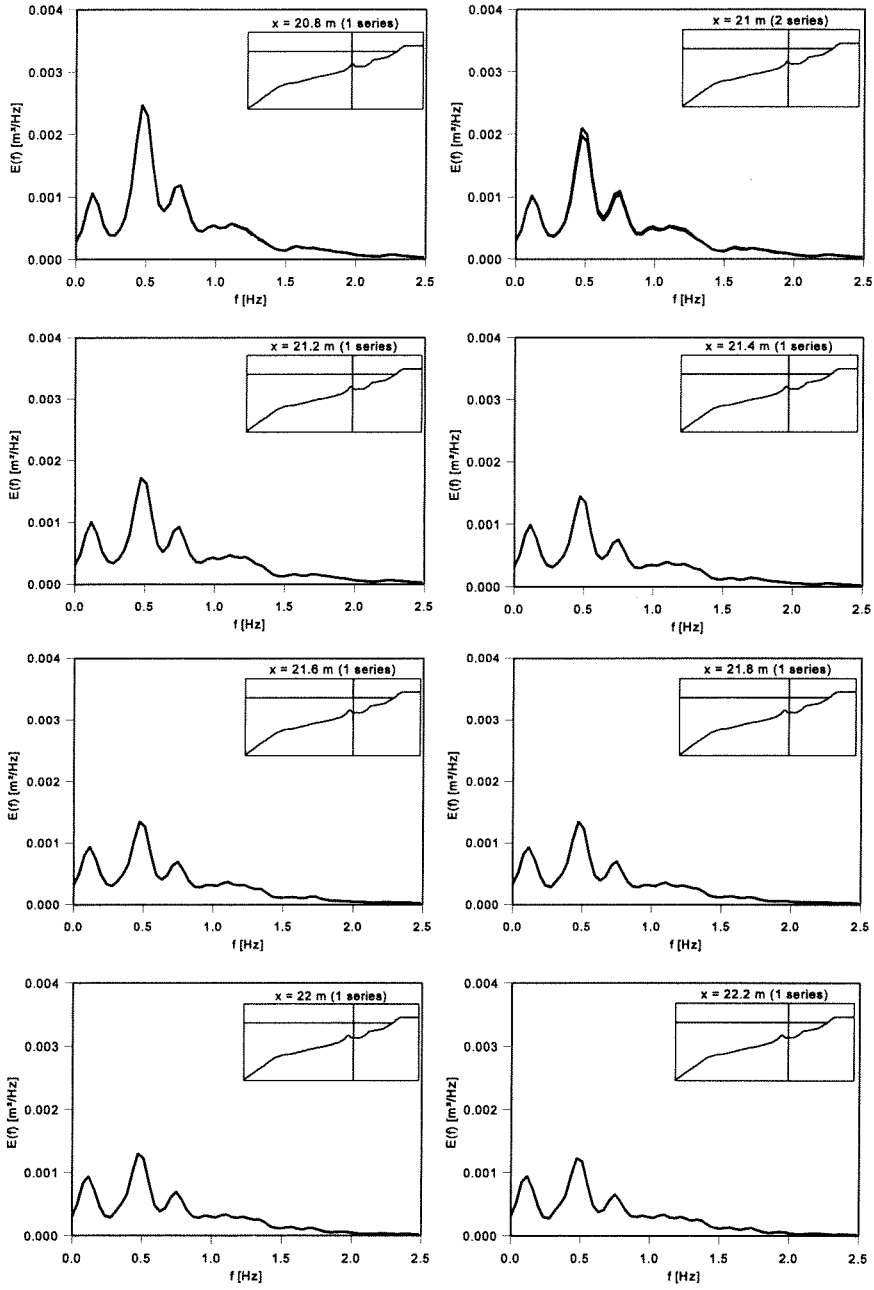


*Figure 3.2e* Energy Density Spectrum of Surface Elevation (1B; x = 20.8 - 22.2 m)

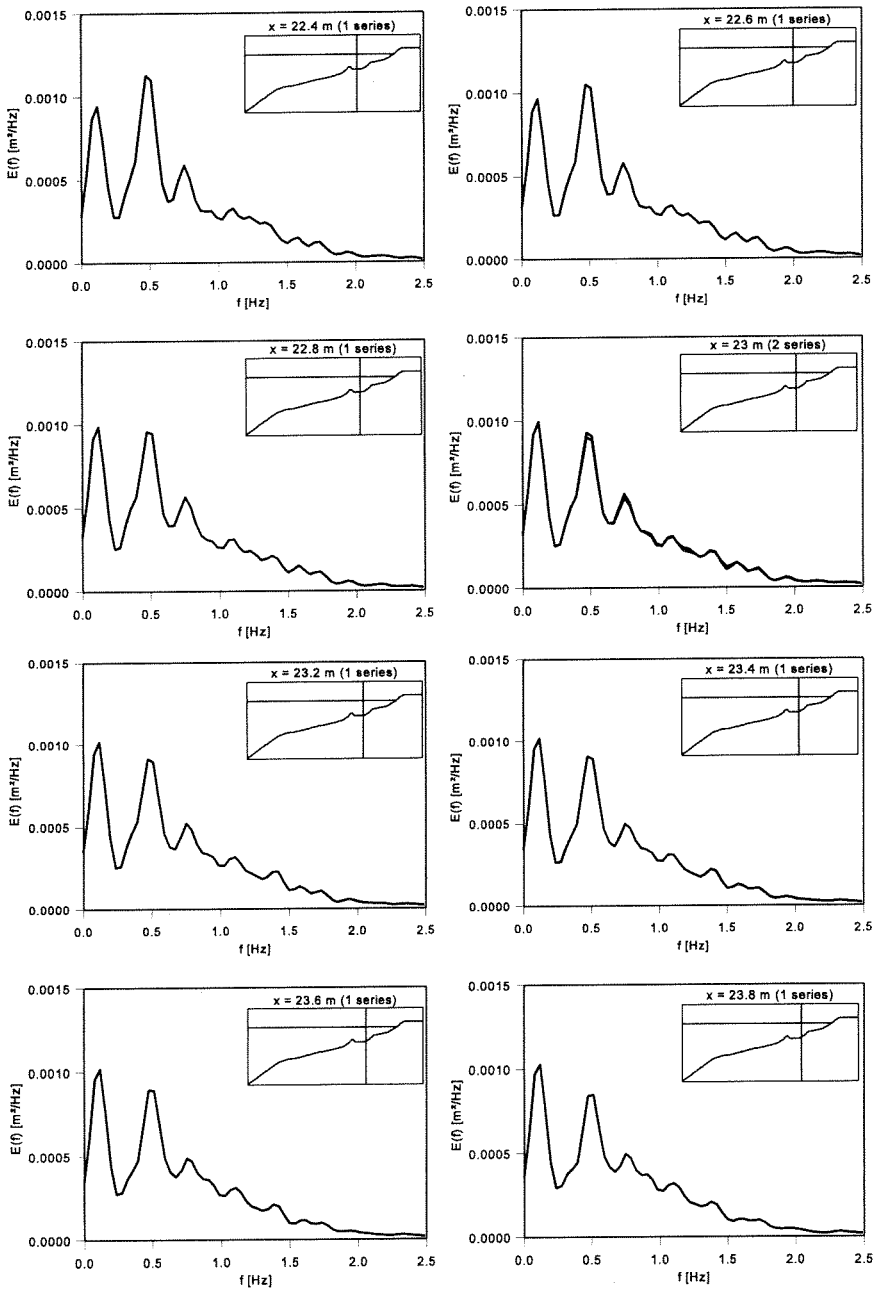


*Figure 3.2f* Energy Density Spectrum of Surface Elevation (1B; x = 22.4 - 23.8 m)

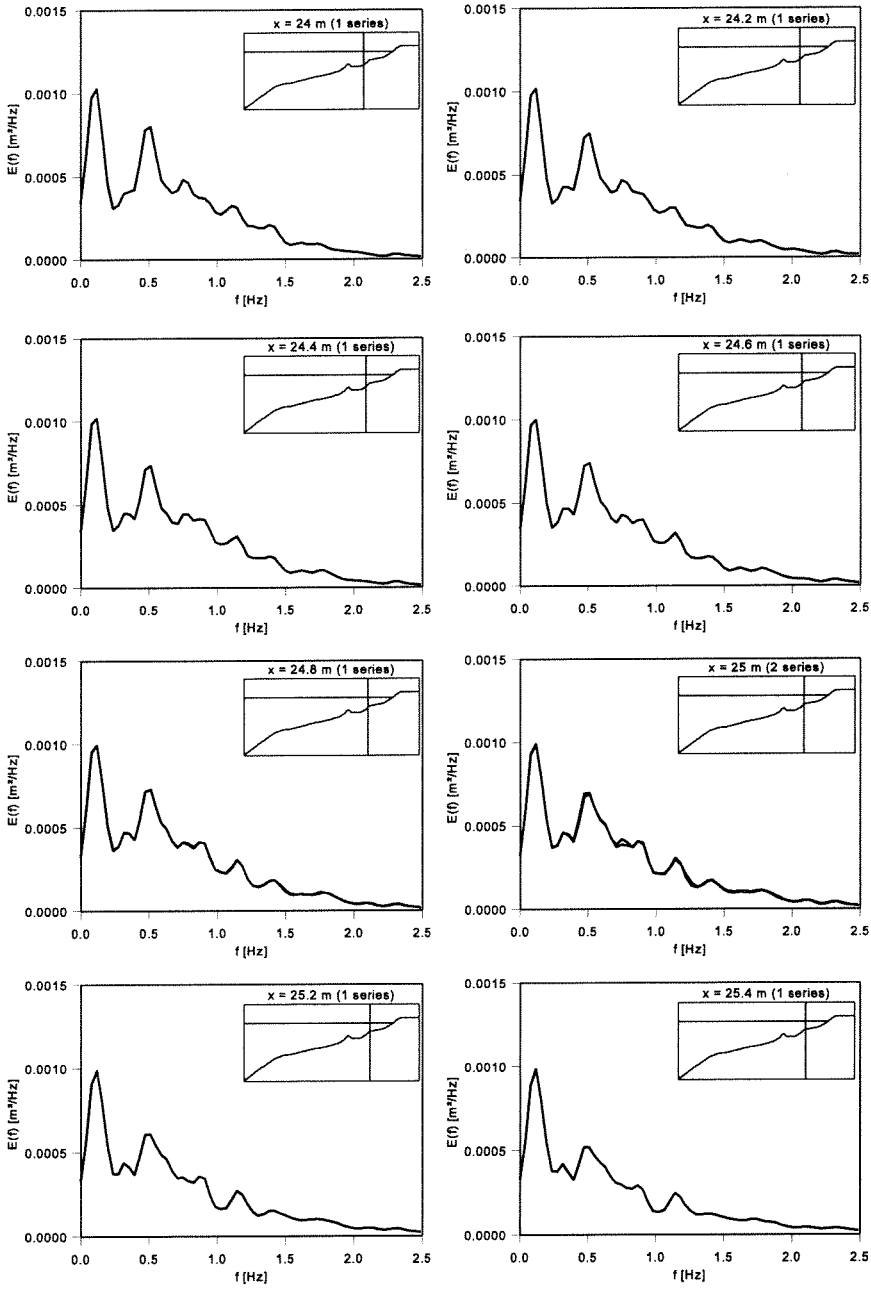


*Figure 3.2g* Energy Density Spectrum of Surface Elevation (1B; x = 24 - 25.4 m)

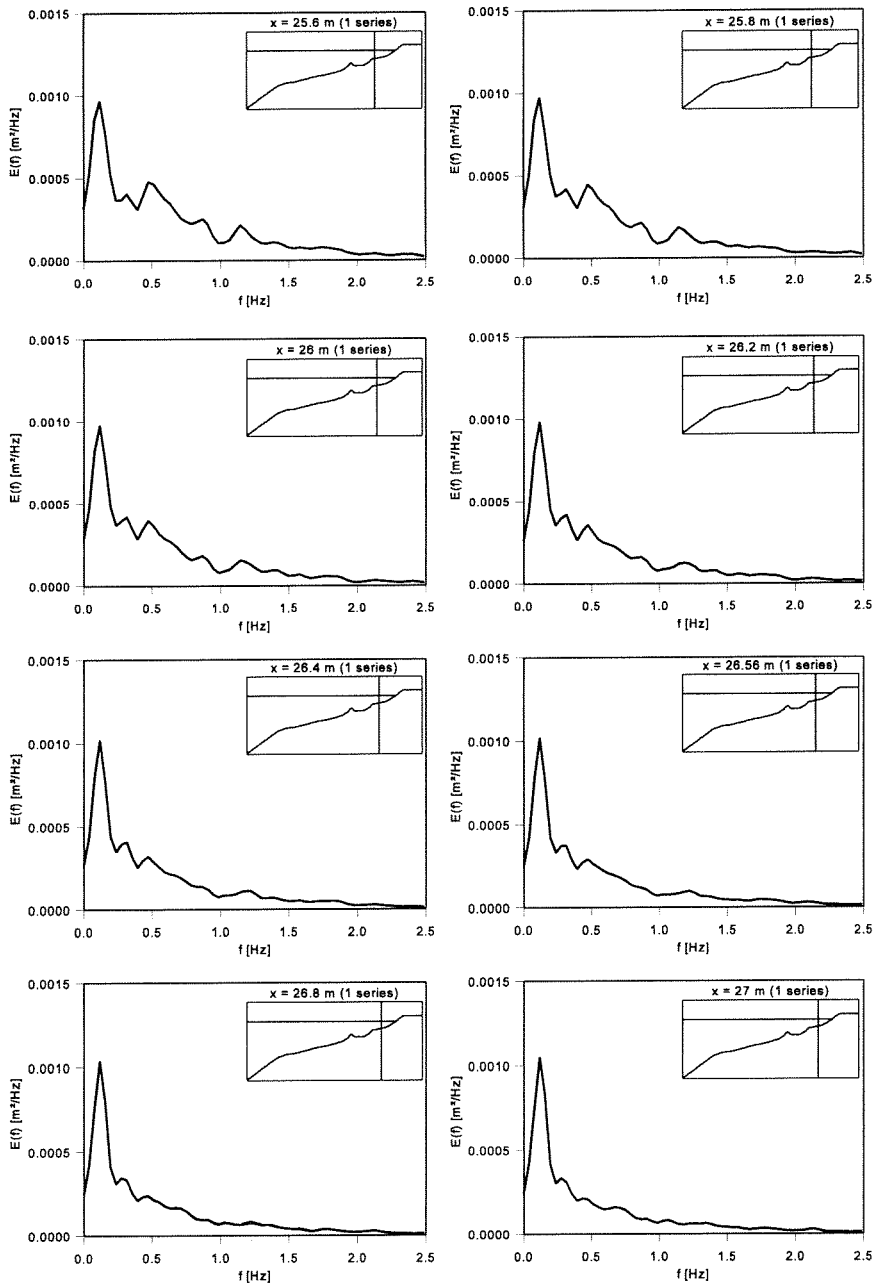


*Figure 3.2h* Energy Density Spectrum of Surface Elevation (1B; x = 25.6 - 27 m)

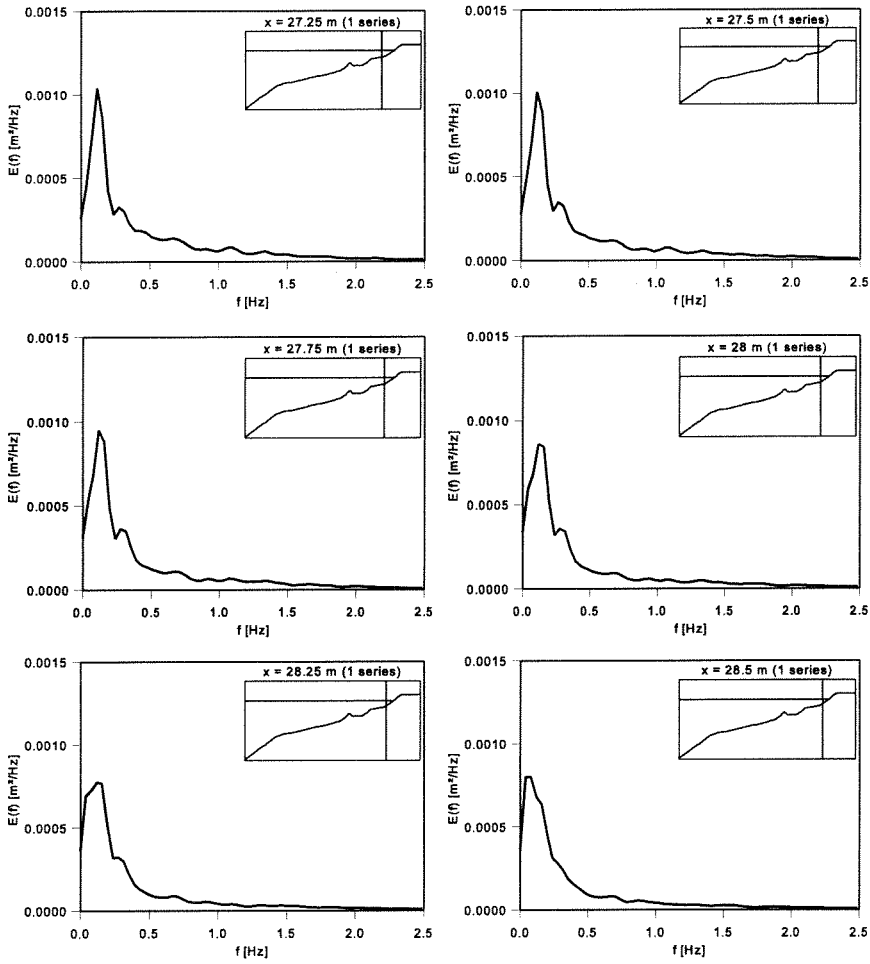


*Figure 3.2i* Energy Density Spectrum of Surface Elevation (1B; x = 27.25 - 28.5 m)

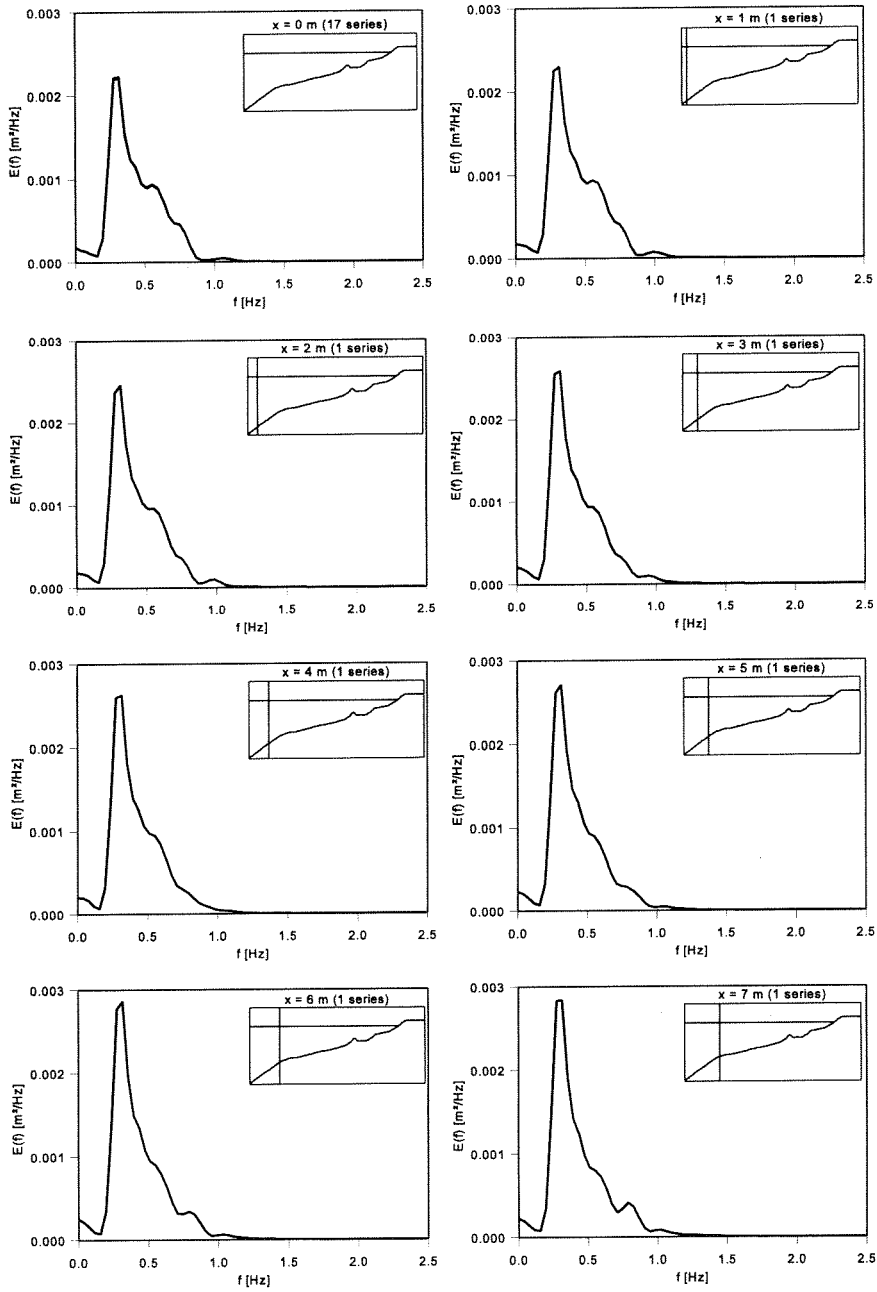


*Figure 3.3a* Energy Density Spectrum of Surface Elevation (1C; x = 0 - 7 m)

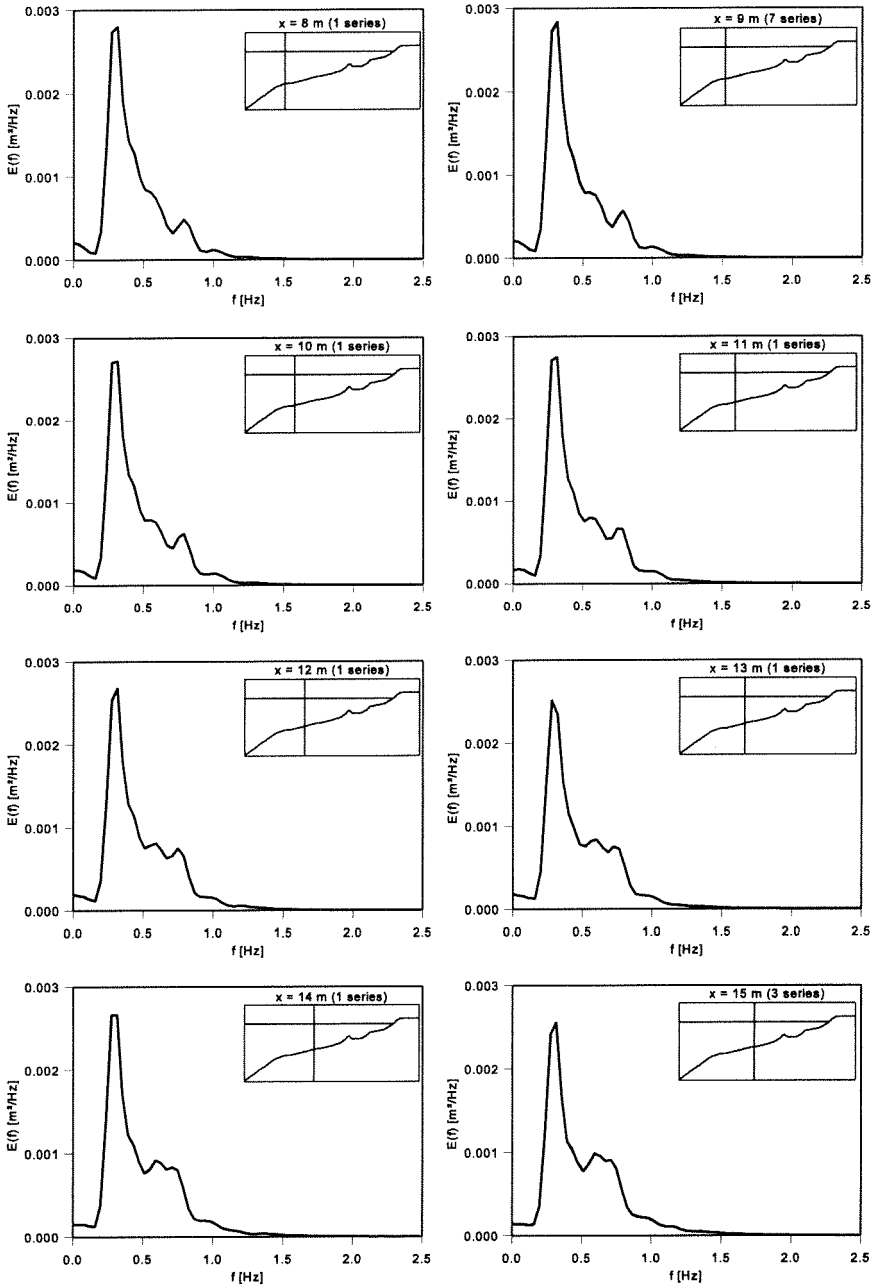


*Figure 3.3b* Energy Density Spectrum of Surface Elevation (1C; x = 8 - 15 m)

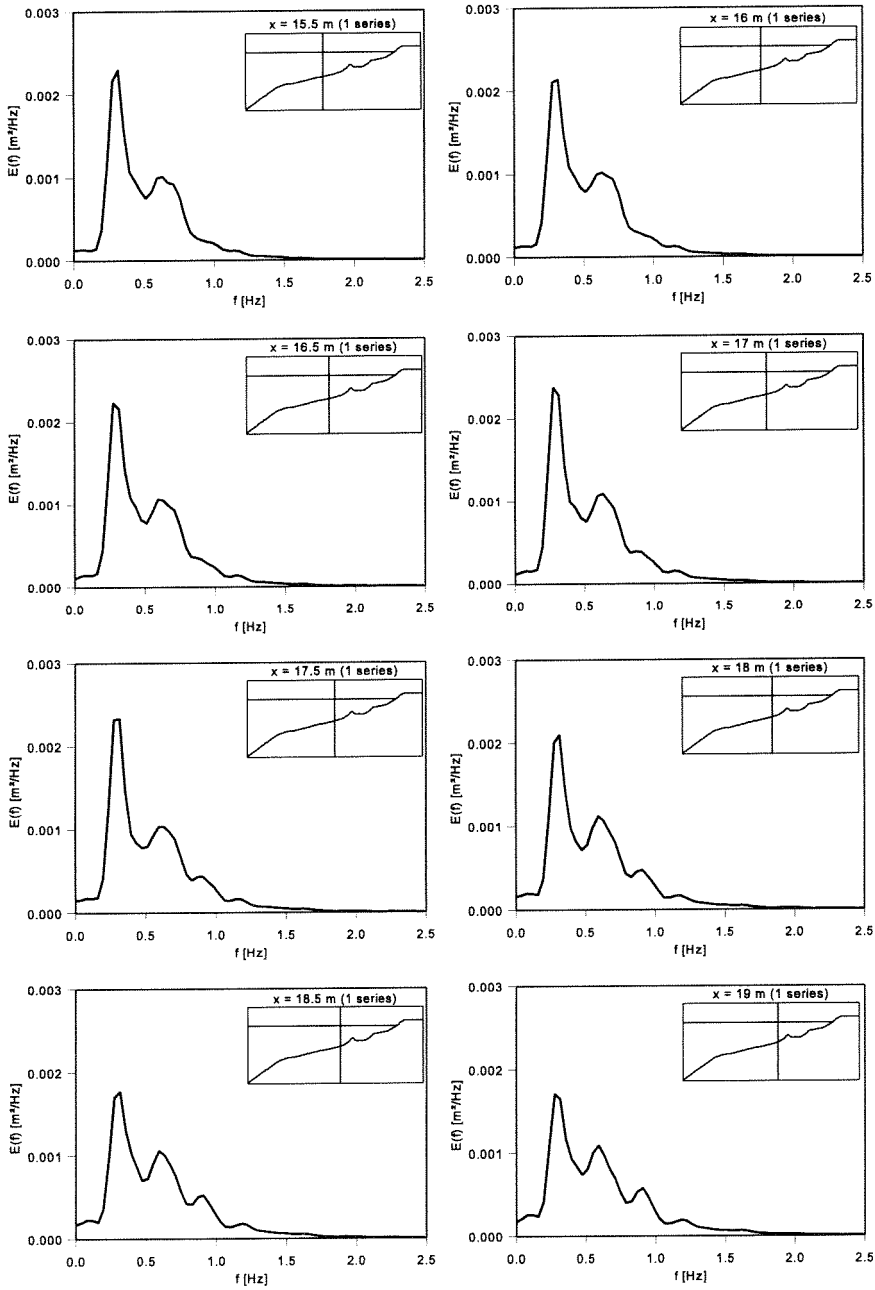


*Figure 3.3c* Energy Density Spectrum of Surface Elevation (1C; x = 15.5 - 19 m)

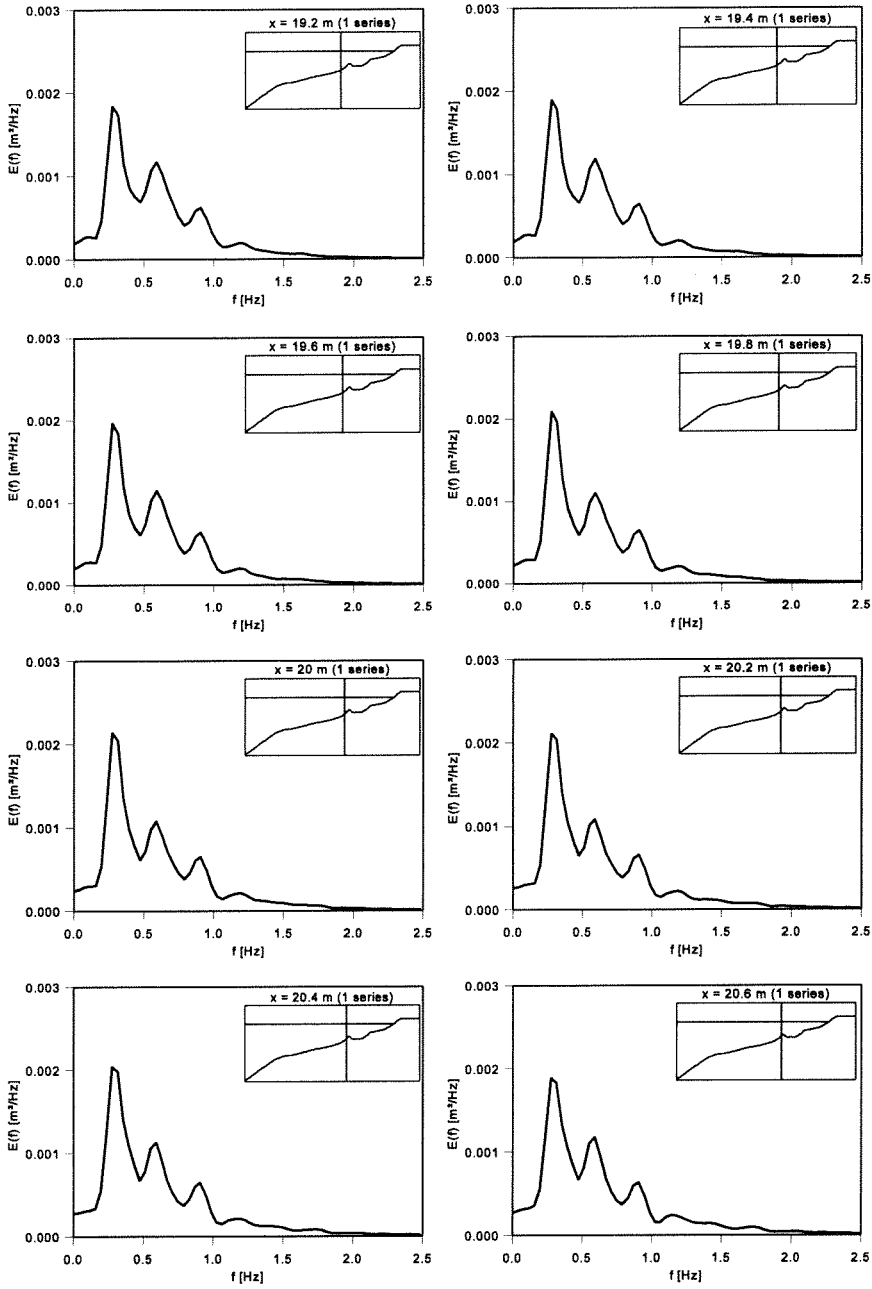


*Figure 3.3d* Energy Density Spectrum of Surface Elevation (1C; x = 19.2 - 20.6 m)

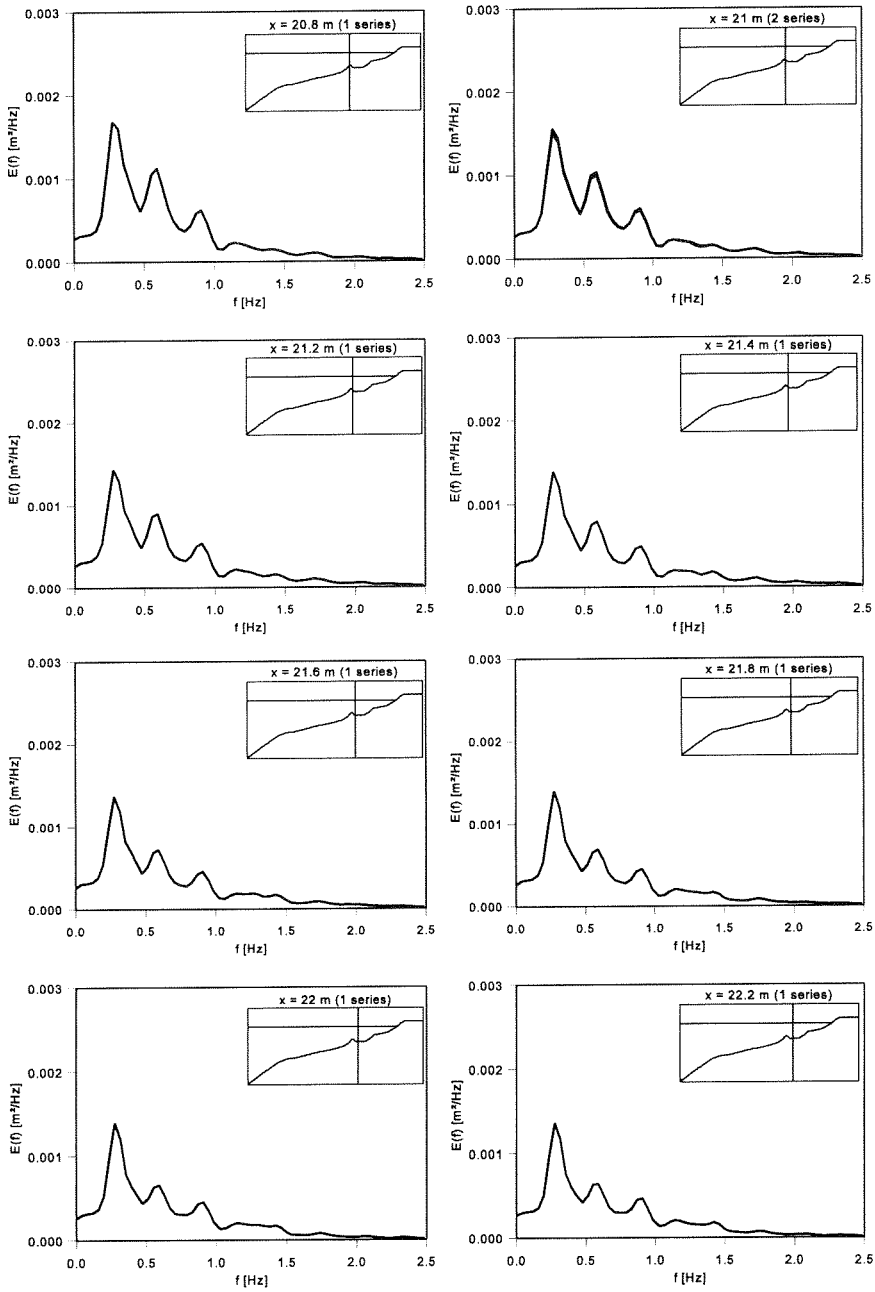


*Figure 3.3e* Energy Density Spectrum of Surface Elevation (1C; x = 20.8 - 22.2 m)

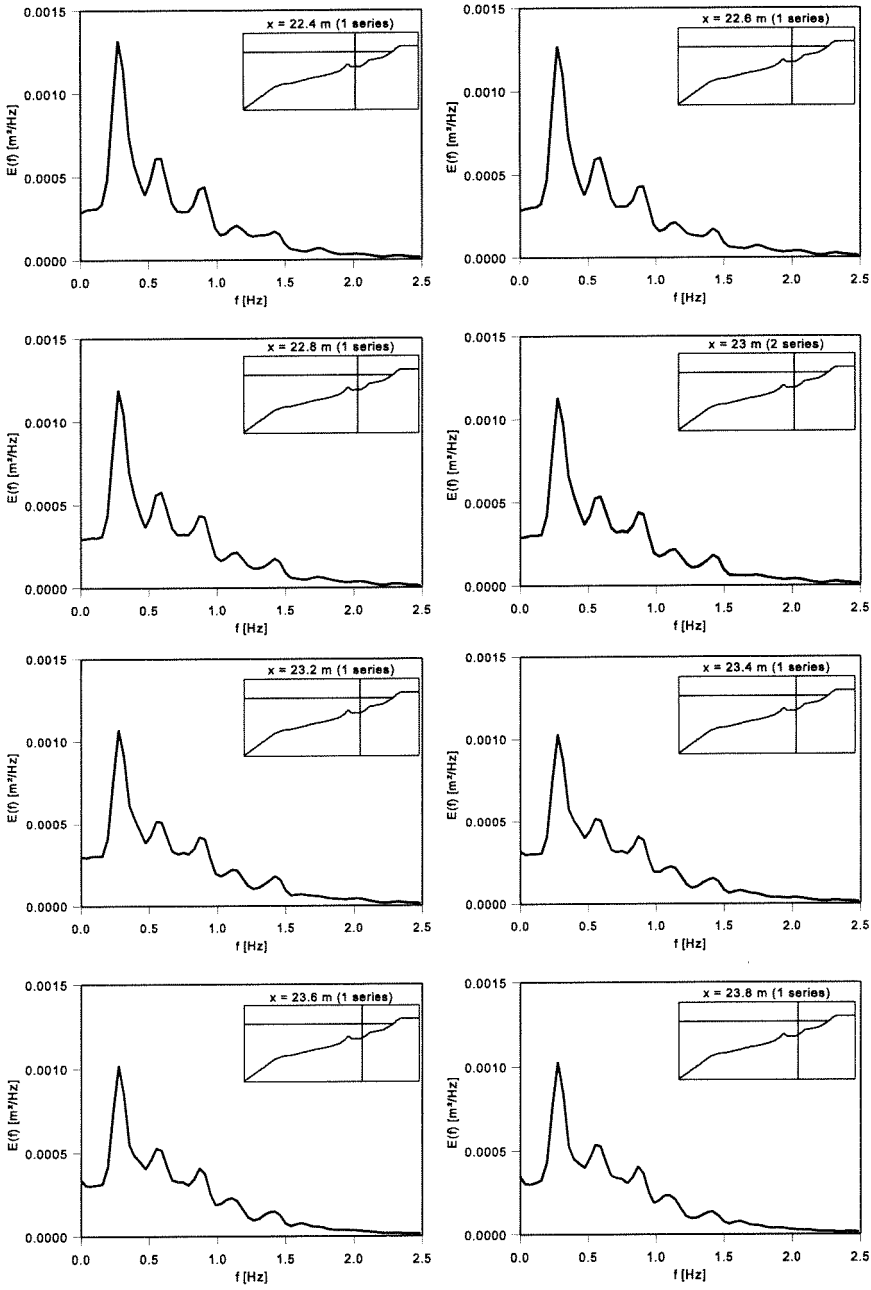


*Figure 3.3f* Energy Density Spectrum of Surface Elevation (1C; x = 22.4 - 23.8 m)

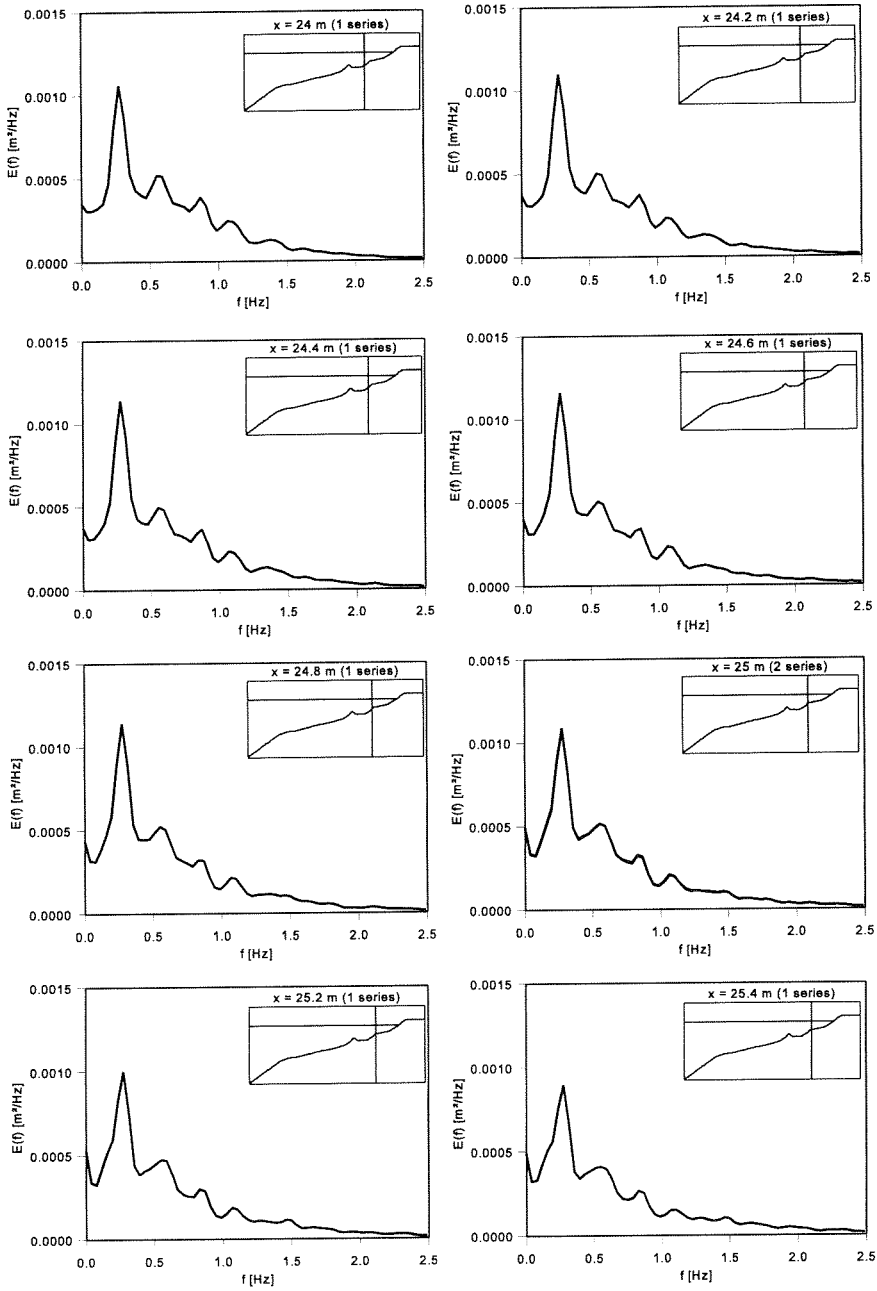


*Figure 3.3g* Energy Density Spectrum of Surface Elevation (1C; x = 24 - 25.4 m)

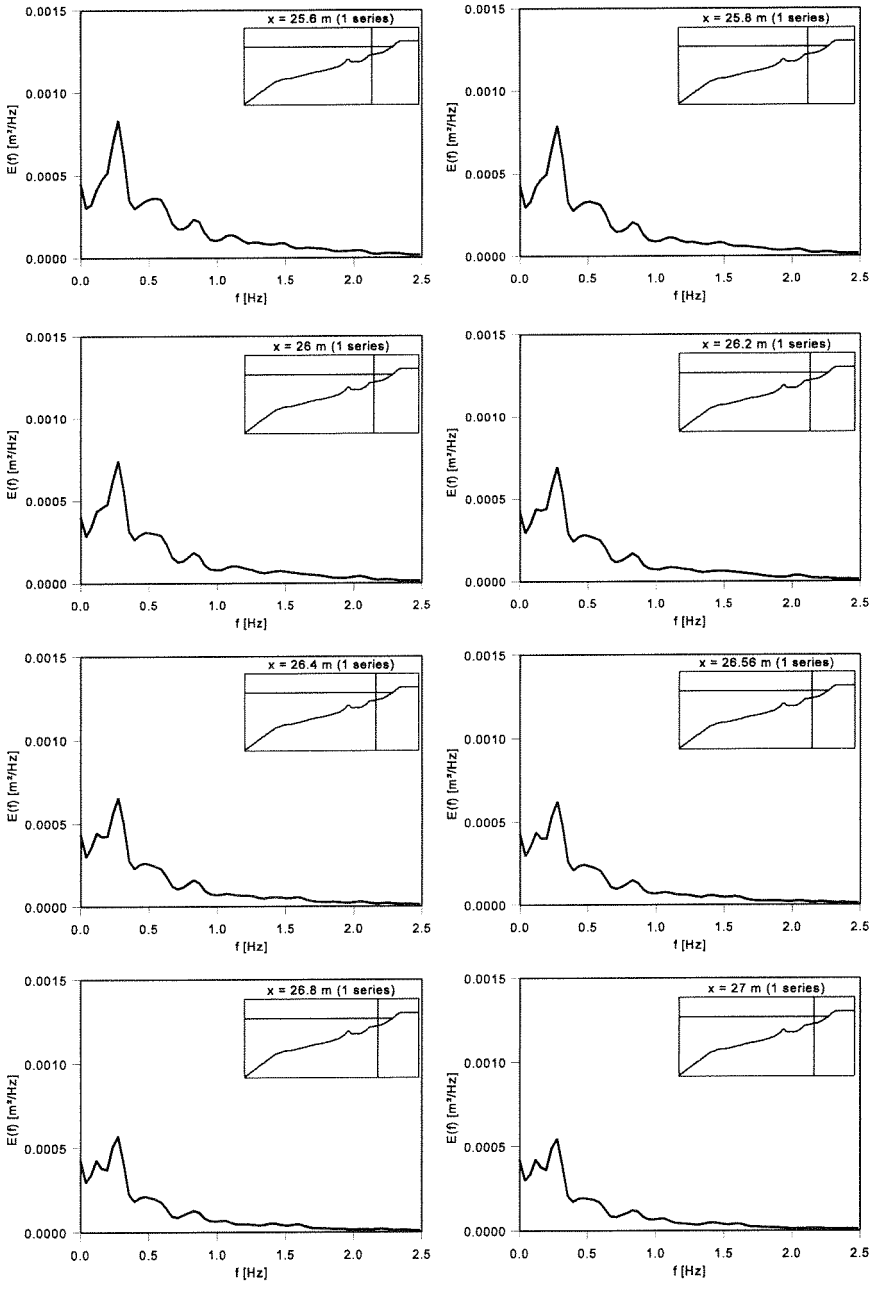


*Figure 3.3h* Energy Density Spectrum of Surface Elevation (1C; x = 25.6 - 27 m)

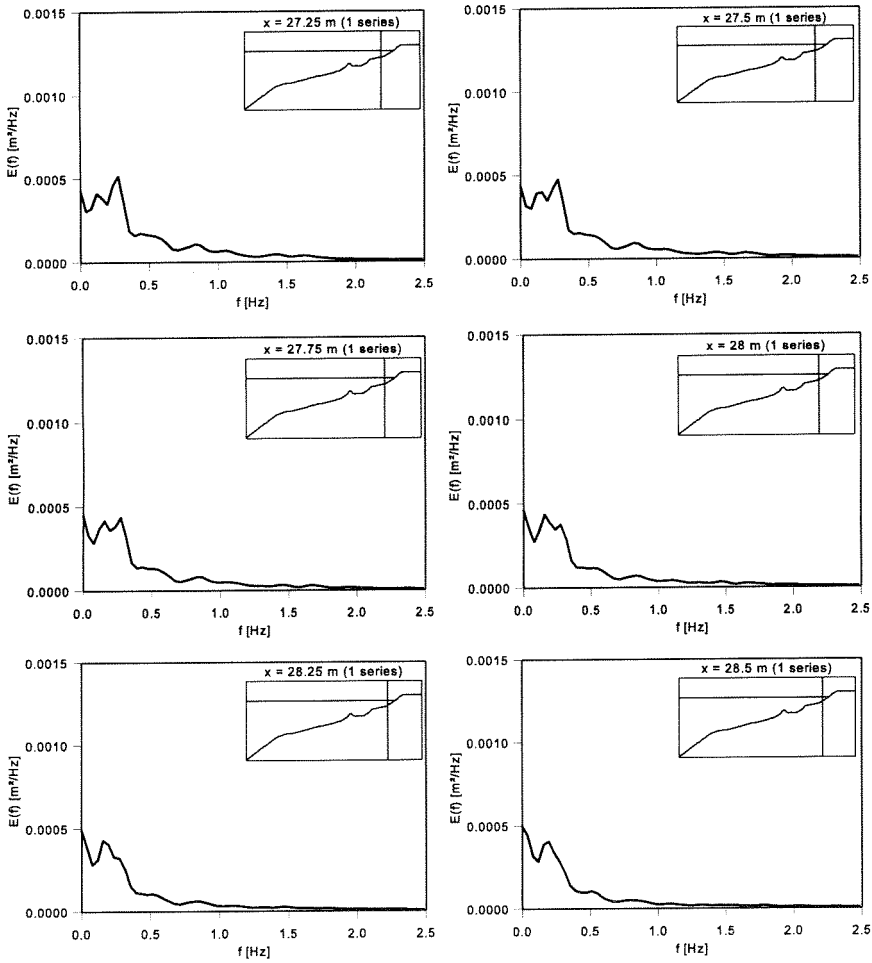


*Figure 3.3i* Energy Density Spectrum of Surface Elevation (1C; x = 27.25 - 28.5 m)

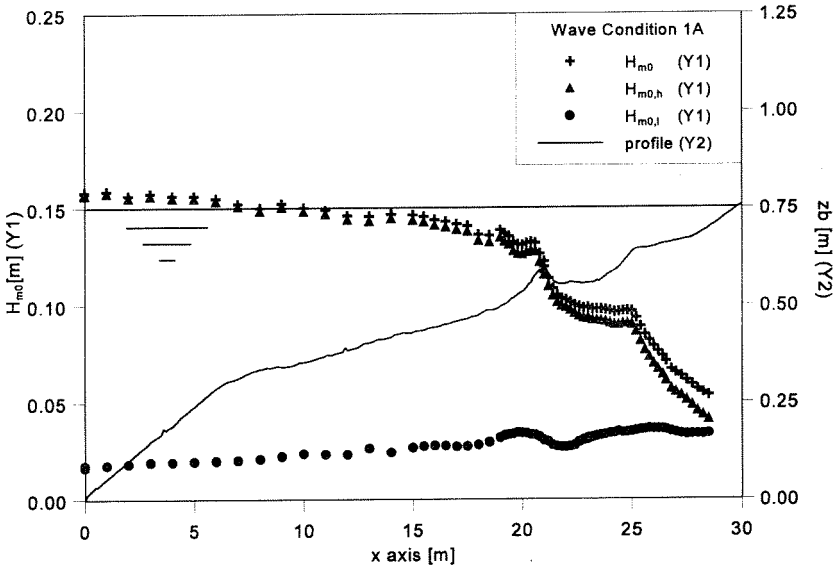


*Figure 3.4* Wave Height $H_{m0}$ (1A)

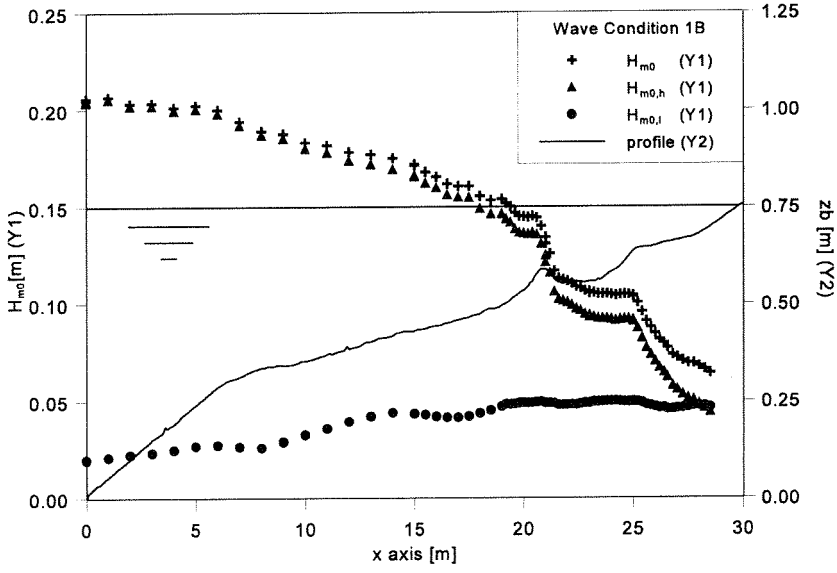


*Figure 3.5* Wave Height $H_{m0}$ (1B)

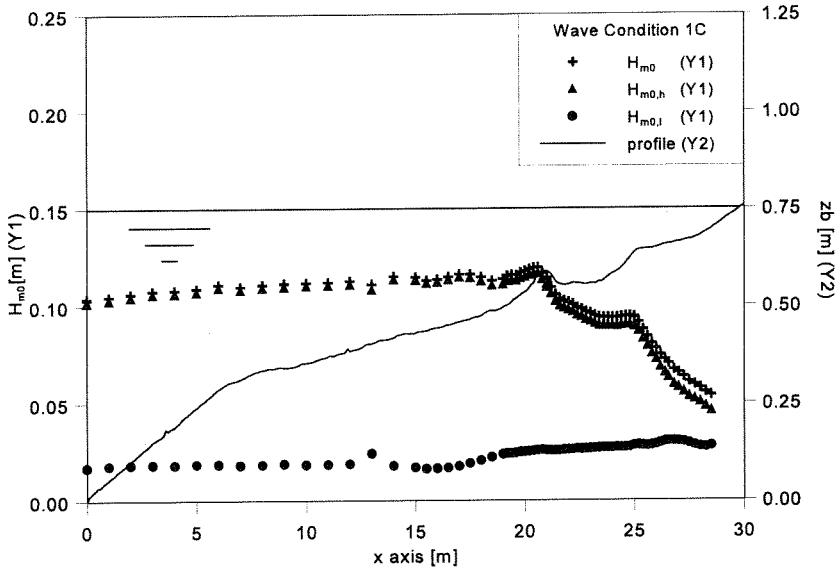


*Figure 3.6* Wave Height $H_{m0}$ (1C)

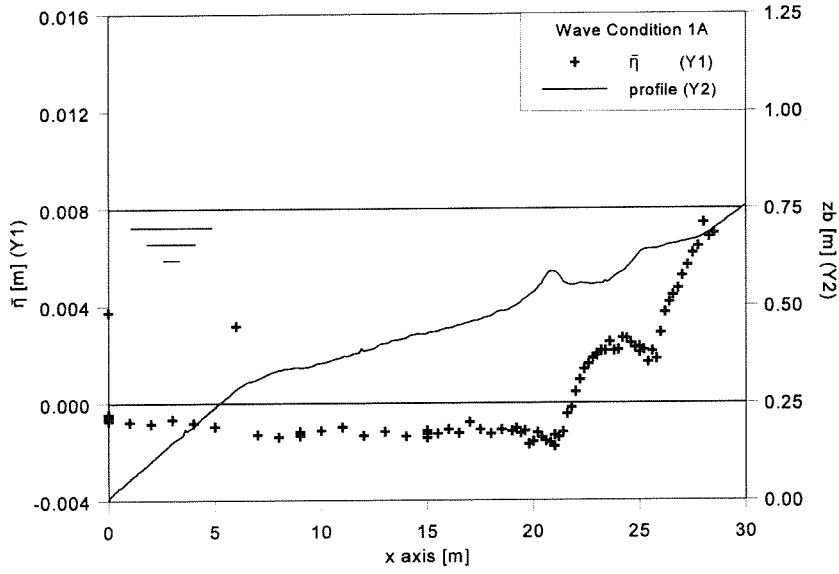


*Figure 3.7* Wave Set-up (1A)

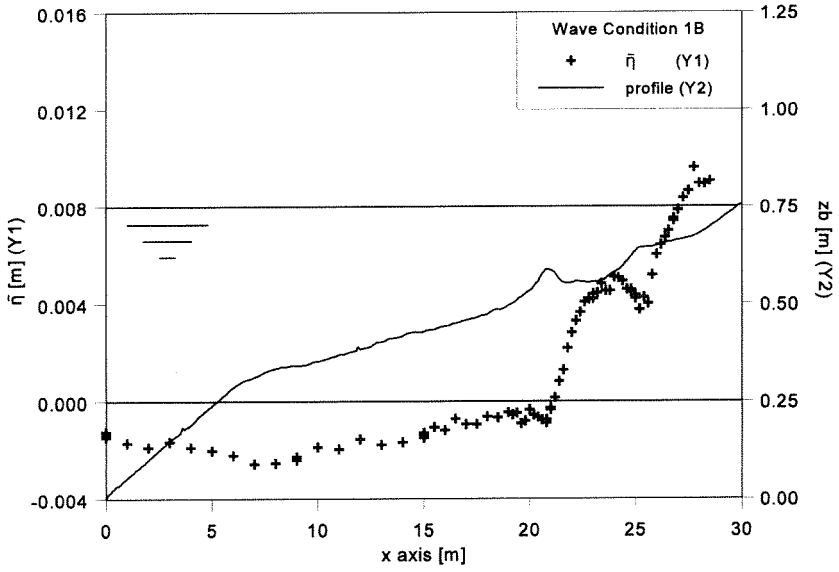


*Figure 3.8* Wave Set-up (1B)

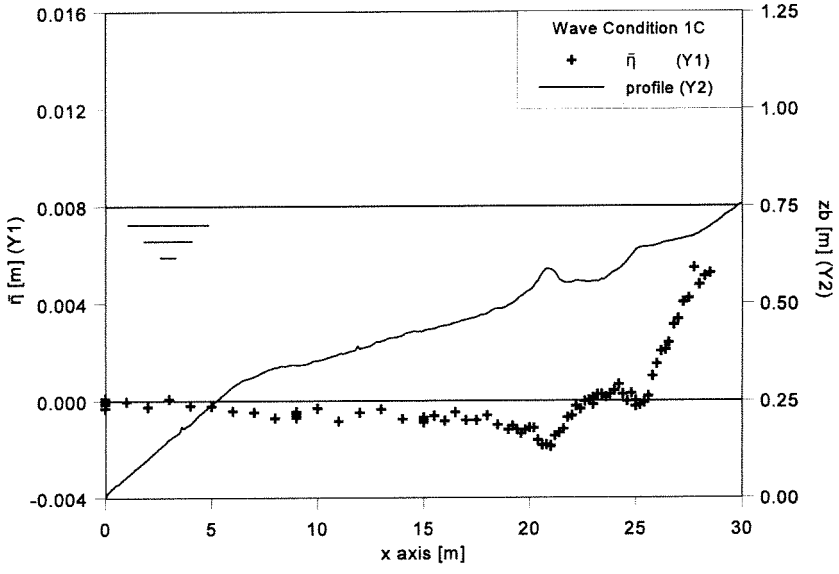


*Figure 3.9* Wave Set-up (1C)

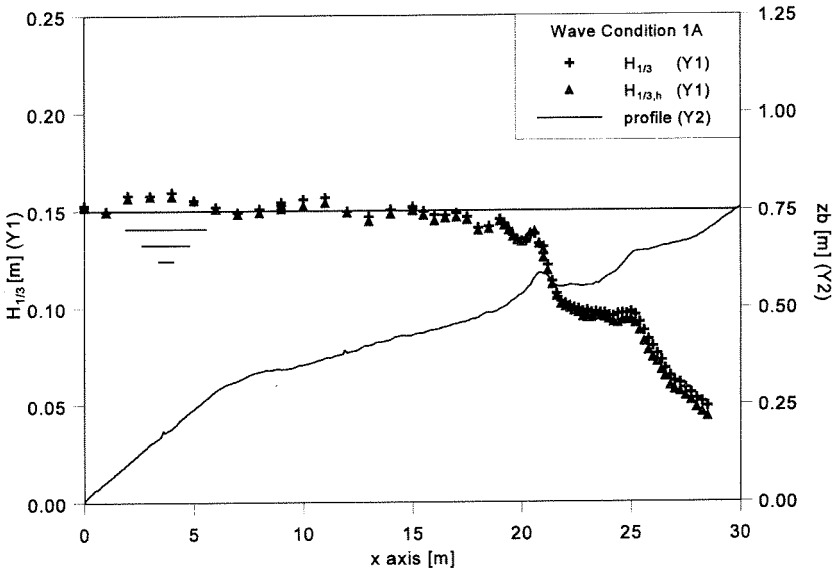


*Figure 3.10* Significant Wave Height; total signal & high-pass filter (1A)

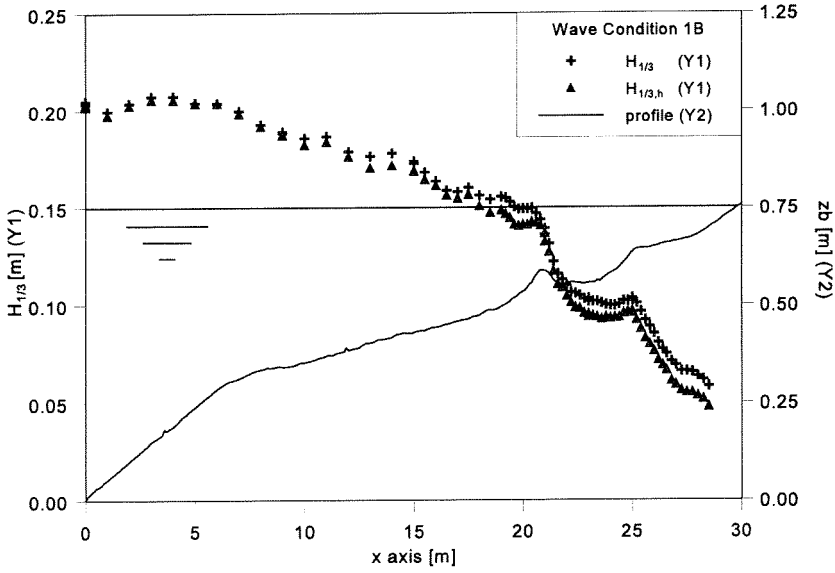


*Figure 3.11* Significant Wave Height; total signal & high-pass filter (1B)

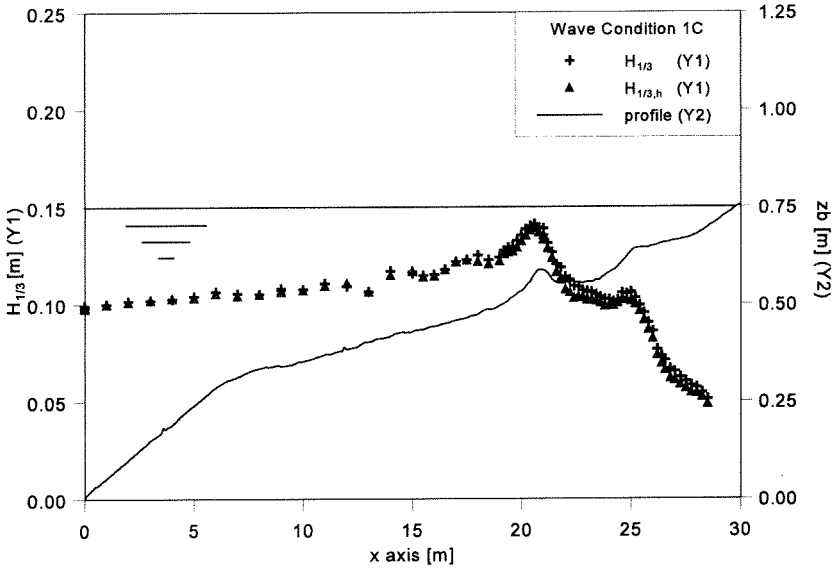


*Figure 3.12* Significant Wave Height; total signal & high-pass filter (1C)

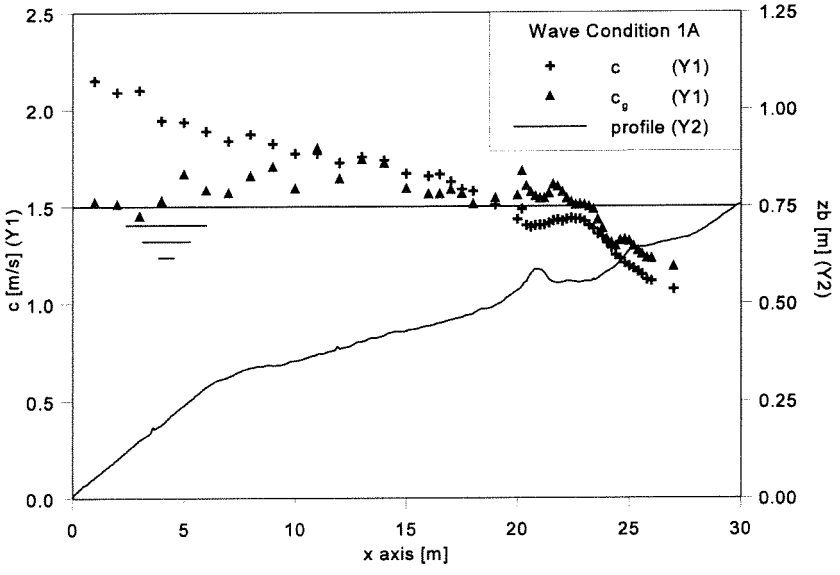


*Figure 3.13* Wave Celerity and Wave Group Celerity (1A)

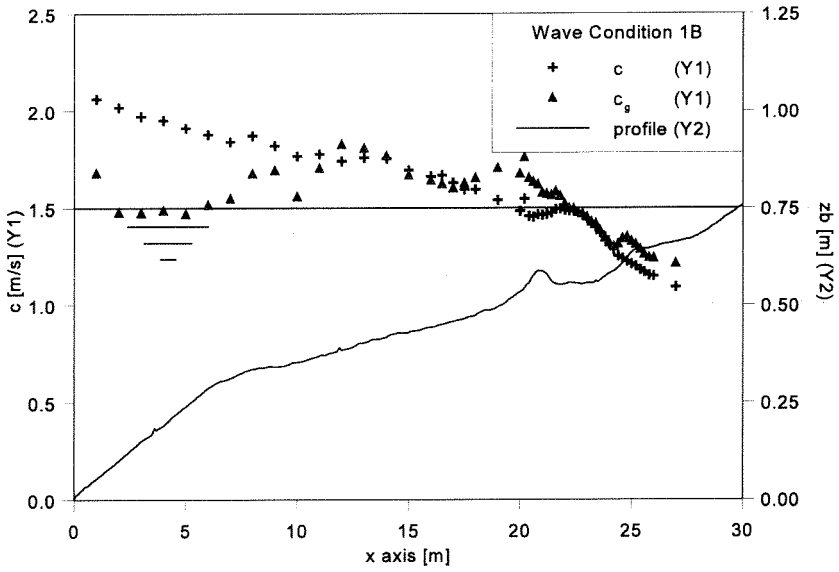


*Figure 3.14* Wave Celerity and Wave Group Celerity (1B)

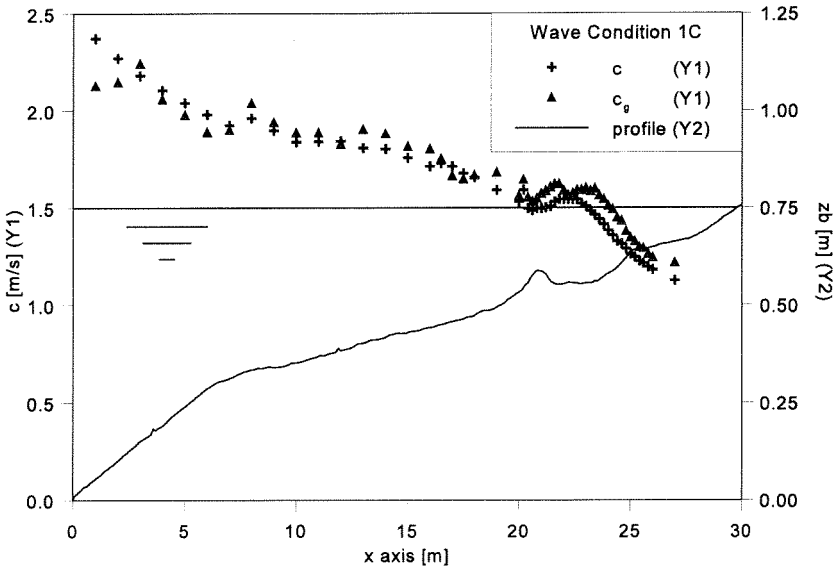


*Figure 3.15* Wave Celerity and Wave Group Celerity (1C)

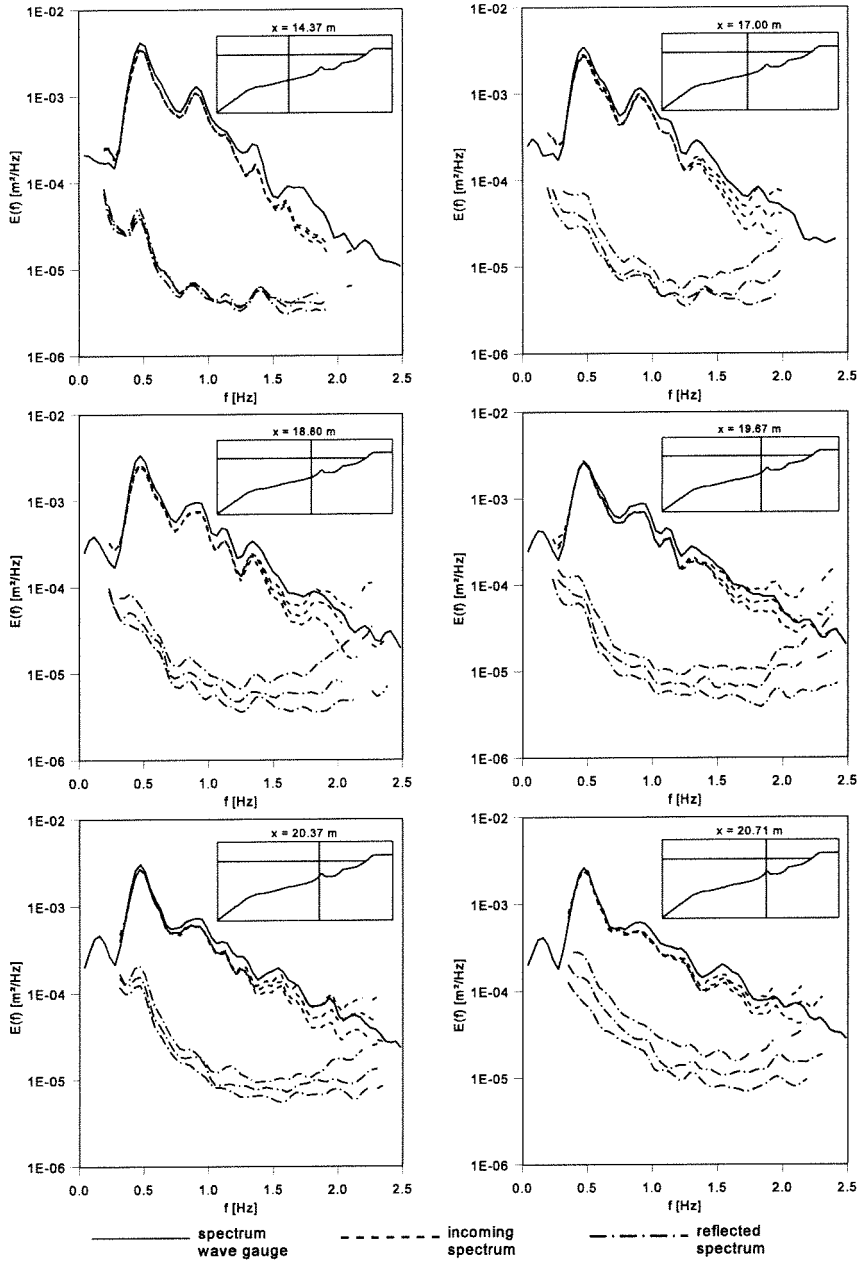


*Figure 3.16a* Energy Density Spectra of Incoming and Reflected Wave Energy (1A)

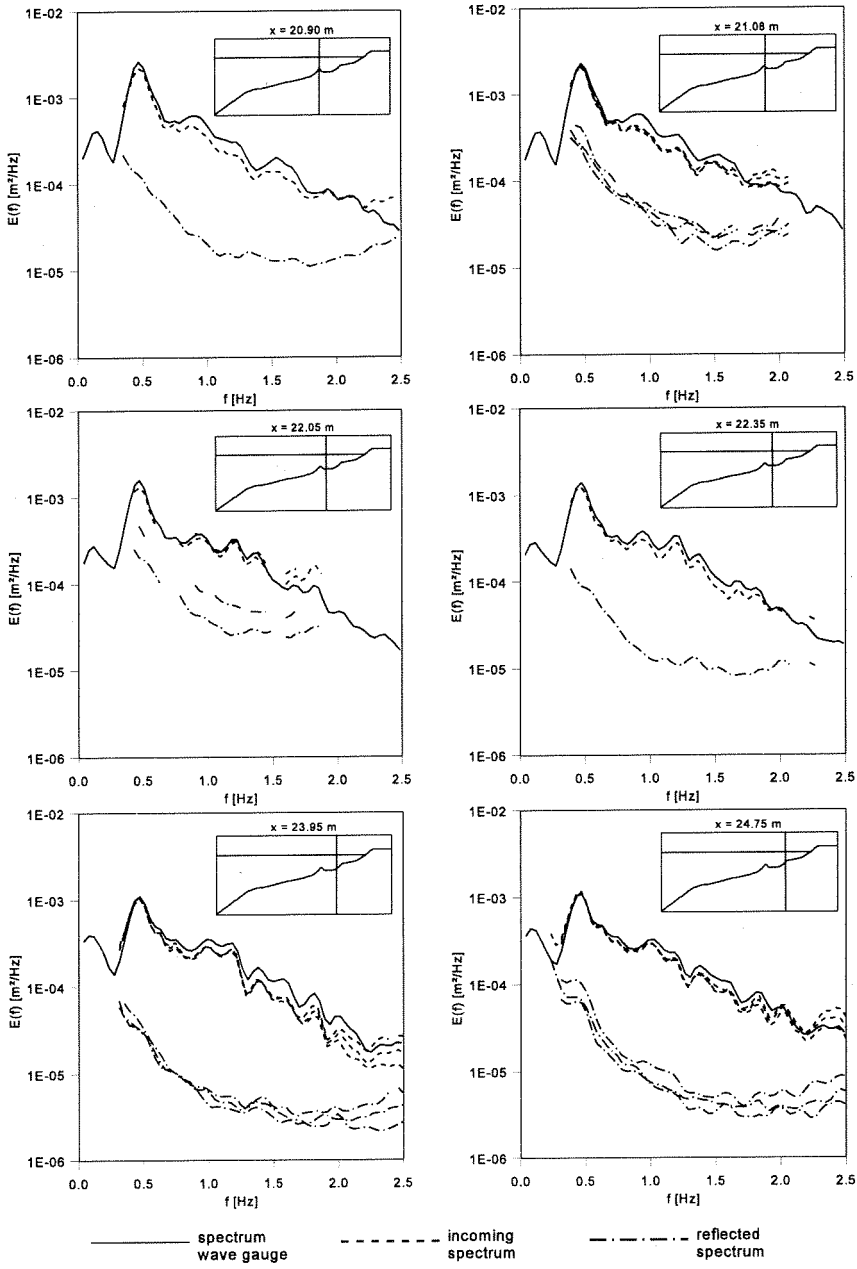


*Figure 3.16b* Energy Density Spectra of Incoming and Reflected Wave Energy (1A)

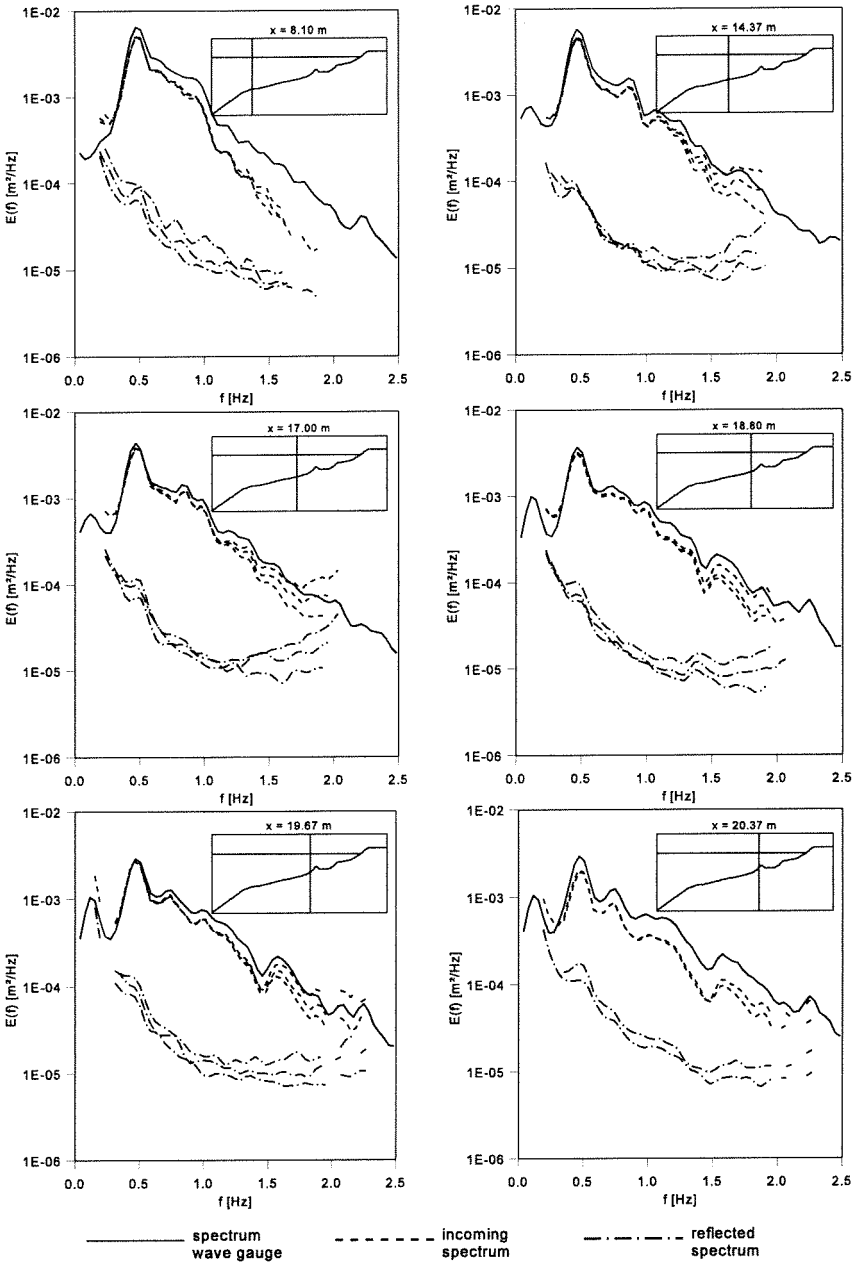


*Figure 3.17a* Energy Density Spectra of Incoming and Reflected Wave Energy (1B)

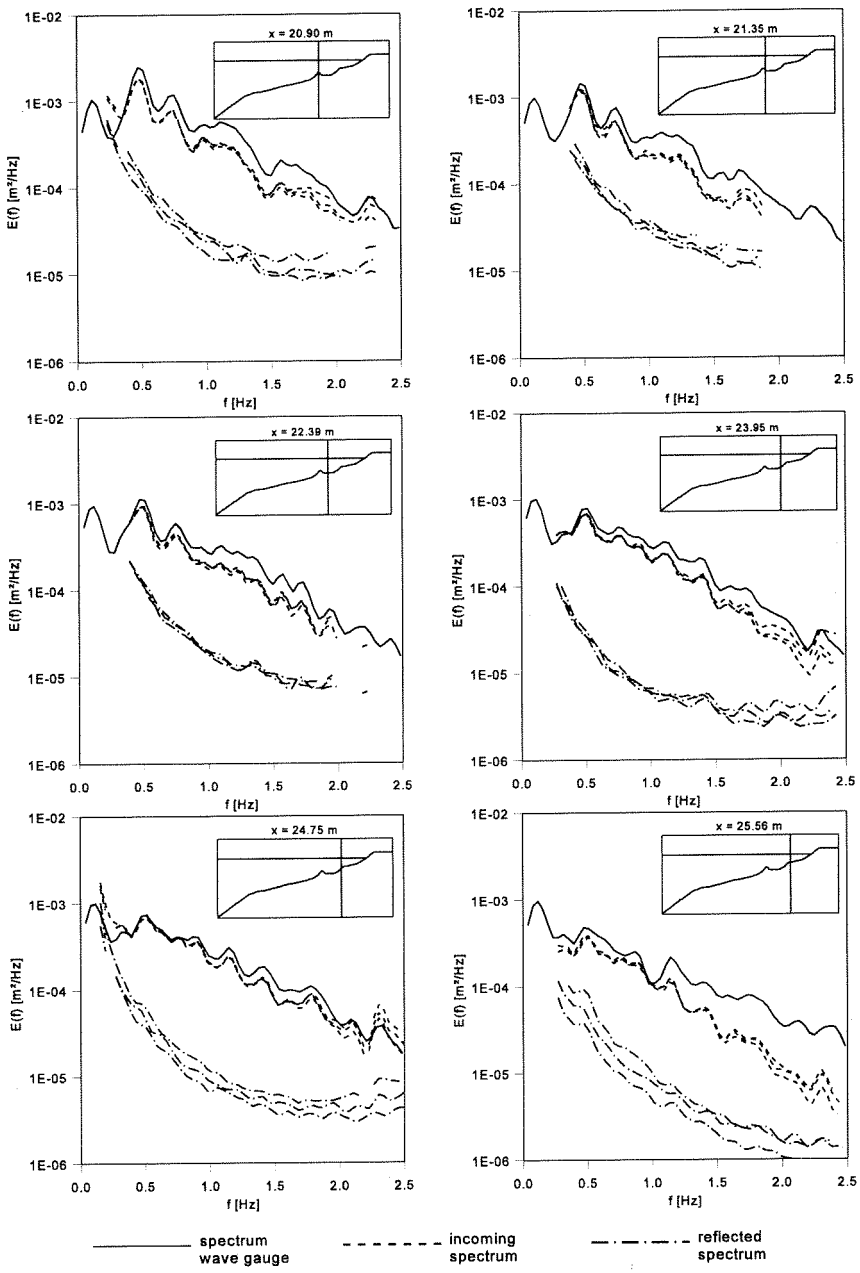


*Figure 3.17b* Energy Density Spectra of Incoming and Reflected Wave Energy (1B)

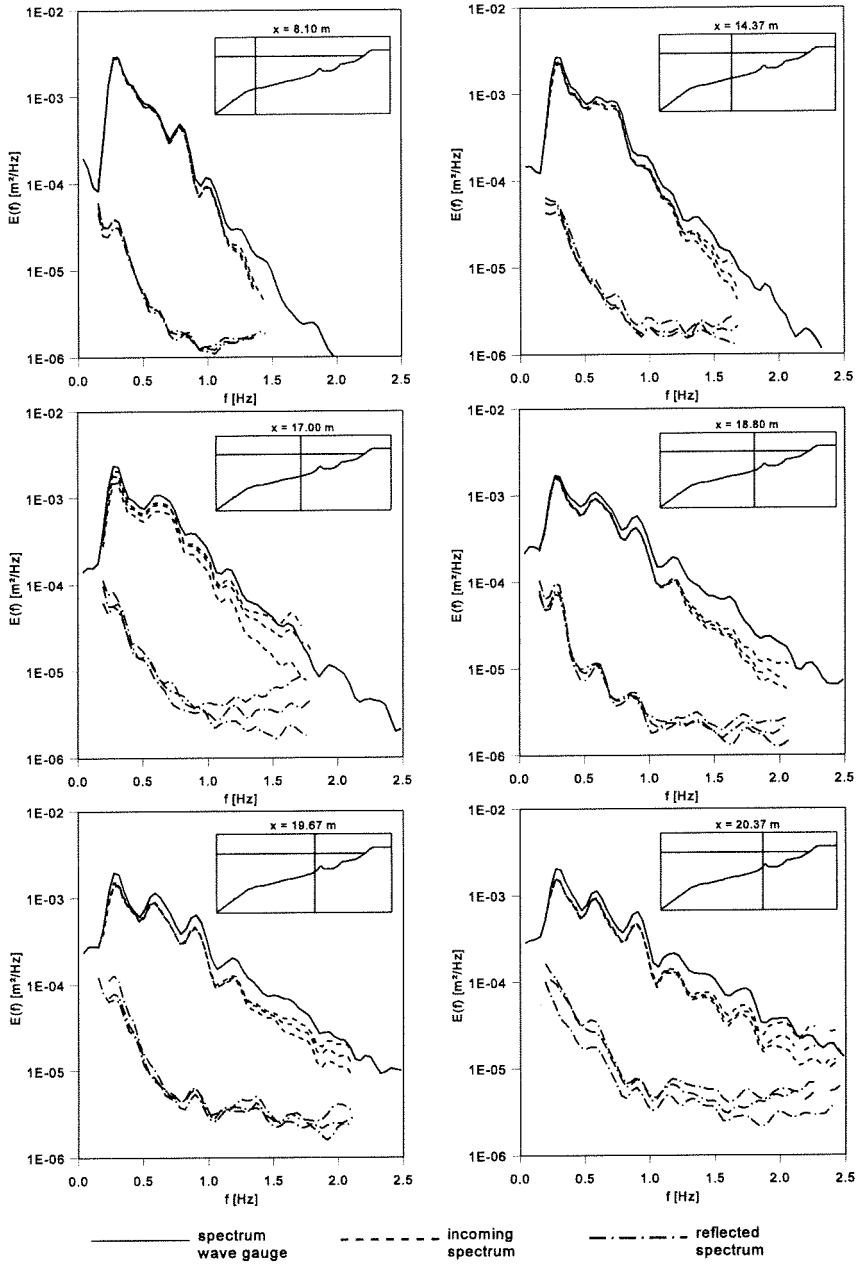


*Figure 3.18a* Energy Density Spectra of Incoming and Reflected Wave Energy (1C)

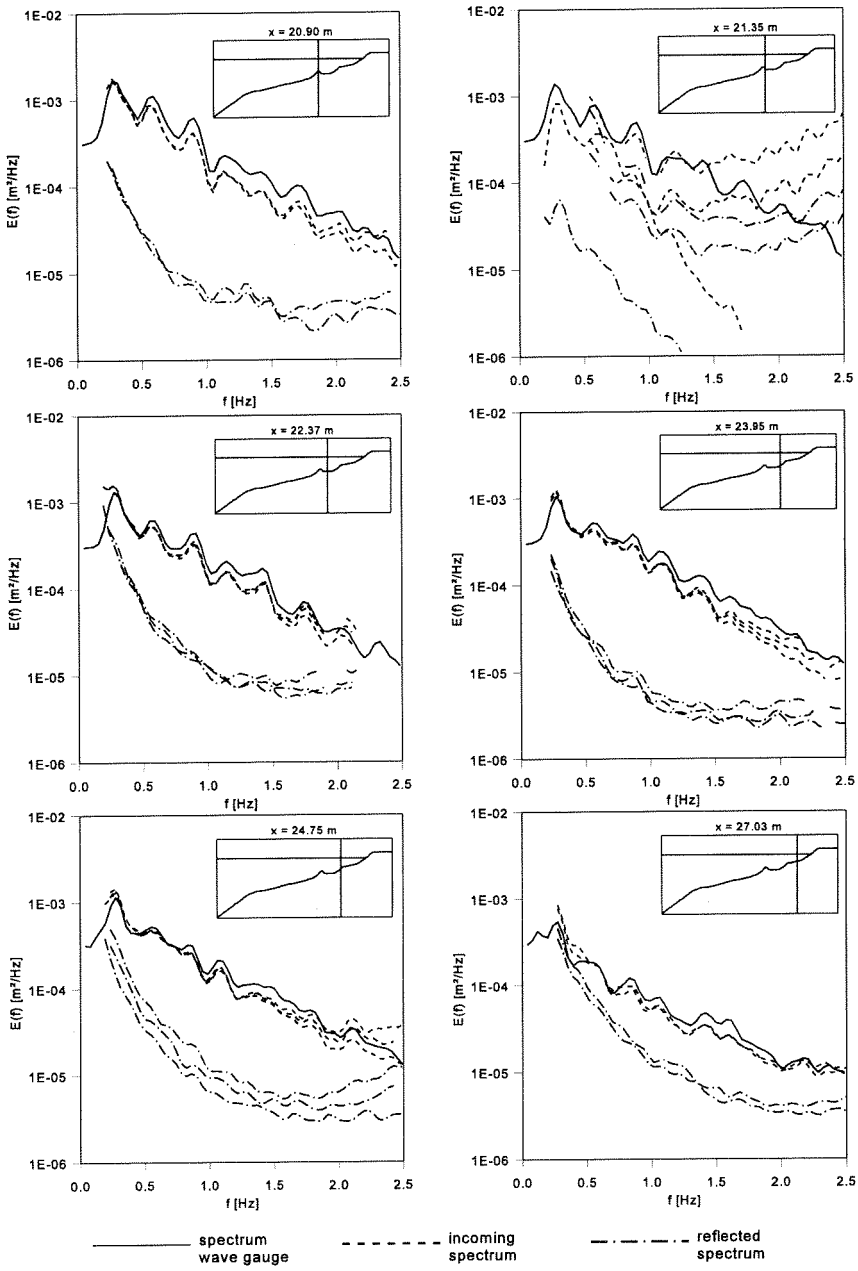


*Figure 3.18b* Energy Density Spectra of Incoming and Reflected Wave Energy (1C)

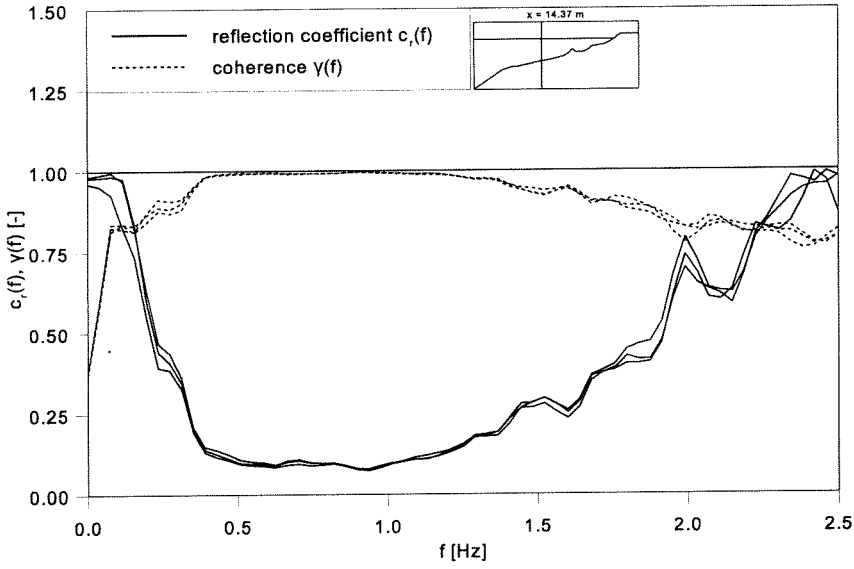


*Figure 3.19* Reflection Coefficient and Coherence outside Breaking Region (1A)

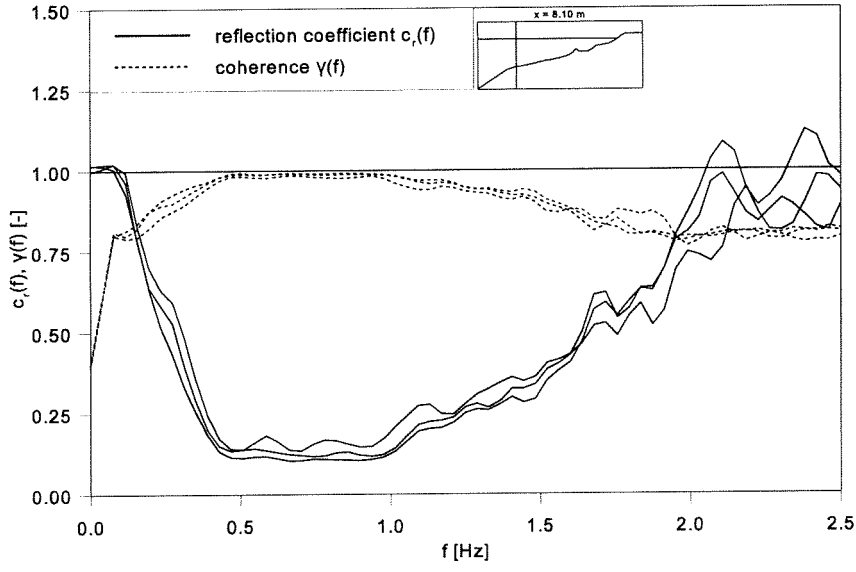


*Figure 3.20* Reflection Coefficient and Coherence outside Breaking Region (1B)

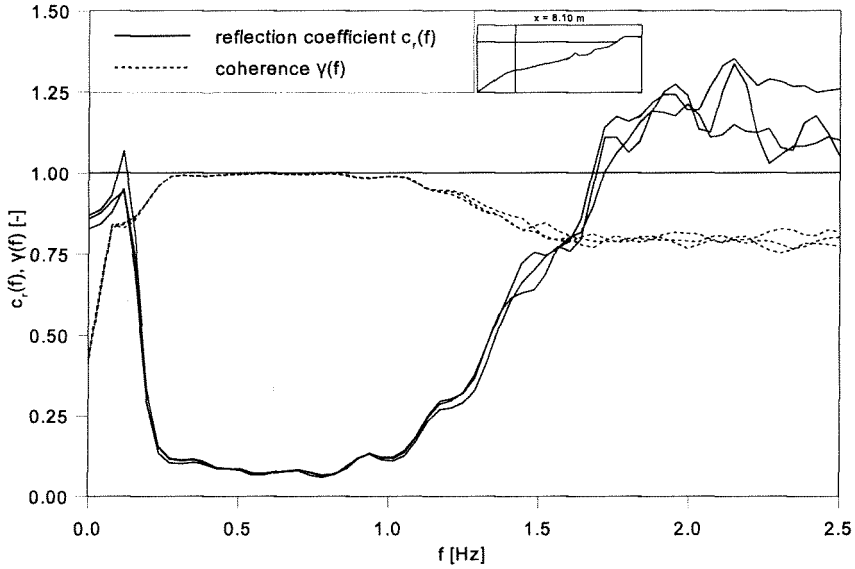


*Figure 3.21* Reflection Coefficient and Coherence outside Breaking Region (1C)

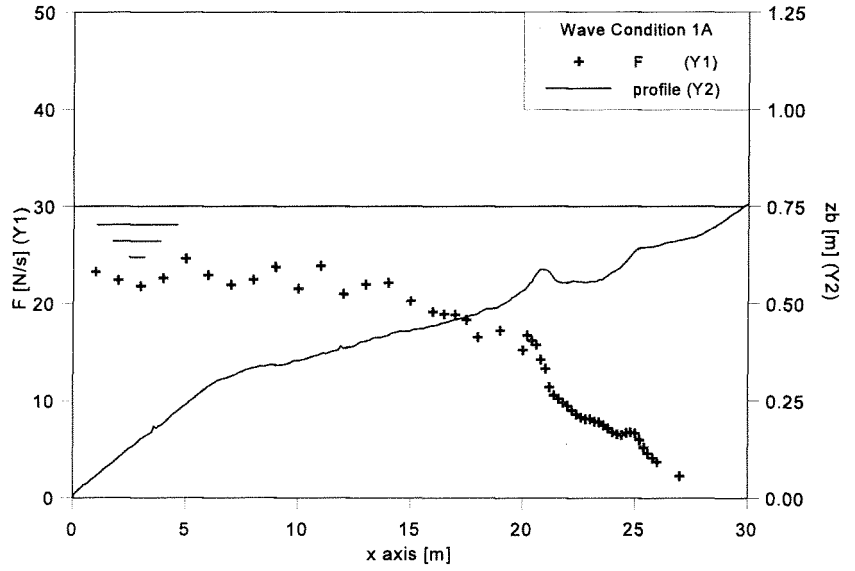


*Figure 3.22* Flux of Wave Energy (1A)

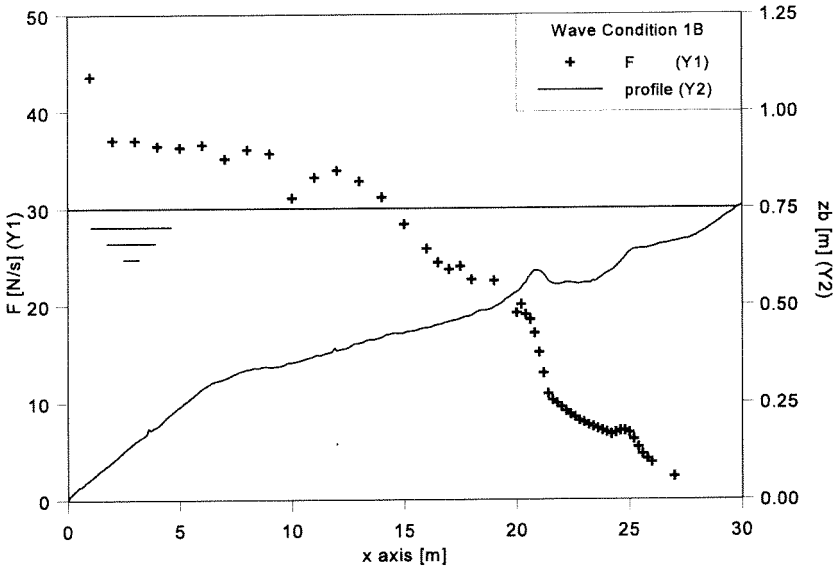


*Figure 3.23* Flux of Wave Energy (1B)

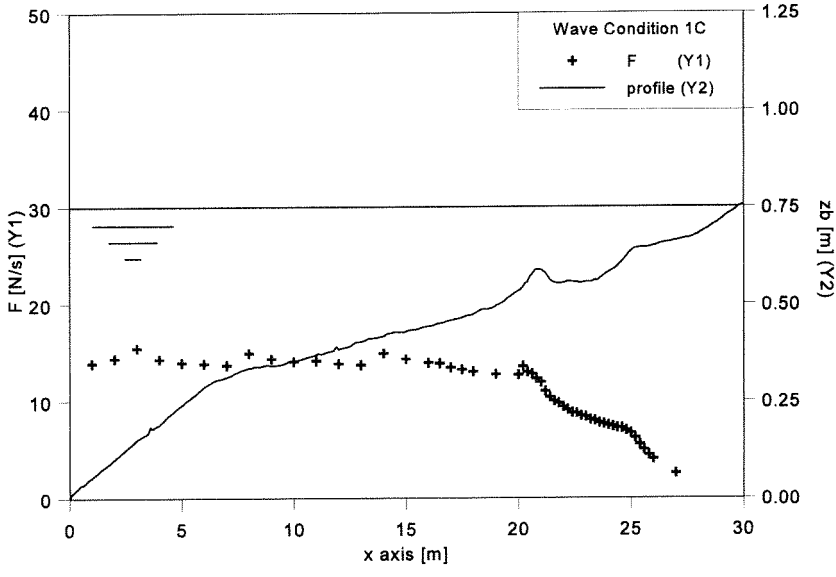


*Figure 3.24* Flux of Wave Energy (1C)

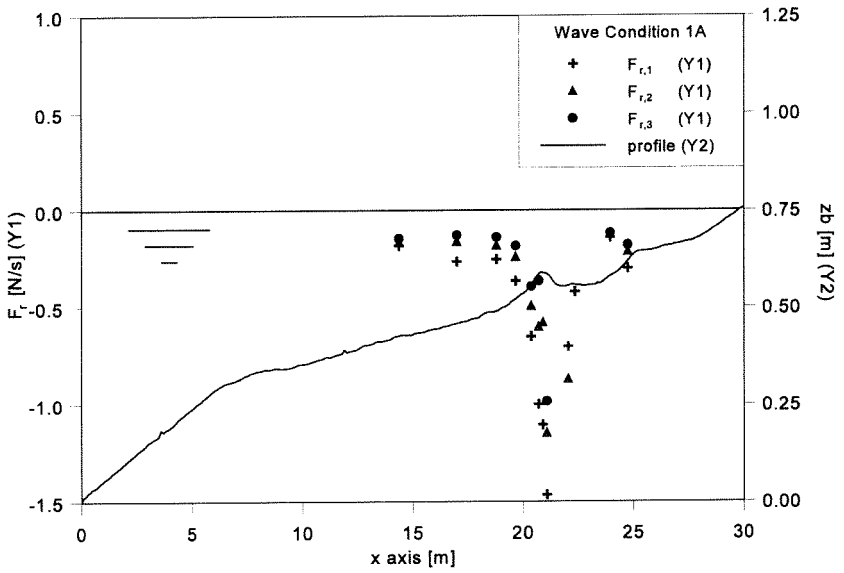


*Figure 3.25* Flux of Reflected Wave Energy (1A)

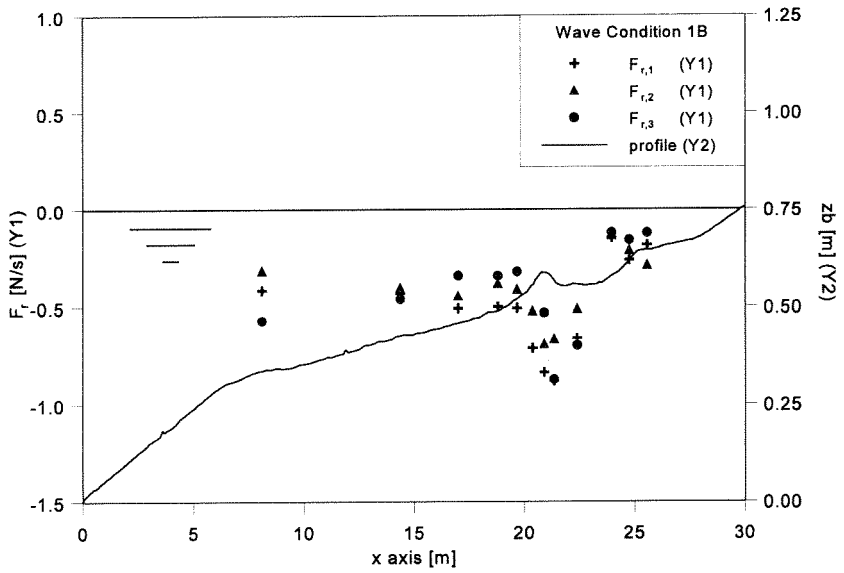


*Figure 3.26* Flux of Reflected Wave Energy (1B)

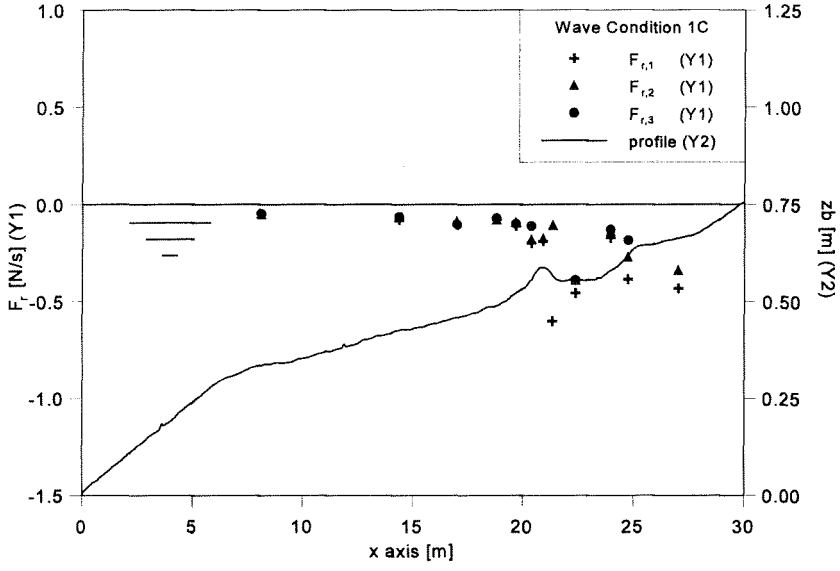


*Figure 3.27* Flux of Reflected Wave Energy (1C)

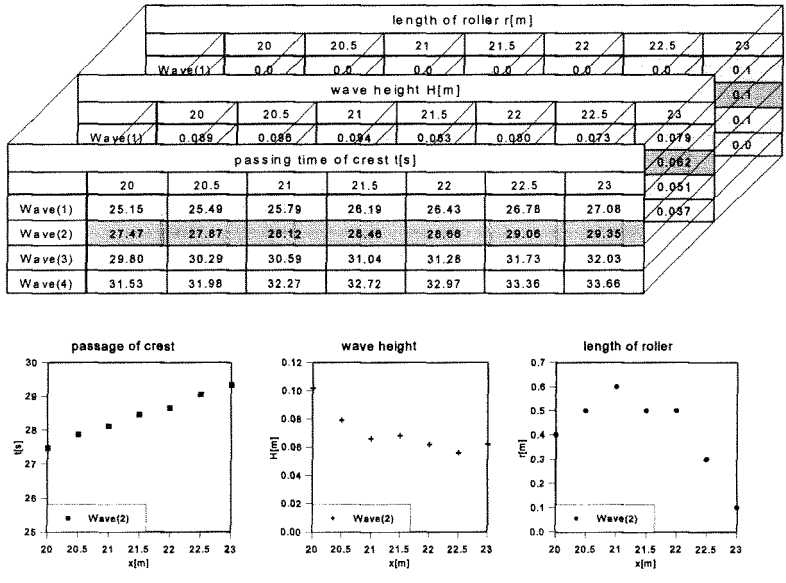


| | 20 | 20.5 | 21 | 21.5 | 22 | 22.5 | 23 |
|---|---|---|---|---|---|---|---|
| Wave(1) | 25.15 | 25.49 | 25.79 | 26.19 | 26.43 | 26.78 | 27.08 |
| Wave(2) | 27.47 | 27.87 | 28.12 | 28.46 | 28.66 | 29.06 | 29.35 |
| Wave(3) | 29.80 | 30.29 | 30.59 | 31.04 | 31.26 | 31.73 | 32.03 |
| Wave(4) | 31.53 | 31.98 | 32.27 | 32.72 | 32.97 | 33.36 | 33.66 |

*Figure 3.28* Analysis of Wave Propagation with Breaking

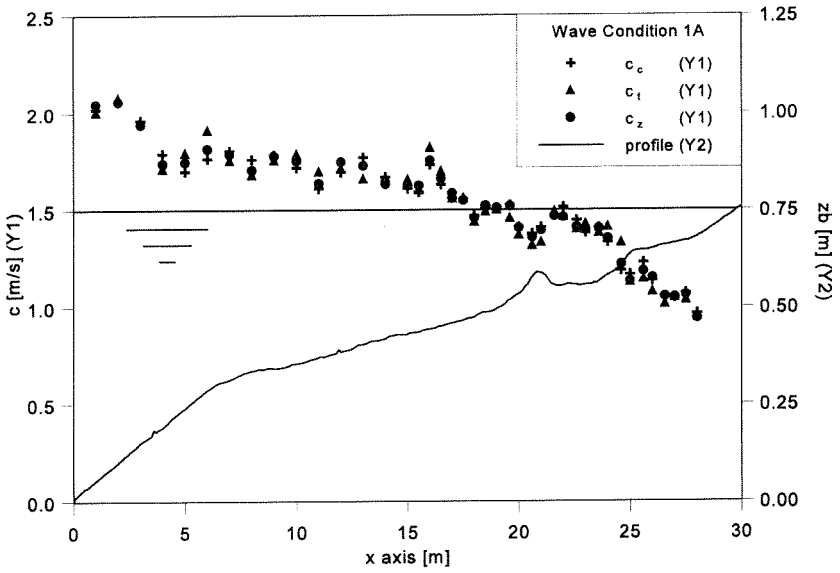


*Figure 3.29* Celerity of Crest, Trough and Zero-Crossing (1A)

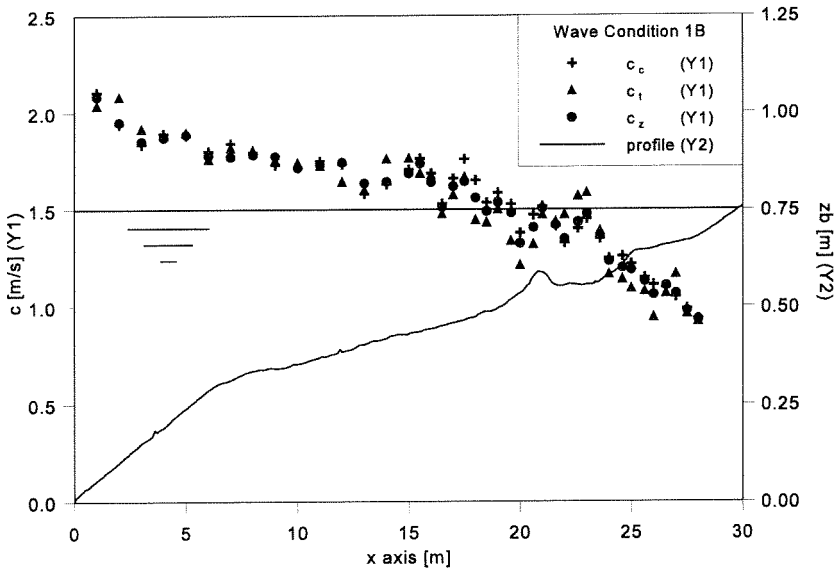


*Figure 3.30* Celerity of Crest, Trough and Zero-Crossing (1B)

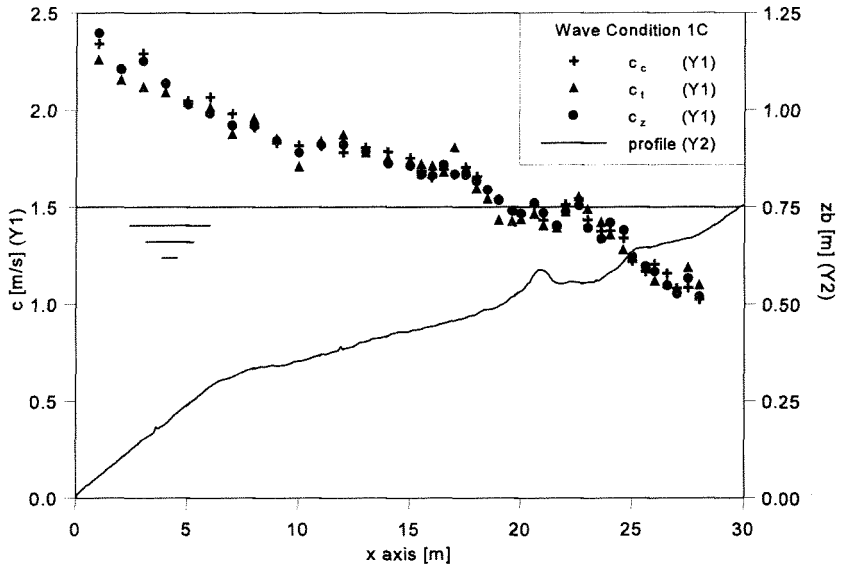


*Figure 3.31* Celerity of Crest, Trough and Zero-Crossing (1C)

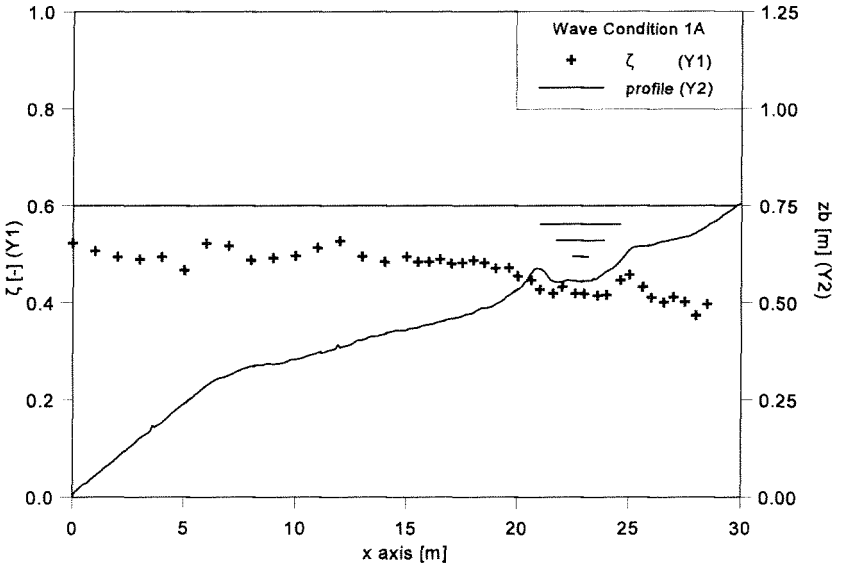


*Figure 3.32* Asymmetry of Waves (1A)

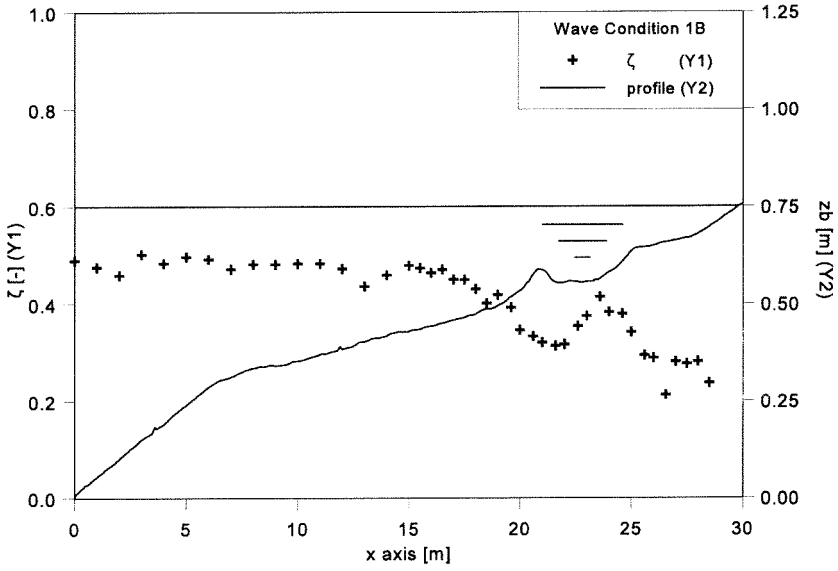


*Figure 3.33* Asymmetry of Waves (1B)

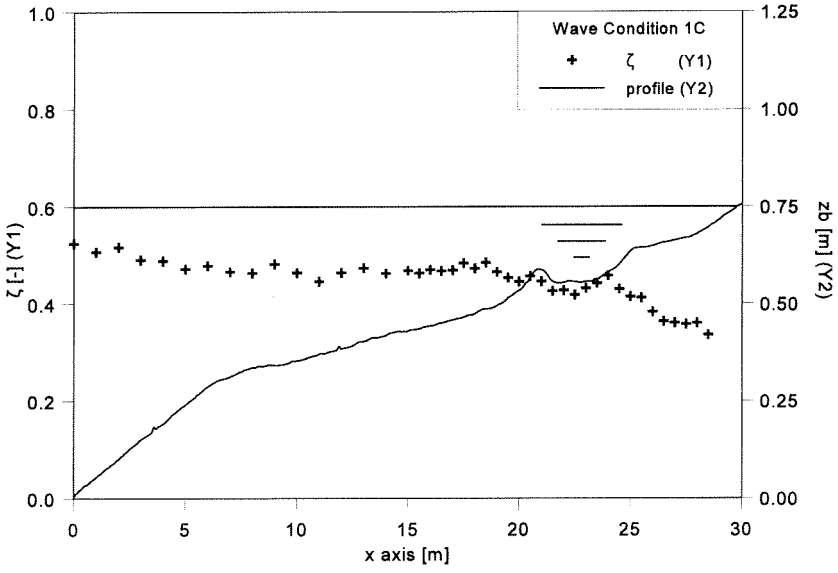


*Figure 3.34* Asymmetry of Waves (1C)

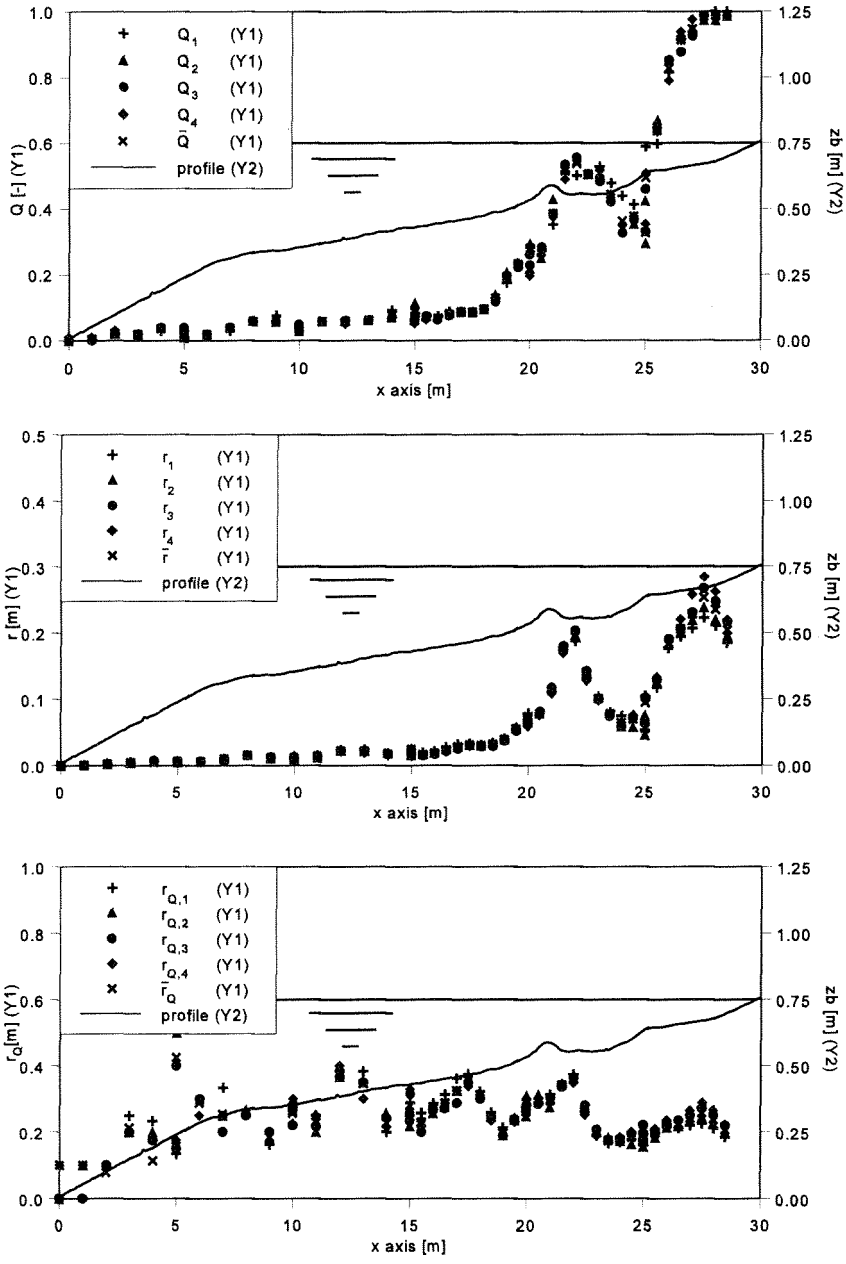


*Figure 3.35* Breaking Characteristics Q, r and $r_Q$ (1A)

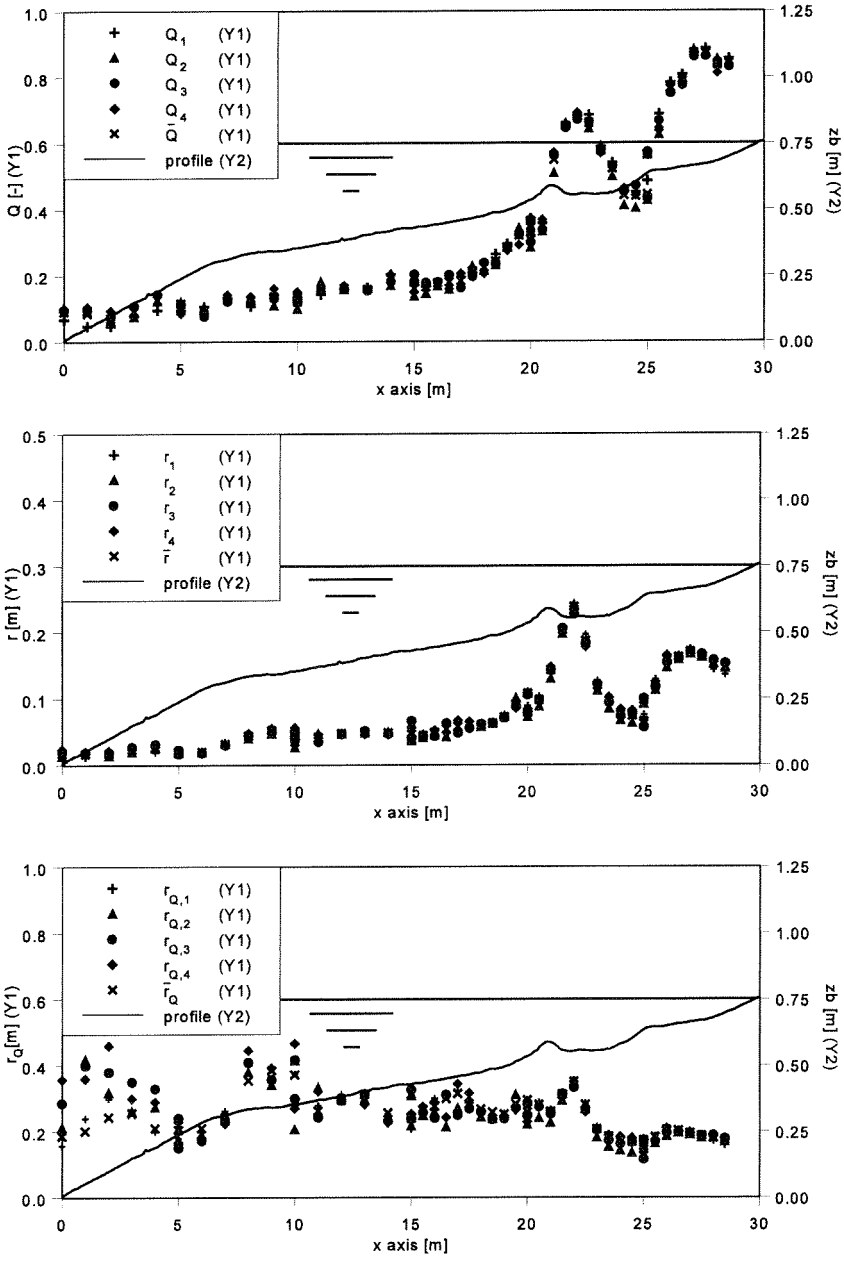


*Figure 3.36* Breaking Characteristics Q, r and $r_Q$ (1B)

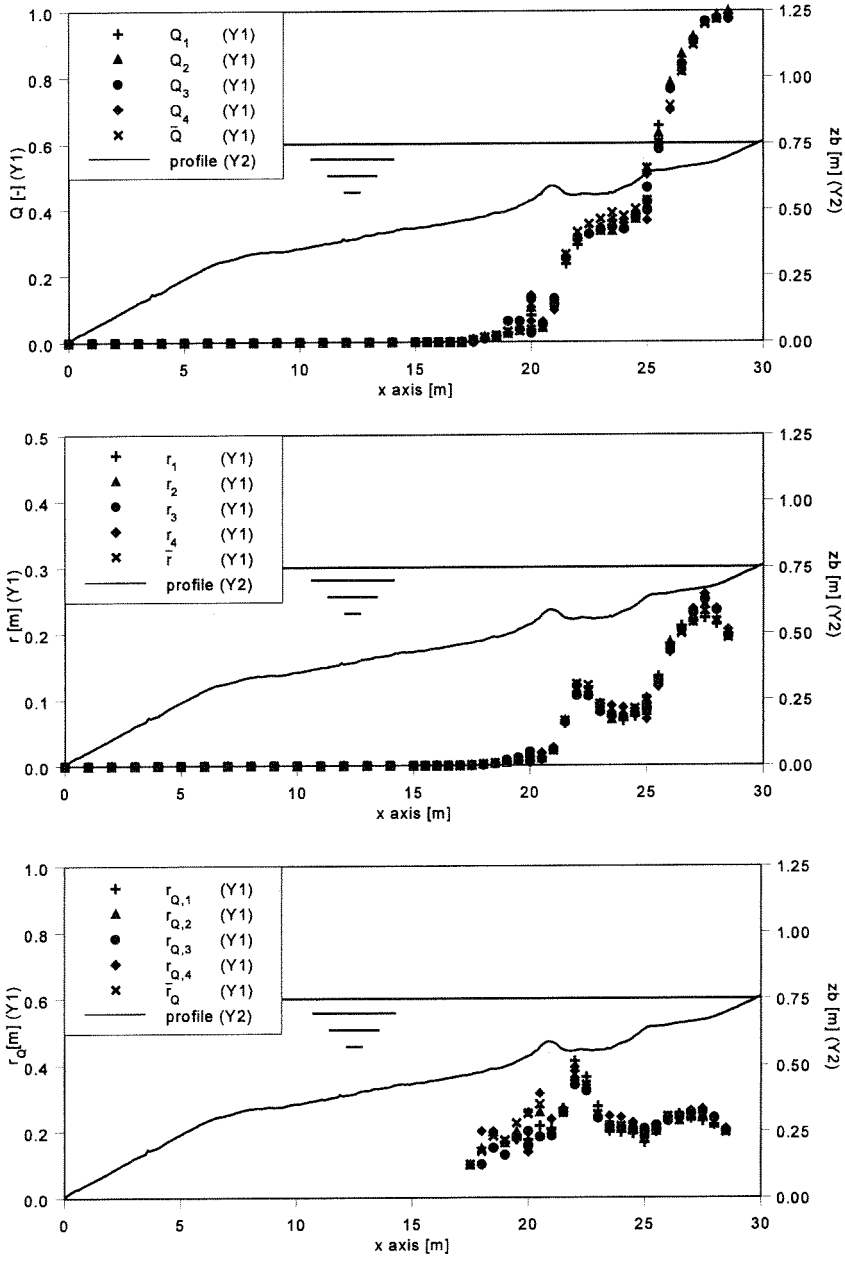


*Figure 3.37* Breaking Characteristics Q, r and $r_Q$ (1C)

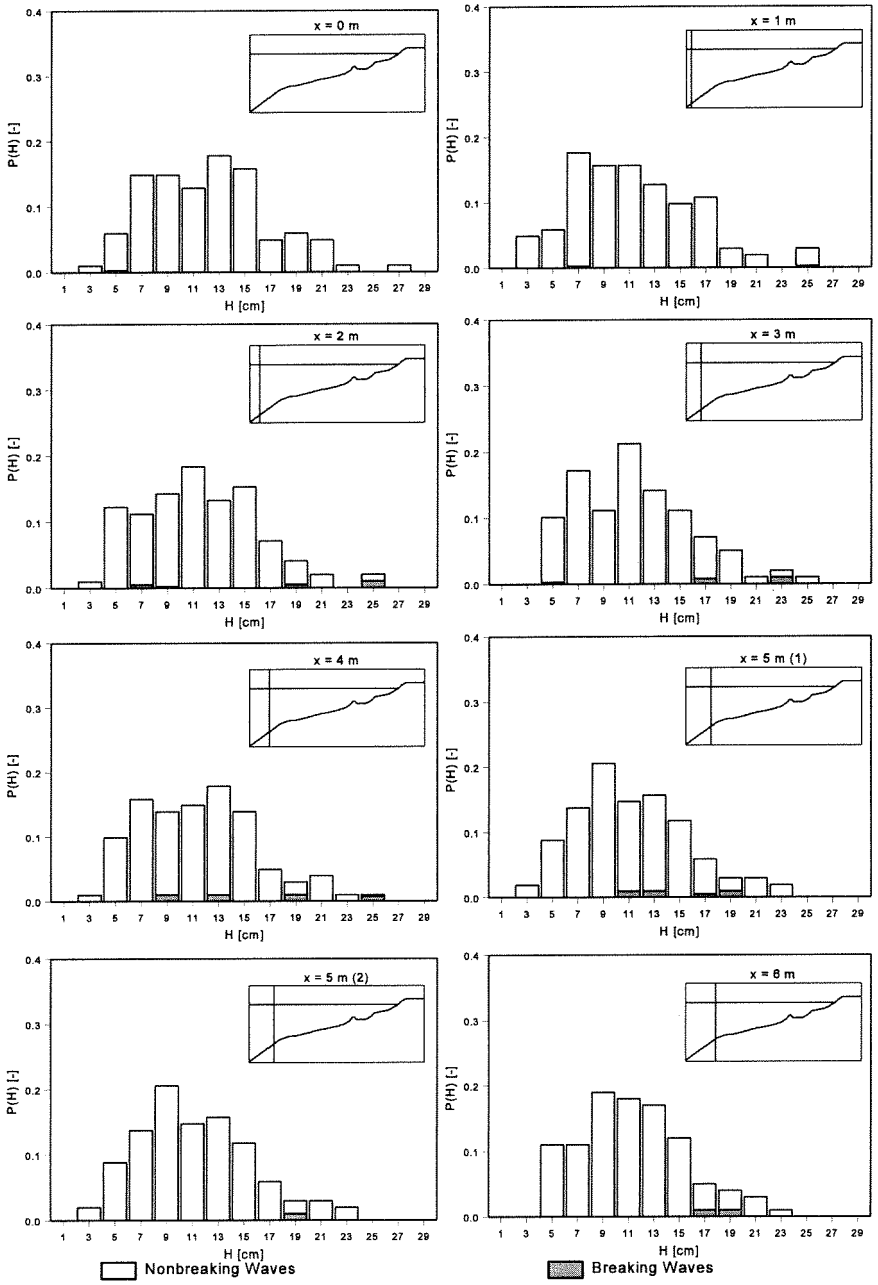


*Figure 3.38a* Wave Height Distribution 1A; Location: x = 0 - 6 m

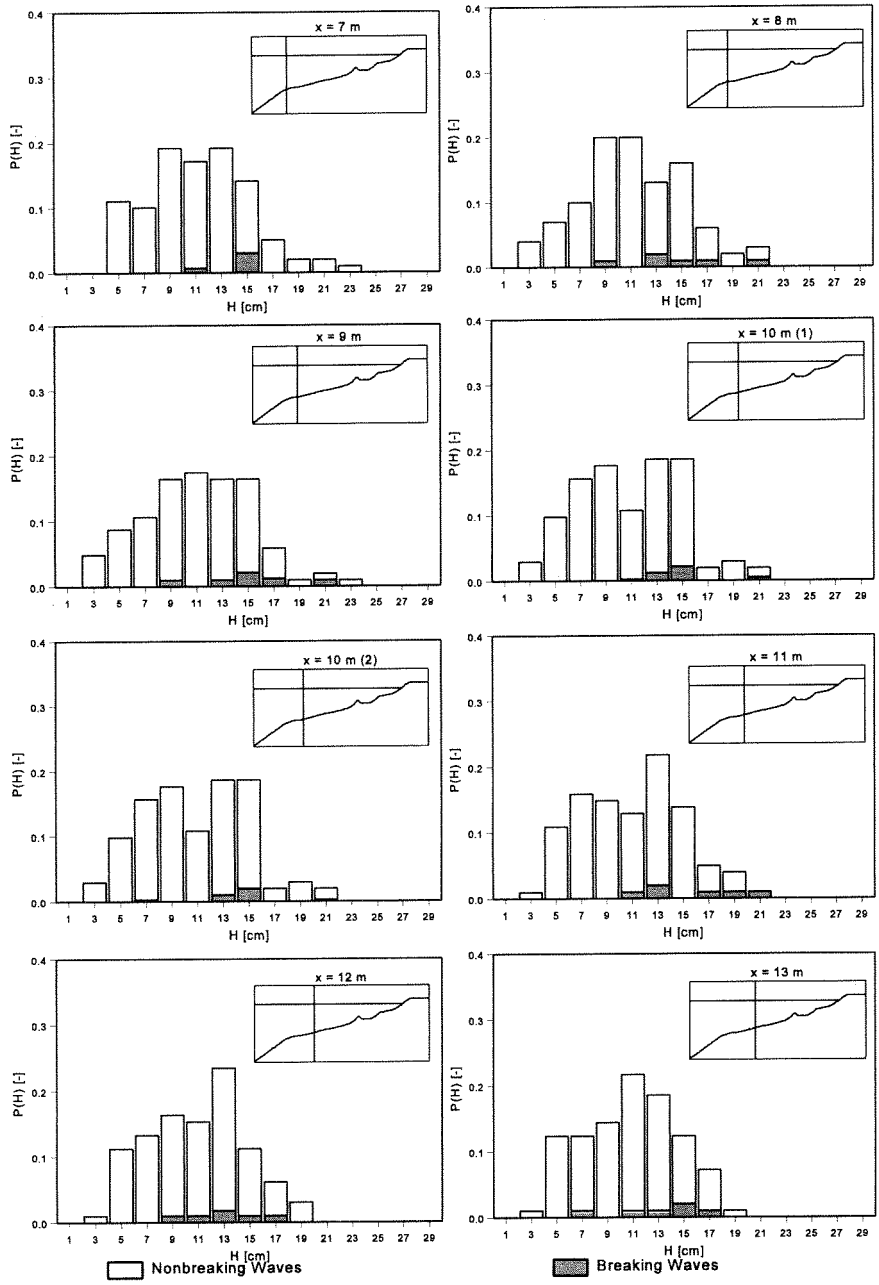


*Figure 3.38b* Wave Height Distribution 1A; Location: x = 7 - 13 m

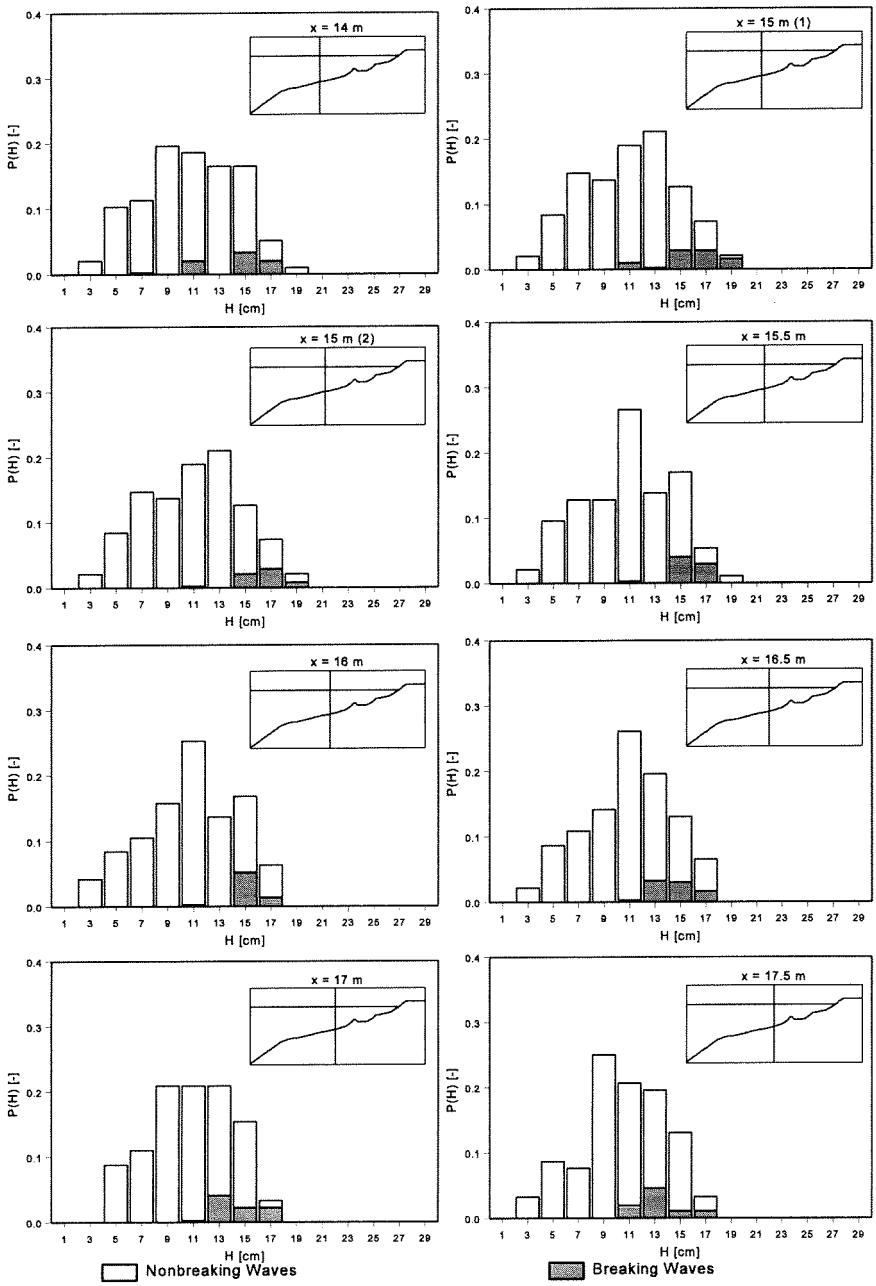


*Figure 3.38c* Wave Height Distribution 1A; Location: x = 14 - 17.5 m

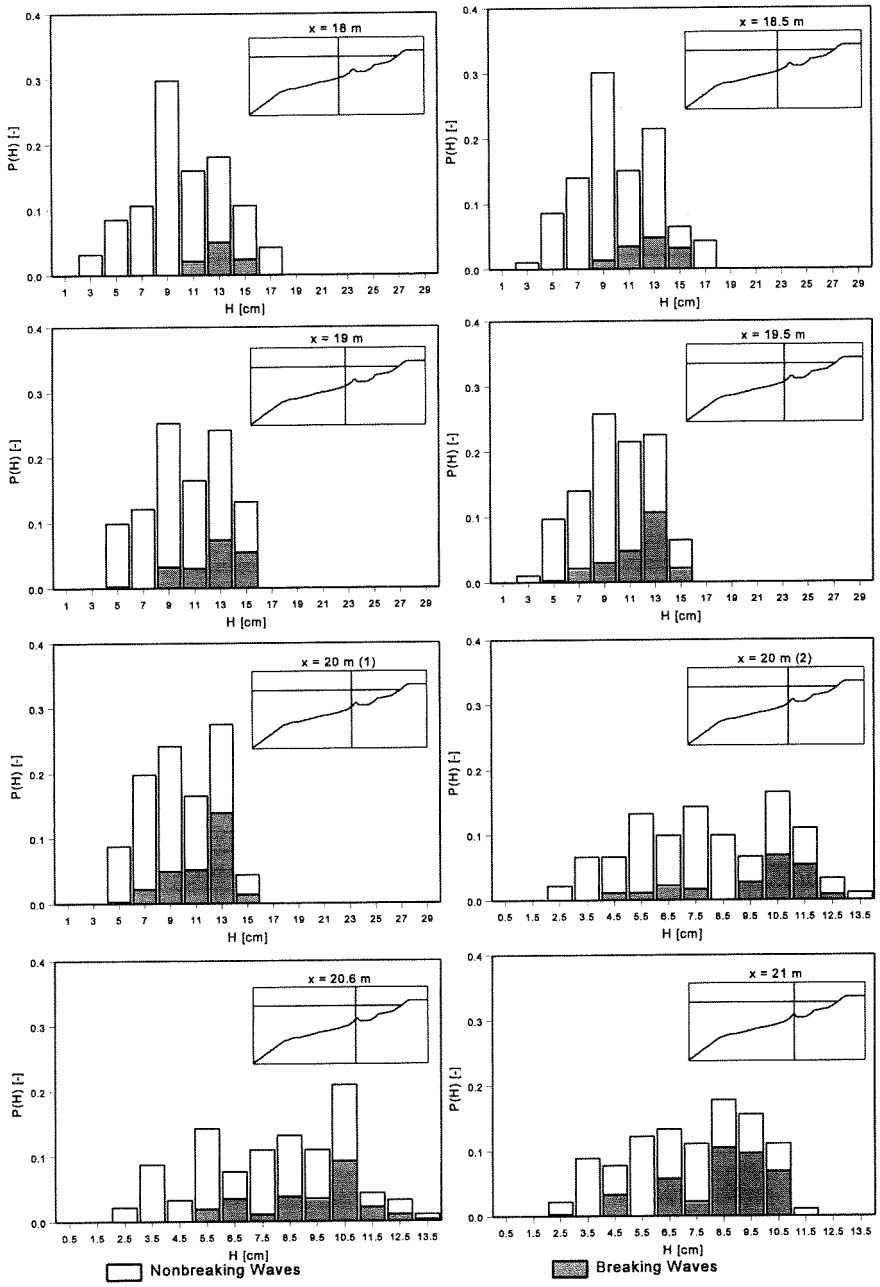


*Figure 3.38d* Wave Height Distribution 1A; Location: x = 18 - 21 m

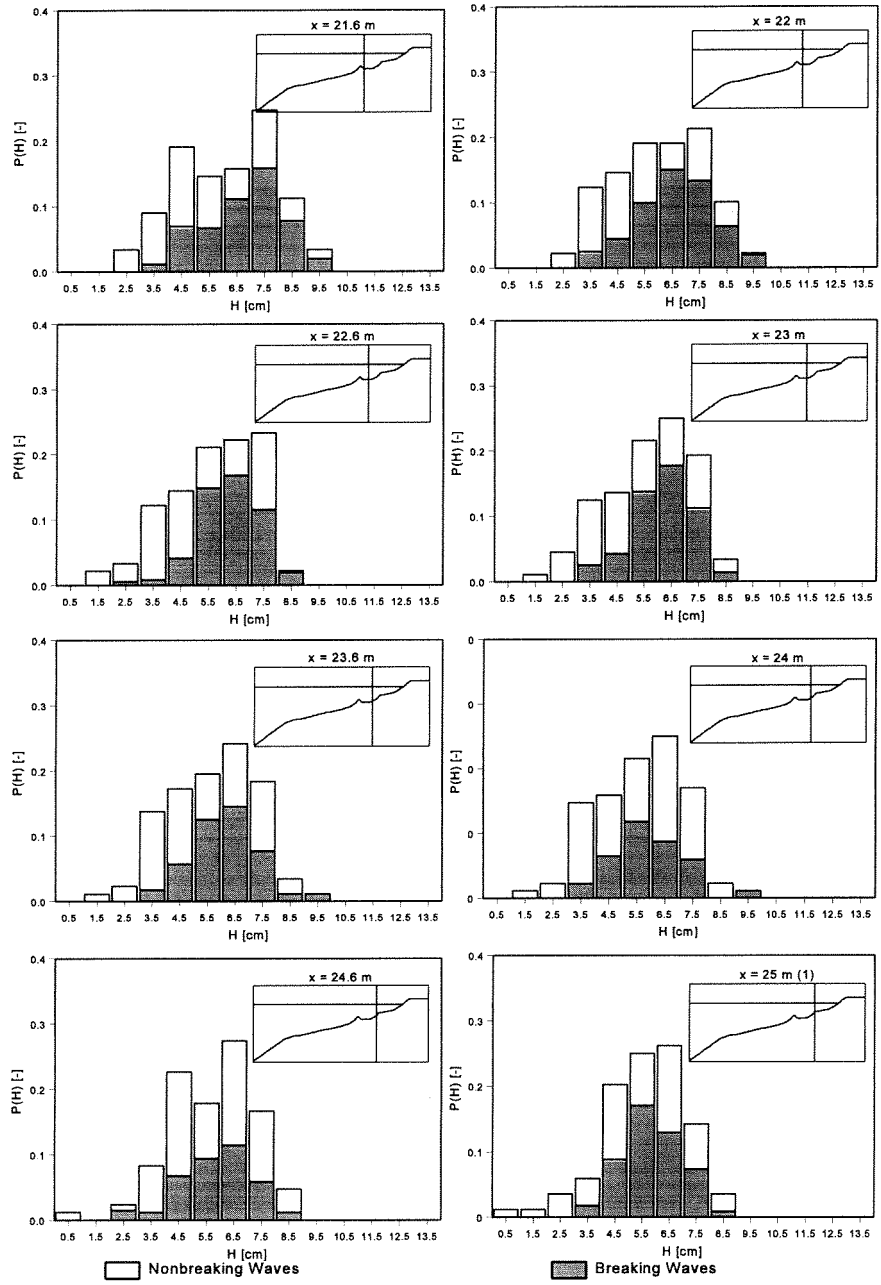


*Figure 3.38e* Wave Height Distribution 1A; Location: x = 21.6 - 25 m

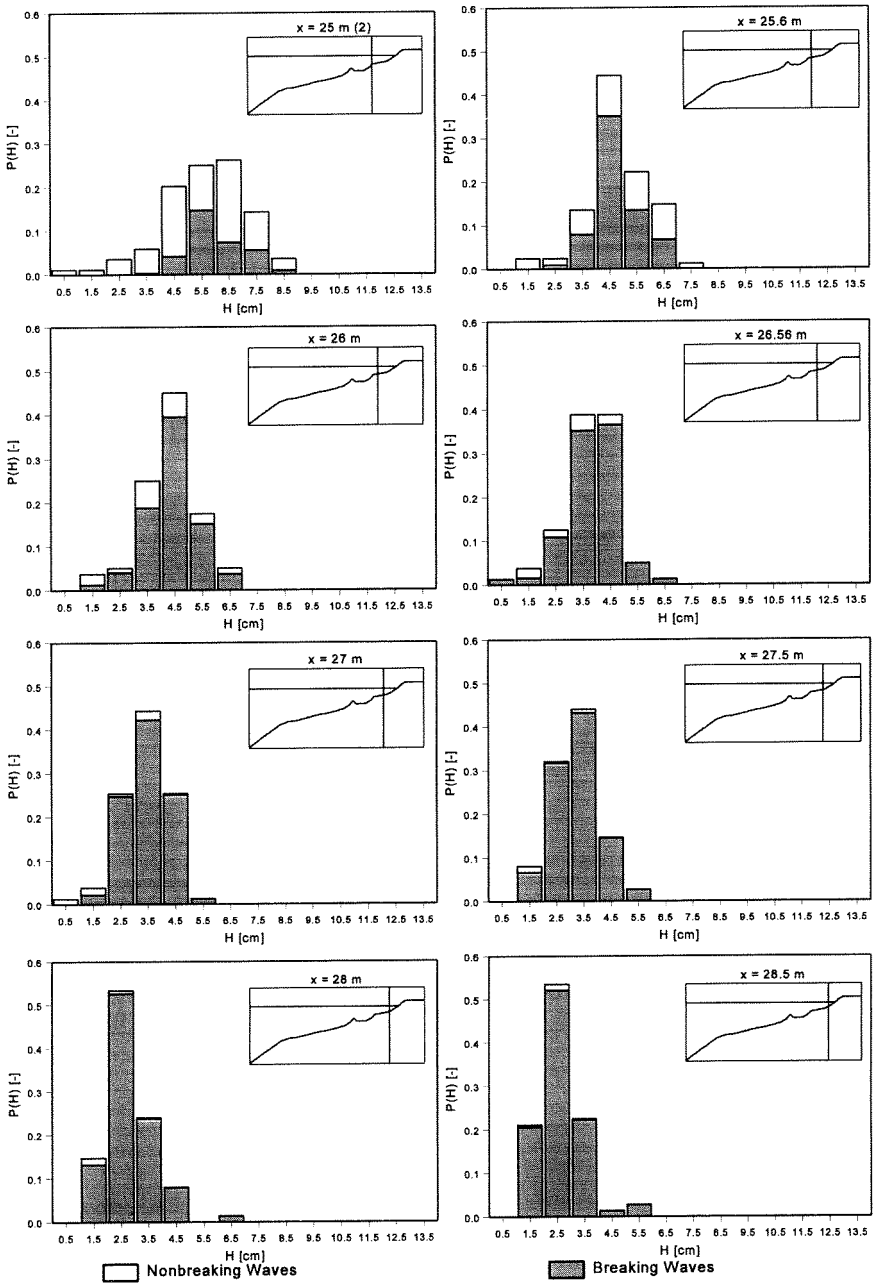


*Figure 3.38f* Wave Height Distribution 1A; Location: x = 25 - 28.5 m

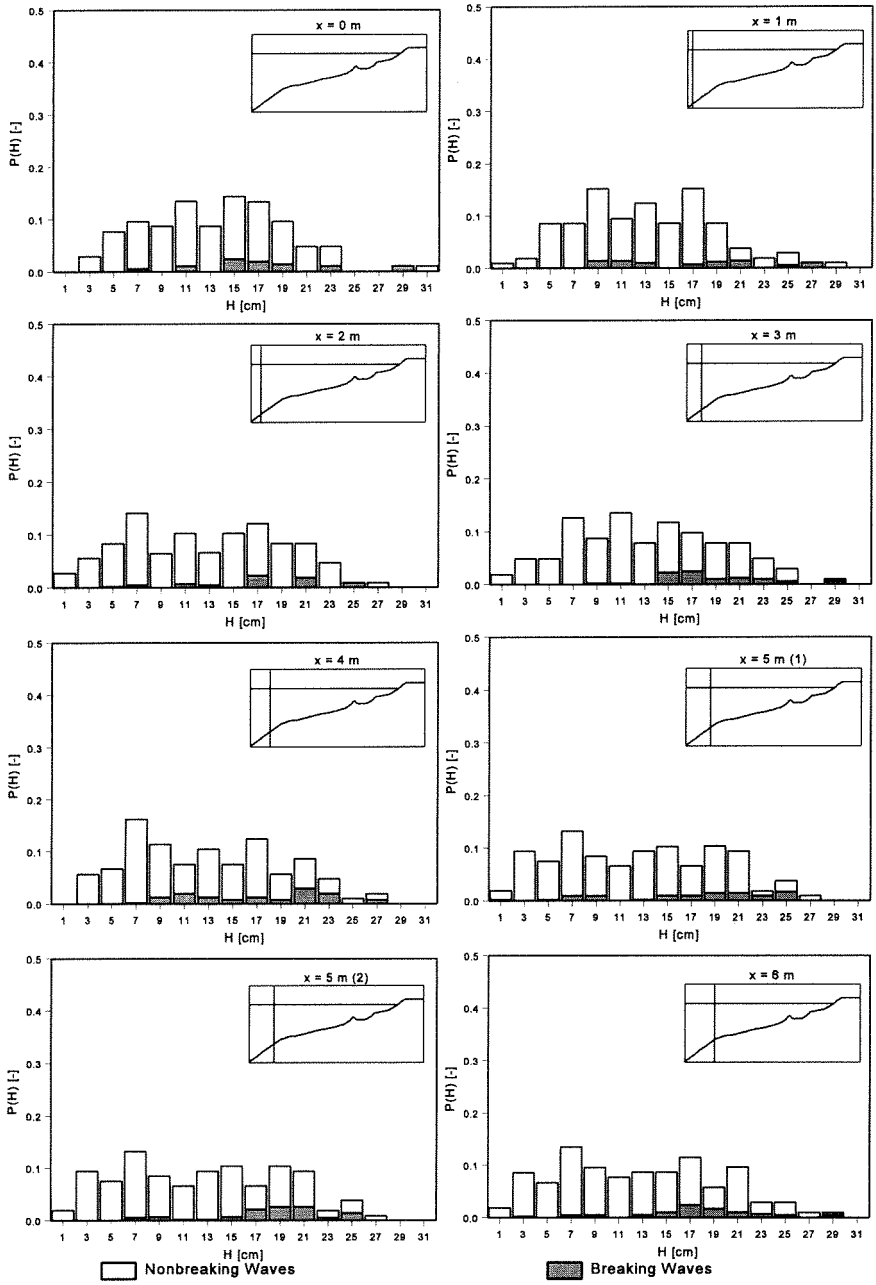


*Figure 3.39a* Wave Height Distribution 1B; Location: x = 0 - 6 m

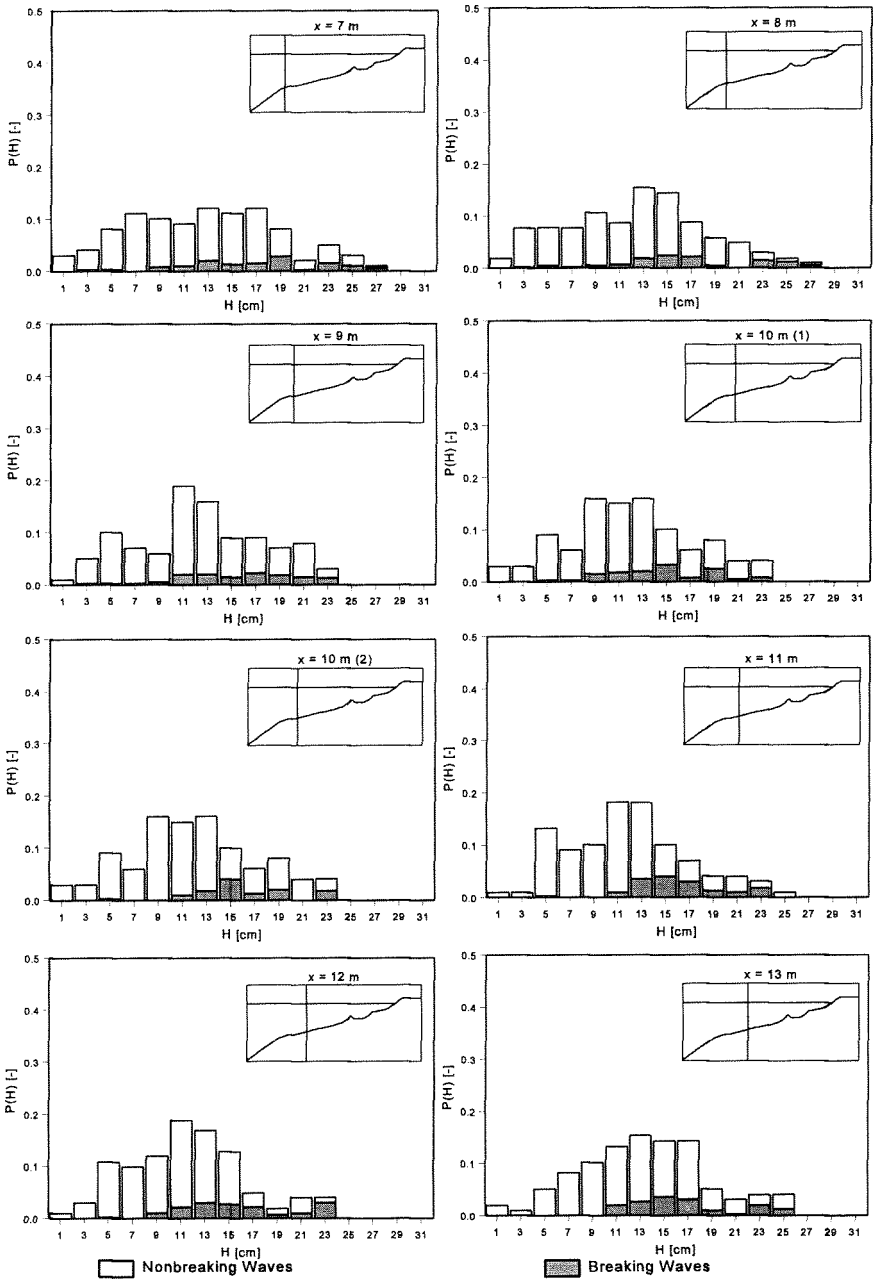


*Figure 3.39b* Wave Height Distribution 1B; Location: x = 7 - 13 m

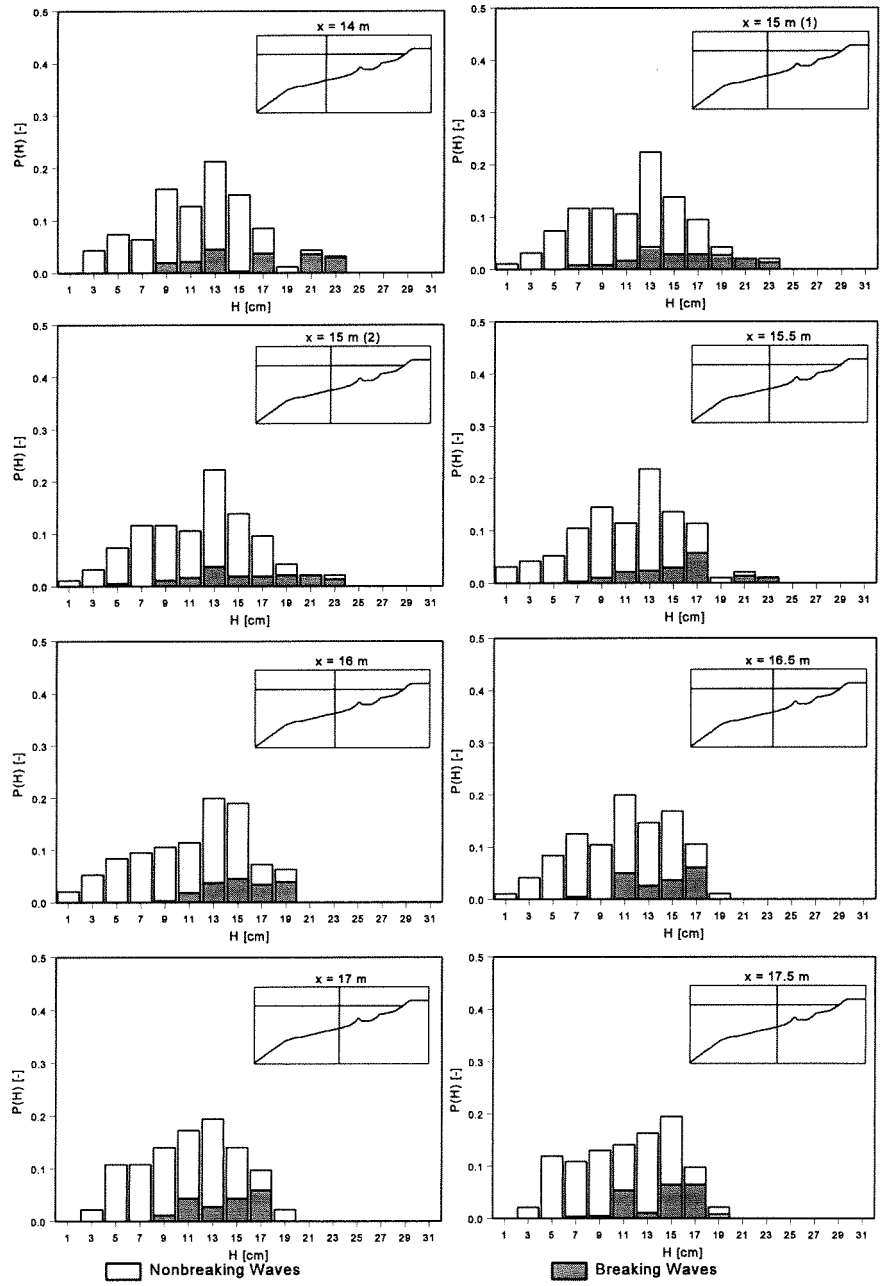


*Figure 3.39c* Wave Height Distribution 1B; Location: x = 14 - 17.5 m

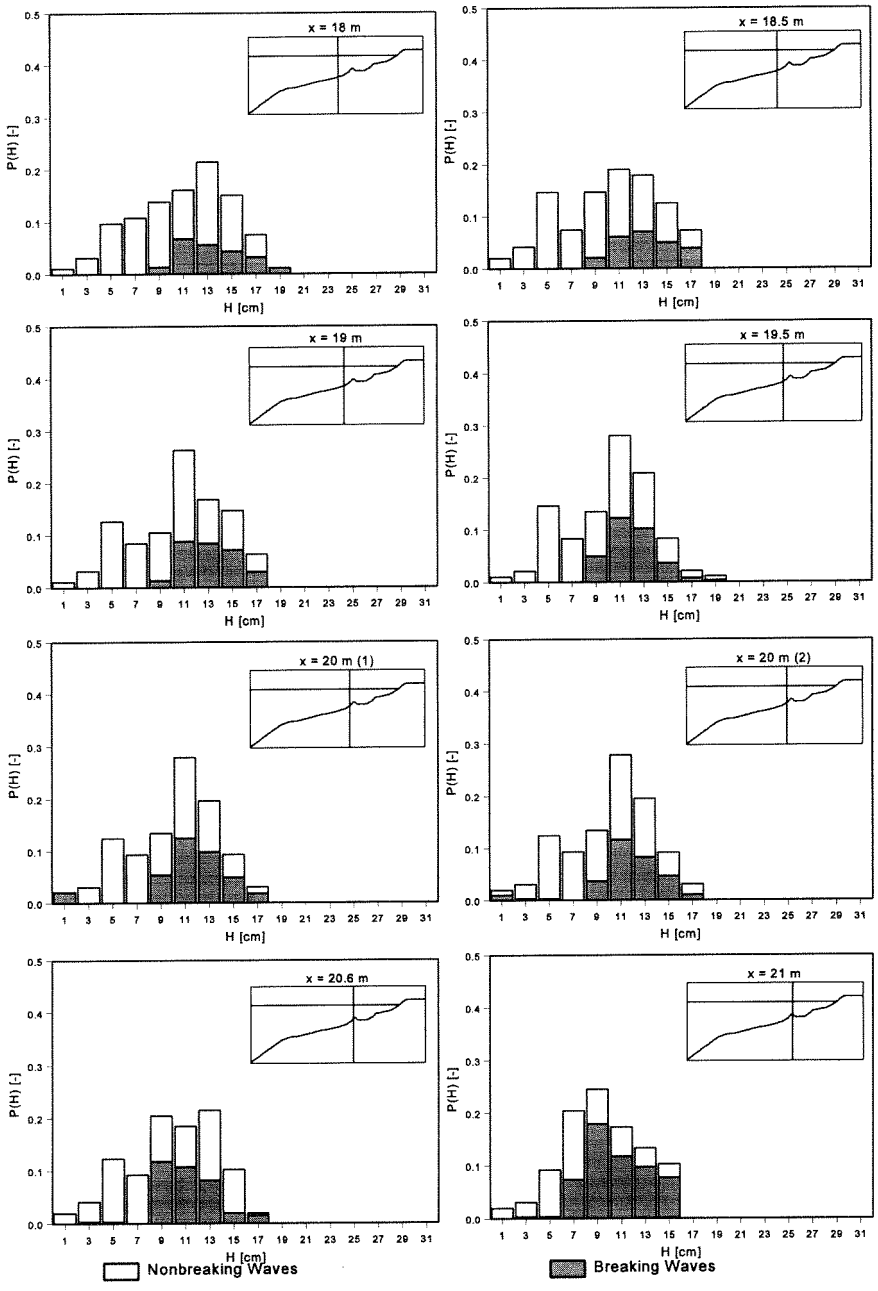


*Figure 3.39d* Wave Height Distribution 1B; Location: x = 18 - 21 m

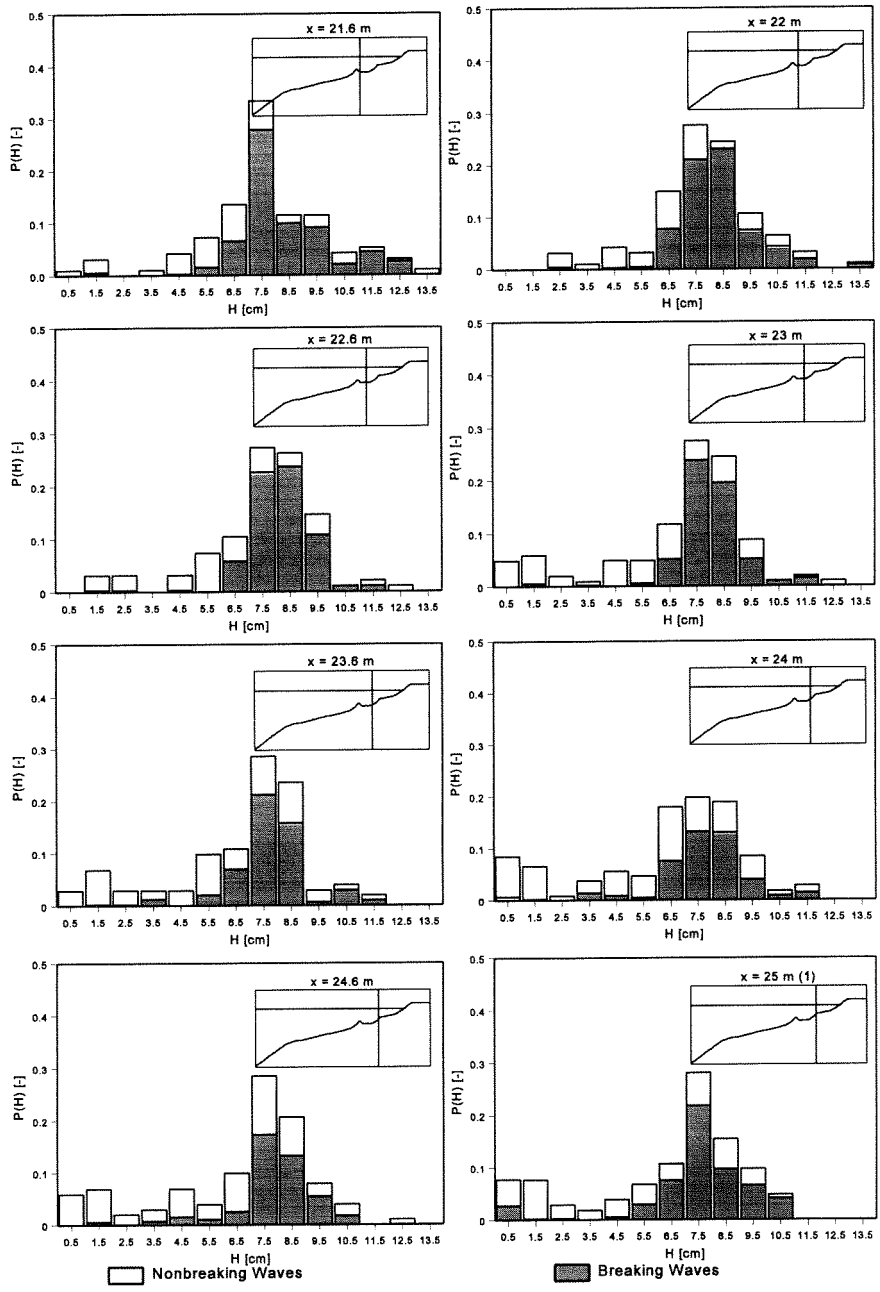


*Figure 3.39e* Wave Height Distribution 1B; Location: x = 21.6 - 25 m

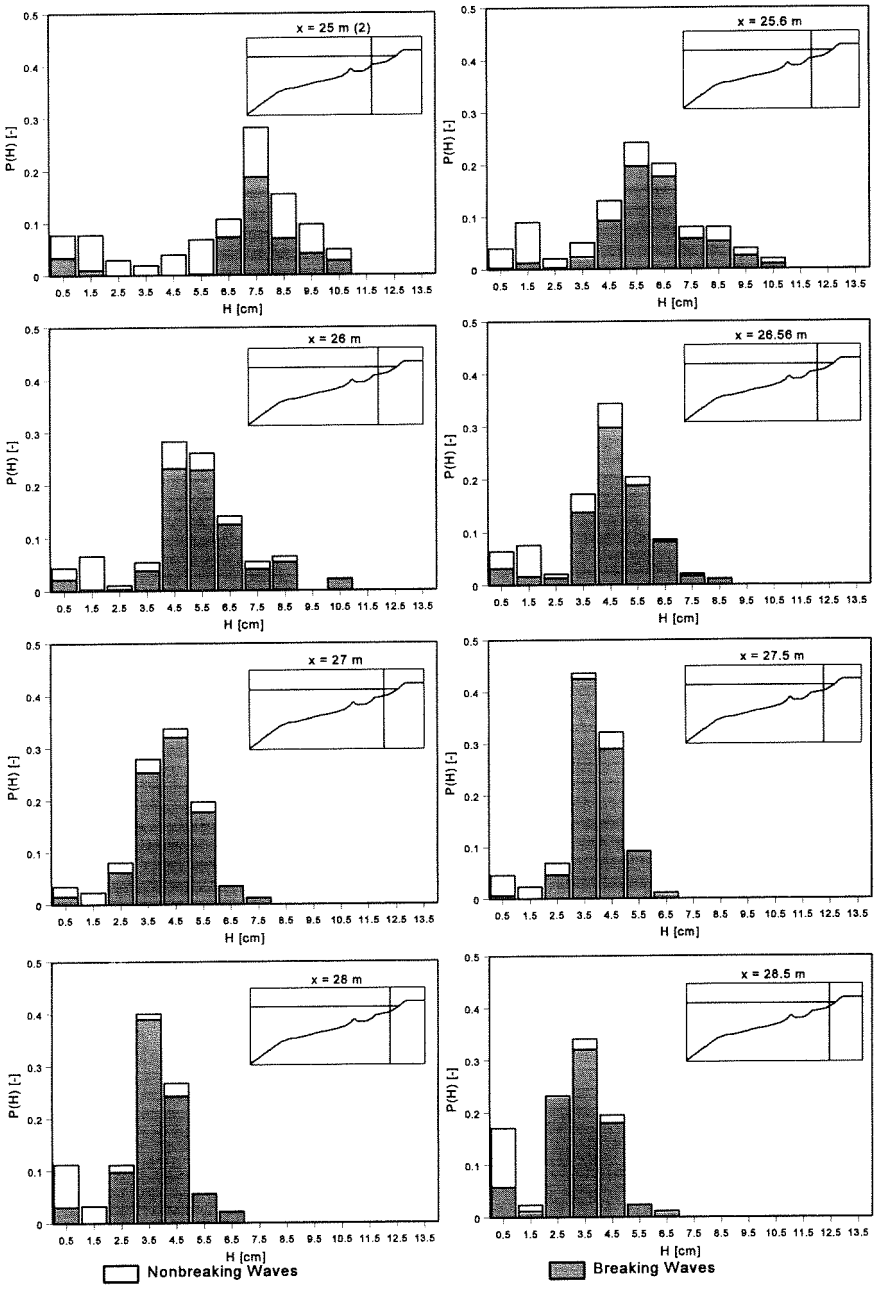


*Figure 3.39f* Wave Height Distribution 1B; Location: x = 25 - 28.5 m

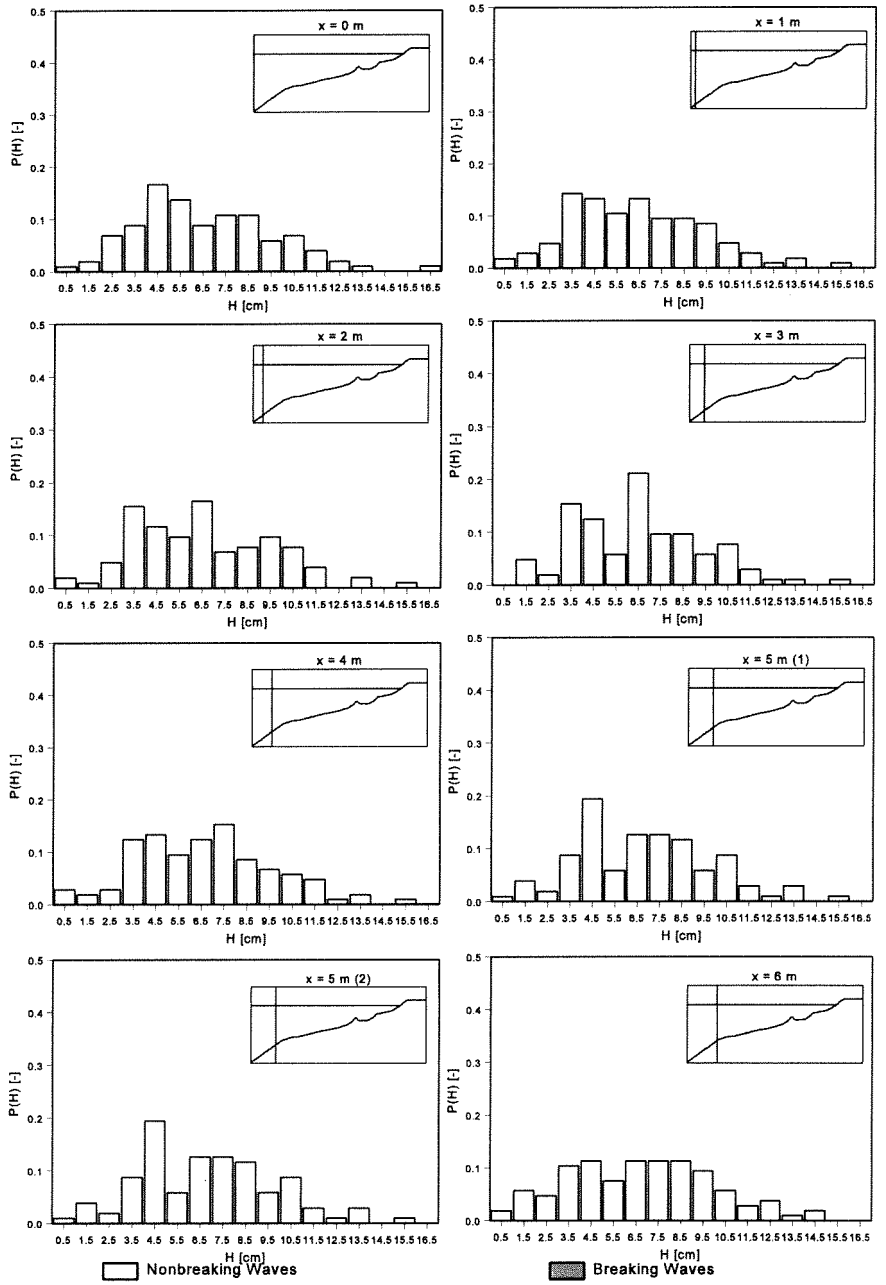


*Figure 3.40a* Wave Height Distribution 1C; Location: x = 0 - 6 m

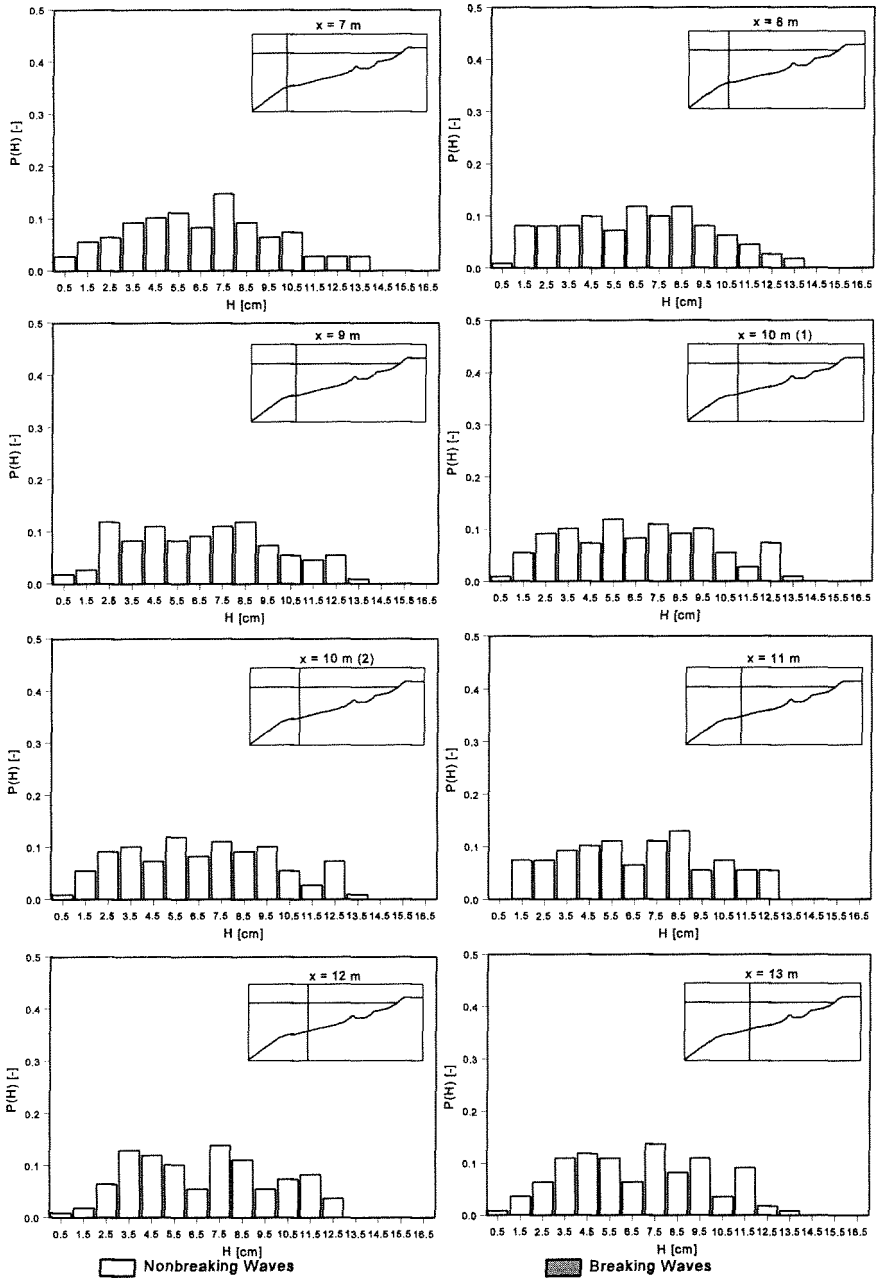


*Figure 3.40b* Wave Height Distribution 1C; Location: x = 7 - 13 m

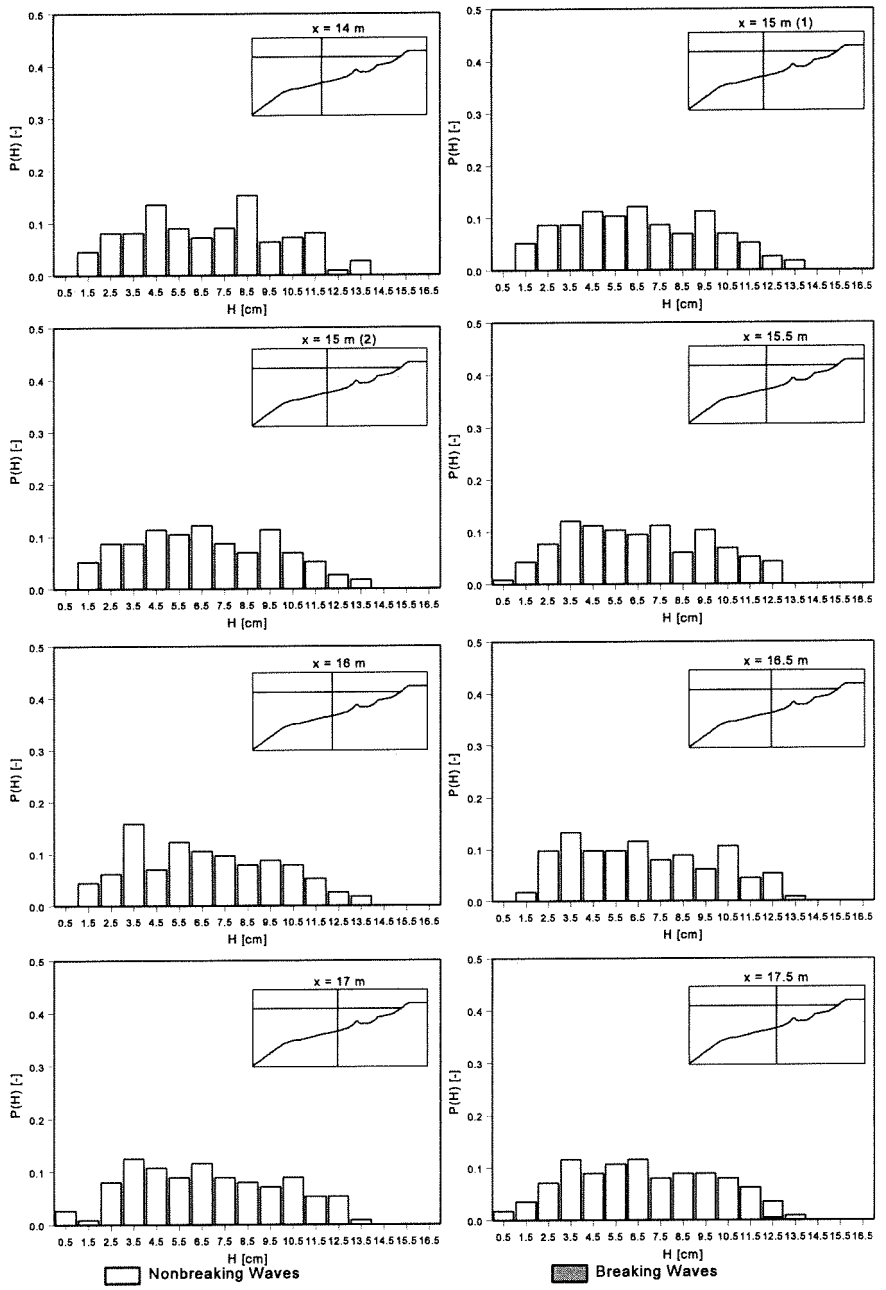


*Figure 3.40c* Wave Height Distribution 1C; Location: x = 14 - 17.5 m

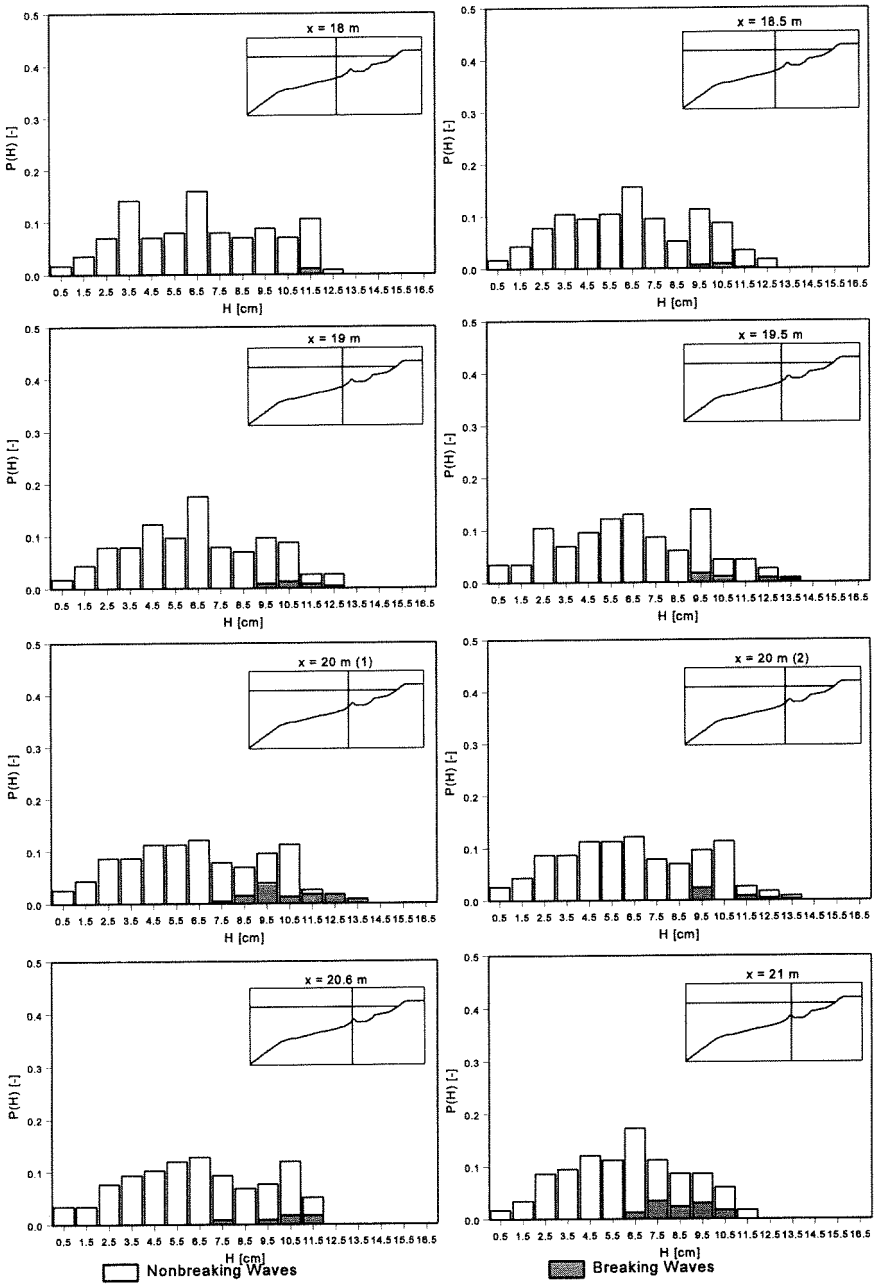


*Figure 3.40d* Wave Height Distribution 1C; Location: x = 18 - 21 m

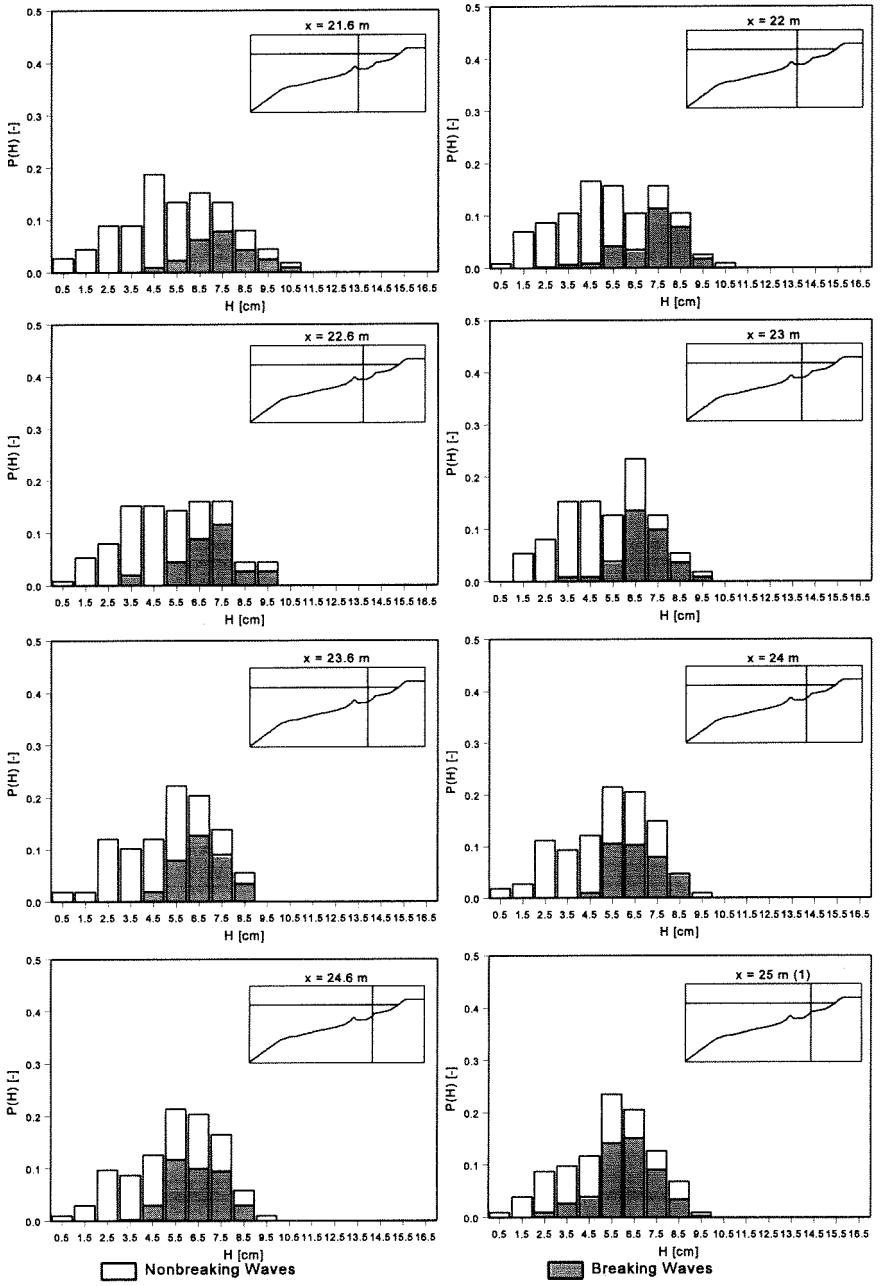


*Figure 3.40e* Wave Height Distribution 1C; Location: x = 21.6 - 25 m

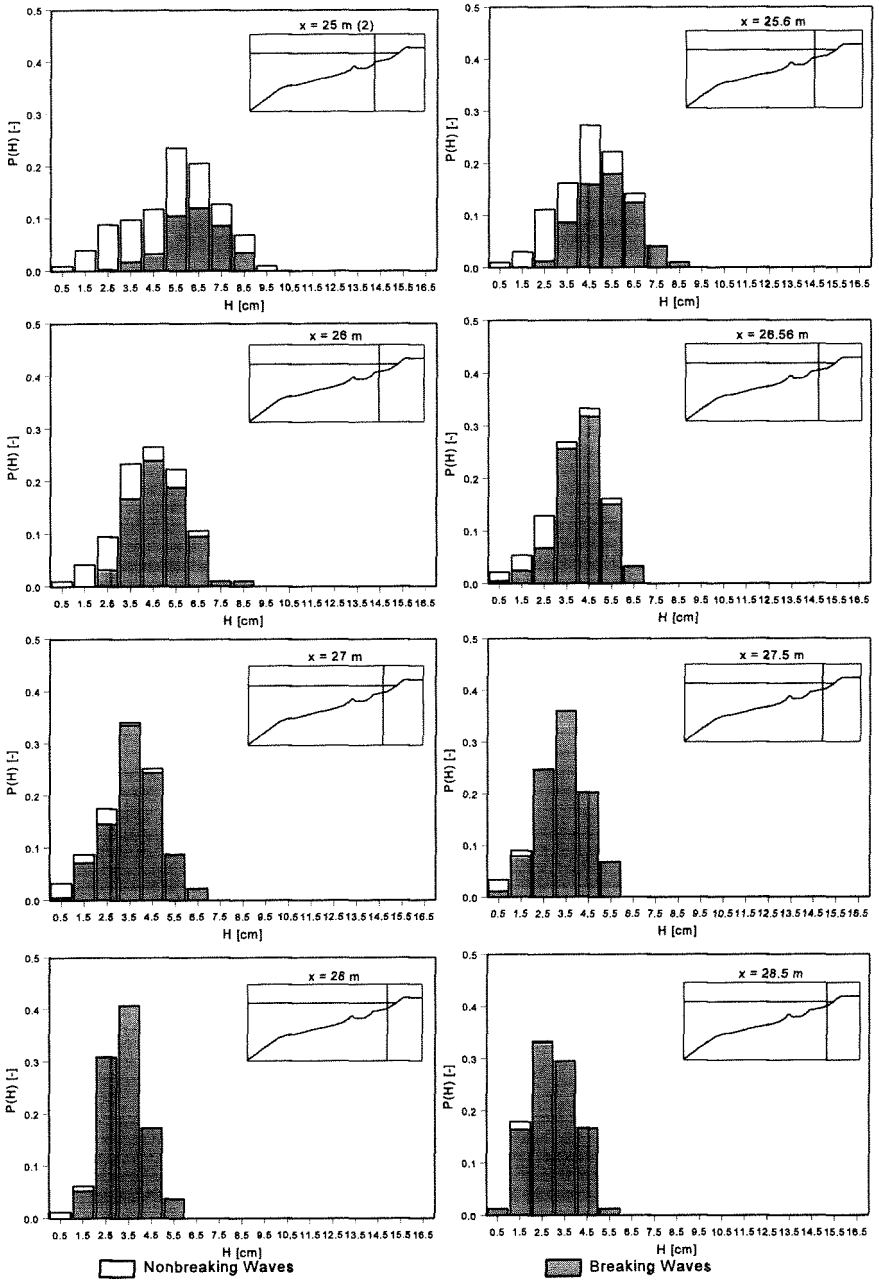


*Figure 3.40f* Wave Height Distribution 1C; Location: x = 25 - 28.5 m

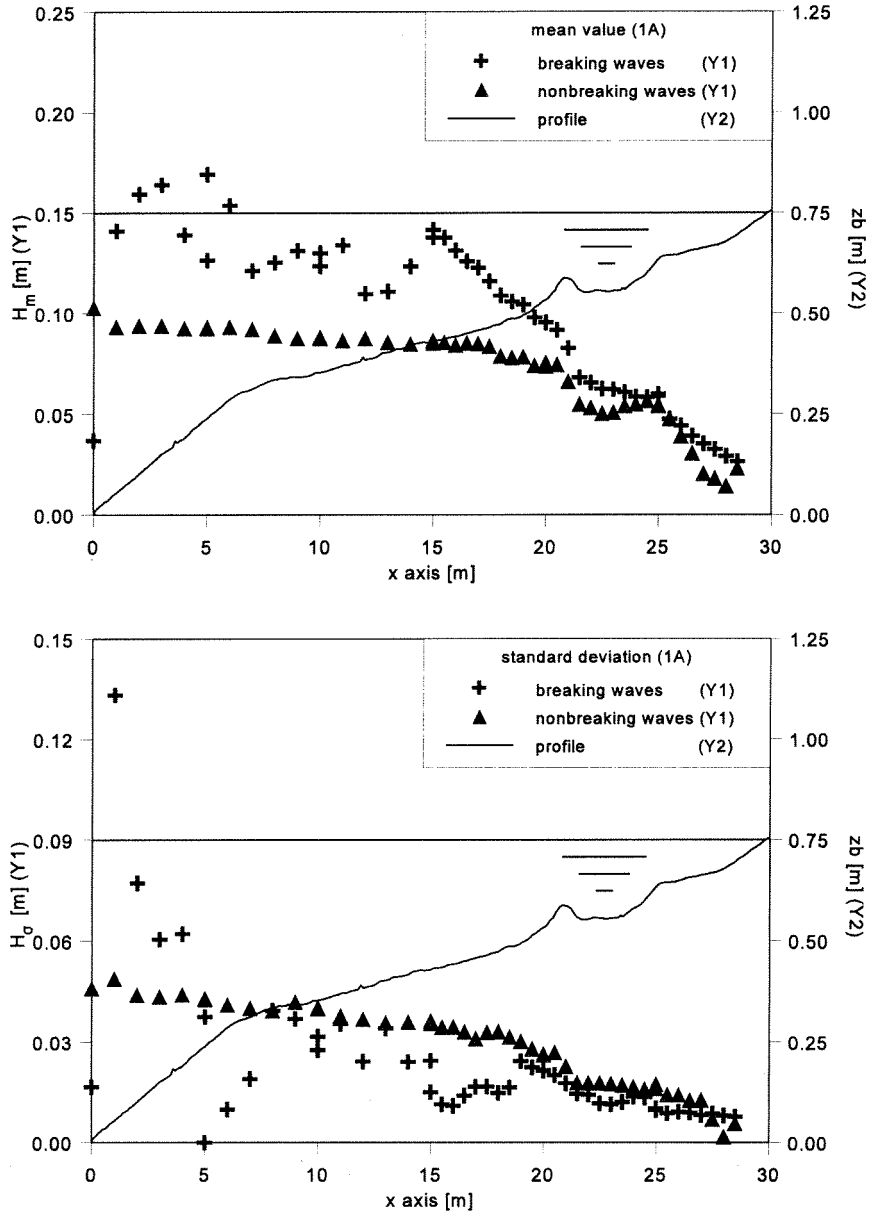


*Figure 3.41* Mean and Standard Deviation Wave Height H (1A)

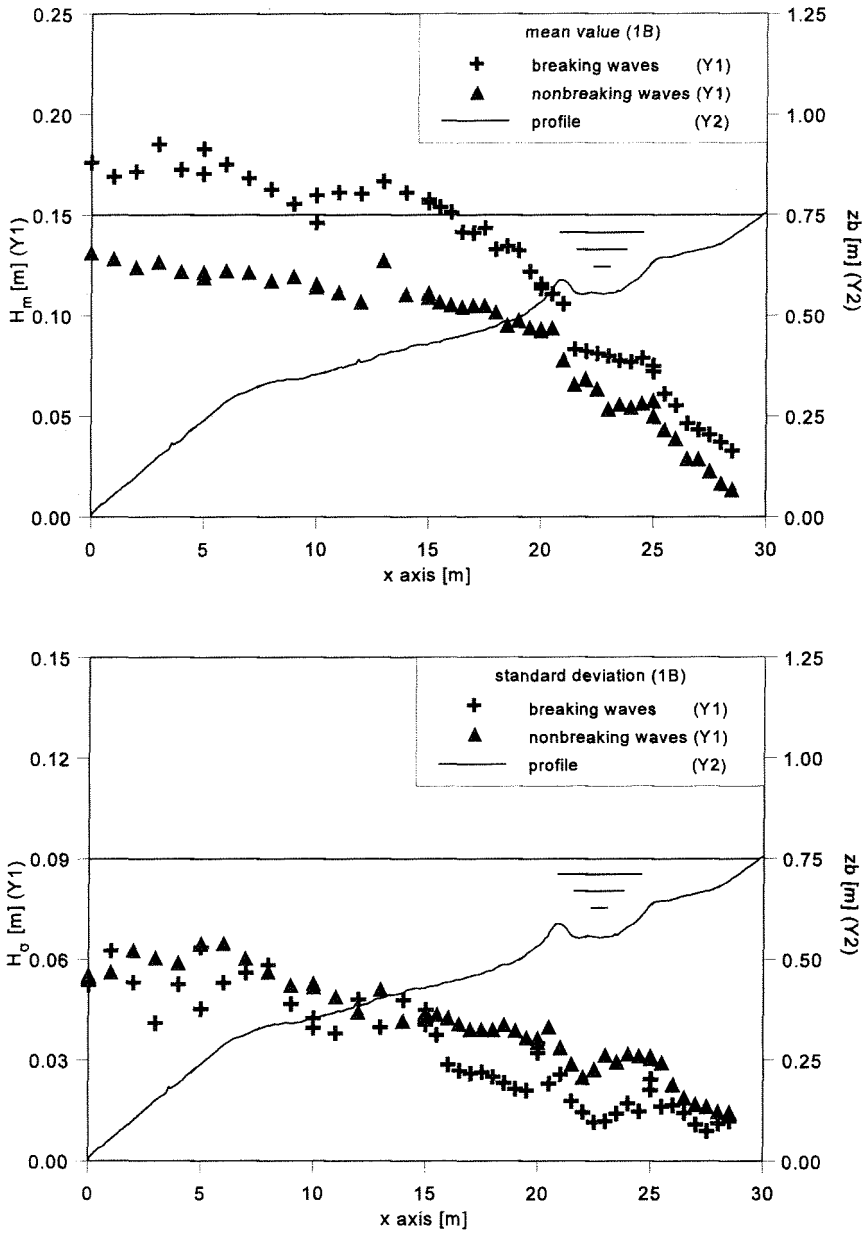


*Figure 3.42* Mean and Standard Deviation Wave Height H (1B)

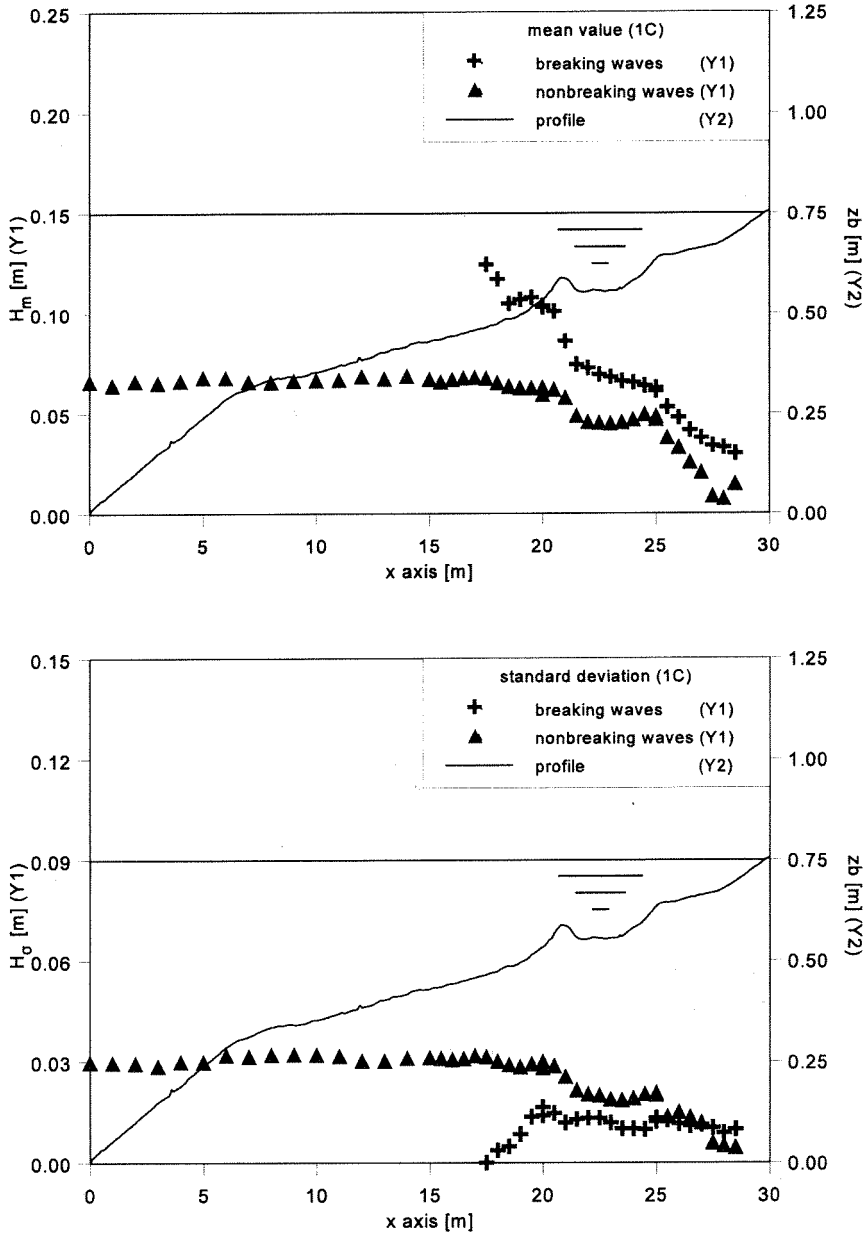


*Figure 3.43* Mean and Standard Deviation Wave Height H (1C)